Summer 7-7-2011

Interactions of Metals and Radicals: A Biochemical Perspective in Tryptophan Dioxygenase

Kednerlin Dornevil
Georgia State University, kdornevil1@student.gsu.edu

INTERACTIONS OF METALS AND RADICALS: A BIOCHEMICAL PERSPECTIVE IN TRYPTOPHAN DIOXYGENASE

by

KEDNERLIN H. DORNEVIL

Under the Direction of Dr. Aimin Liu

ABSTRACT

An intriguing mystery about tryptophan 2, 3-dioxygenase is its hydrogen peroxide-triggered enzyme reactivation from the resting ferric oxidation state to the catalytically active ferrous form. In this study, we found that such an odd Fe(III) reduction by an oxidant depends on the presence of L-Trp, which ultimately serves as the reductant for the enzyme. In the peroxide reaction with tryptophan 2, 3-dioxygenase, a previously unknown catalase-like activity was detected. A ferryl species (δ = 0.055 mm/s and ΔE_Q = 1.755 mm/s) and a protein-based free radical (g = 2.0028 and 1.72 millitesla linewidth) were characterized by Mössbauer and EPR spectroscopy, respectively. This is the first compound *E*S-type of ferryl intermediate from a heme-based dioxygenase characterized by EPR and Mössbauer spectroscopy. Density functional theory calculations revealed the contribution of secondary ligand sphere to the spectroscopic properties of the ferryl species. A Trp-Trp dimer and a monooxygenated L-Trp were both observed as the enzyme reactivation by-products by mass spectrometry. Together, these results lead to the unraveling of an over 60-year old mystery of peroxide reactivation mechanism.

INDEX WORDS: Tryptophan dioxygenase, Radical, Methylamine dehydrogenase, Electron paramagnetic spectroscopy, Mössbauer spectroscopy,

INTERACTIONS OF METALS AND RADICALS: A BIOCHEMICAL PERSPECTIVE IN TRYPTOPHAN DIOXYGENASE

by

KEDNERLIN H. DORNEVIL

A Thesis Submitted in Partial Fulfillment of the Requirements for the Degree of

Master of Science

In the College of Arts and Sciences

Georgia State University

2011

INTERACTIONS OF METALS AND RADICALS: A BIOCHEMICAL PERSPECTIVE IN TRYPTOPHAN DIOXYGENASE

by

KEDNERLIN H. DORNEVIL

Chair: Dr. Aimin Liu

Committee: Dr. Dabney Dixon

Dr. Ivaloy Ivanov

Electronic Version Approved:

Office of Graduate Studies

College of Arts and Sciences

Georgia State University

July 2011

DEDICATION

I would like to dedicate this thesis to my mother, Nesline Paul and sister, Chrissie Dornevil. It is because of their support I am able to accomplish so much.

ACKNOWLEDGEMENTS

I would like to acknowledge my advisor, Dr. Aimin Liu for his tremendous support during my stay in his lab. It is because of his beliefs in my abilities that I have been able to succeed. Thank you for helping me become a better scientist.

I would like to acknowledge Dr. Rong Fu, who left me a beautiful project to work on after her graduation. I am very grateful for the training and guidance she gave me. I can only hope that I can leave my mark on this project like you have.

I would like to acknowledge all my lab members, Dr. Vesna de Serano, Yan Chen, Jaifeng Geng, Fange Liu, Ian Davis, Xiaoxi Wei, Luo Hu, and Imran Rehmani. During my time here we have made many memories together that I will forever cherish. Thank you.

Last but not least. I would like to thank my committee members, Dr. Dixon and Dr. Ivanov for their precious time during the summer to serve on my committee. I have received excellent support and thank you both for having my best interest at heart.

TABLE OF CONTENT

LIST OF FIGURES

LIST OF TABLES

LIST OF SCHEMES

ABBREVIATIONS

5’-deoxyadenosyl	5’-dA
Acylated pyruvate formate lyase	acyl-PFL
Acylated coenzyme A	AcCoA
L-α-aminoadipoyl-L-cysteinyl-L-valine	ACV
adenosylcobalamine	AdoCbl
Ascorbate Peroxidase	APX
Catalase I	Cat I
Cytochrome *c* peroxidase	CcP
Cupriavidus metallidurans TDO	*Cm*TDO
Chloroperoxidase I	CPO I
Compound ES	Cpd ES
Compound I	Cpd I
Cysteine	Cys
Density functional theory	DFT
Deoxyribonucleoside triphosphate	dNTP
Electronspray ionization-mass spectrometry	ESI-MS
Electron nuclear double resonance	ENDOR
Electron paramagnetic resonance	EPR
Galactose Oxidase	GAO
High-field EPR	HFEPR
Histidine	His
Horseradish peroxidase I	HRP I
Coenzyme A	HSCoA

Cysteine	Cys
Hydroxyurea	HU
Glycine	Gly
Indoleamine 2,3-dioxygenase	IDO
Isopenicillin *N* synthase	IPNS
Kilodalton	kDa
Liquid chromatography	LC
Lignin peroxidase I	LiP I
Lysine 2, 3-aminomutase	LAM
Methylamine dehydrogenase	MauG
methylmalonyl-CoA mutase	MCM
Mass spectrometry	MS
Nicotinamide adenine dinucleotide phosphate	NADPH
N-formylkynurenine	NFK
Cytochrome P450	P450
Pyruvate formate lyase	PFL
Prostaglandin endoperoxide G_2	PGG_2
Prostaglandin H synthase	PGHS
Pyruvate oxidase	POX
Photosystem II	PSII
Ribonucleotide reductase	RNR
S-adenosylmethionine	SAM
Tryptophan 2,3-dioxygenase	TDO
Tryptophan	Trp
Tryptophan tryptophylquinone	TTQ

Tyrosine	Tyr
Wild type	WT

CHAPTER 1

INTRODUCTION

1.1 *Introduction*

Radicals became accessible to chemist more than 100 years ago when Gomberg prepared the first stable free radical, triphenylmethyl (*1*). Since then, numerous other radical systems have been prepared and characterized (*2*). The discovery of ribonucleotide-diphosphate reductase (RNR) and its tyrosyl radical (*3, 4*) introduced the idea that a radical could be biologically competent and stable, which has stirred up great interest in the scientific community (*5, 6*). It was assumed that because of their unstable nature, radicals were not suitable for utilization in the controlled and specific chemistry that occurs inside an enzyme's active site. However the discovery of radical enzymes such as, RNR and photosystem II (PSII), have opened a new field of radical enzymology in biochemistry and has led to the reconsideration of the ability to use these highly reactive species in a controlled manner. RNR has the ability to generate a stable tyrosyl radical (*7*) and utilize this radical to carry out the reduction of ribonucleotide to deoxyribonucleotide by the replacement of the C2'-OH with a proton (eq 1). Photosystem II oxidizes two water molecules to oxygen (eq 2) and utilizes two tyrosyl radicals, $Y_Z\cdot$ and $Y_D\cdot$, to carry out this process. These findings have also led to the creation of the radical SAM superfamily of enzymes which are represented by the enzymes lysine 2, 3-aminomutase (LAM), pyruvate formate-lyase, and anaerobic RNR class III. These enzymes have a common cysteine motif CX_3CX_2C that coordinates to a [4Fe-4S] cluster (*8-11*). *S*-adenosylmethionine (SAM) is also utilized as either a cofactor or cosubstrate to generate a 5'-deoxyadenosyl (5'-dA•) radical. The reactions presented in equations 1 and 2 are some of the most essential for life, this highlights the important roles that radicals have in nature

$$NDP + 2\ e^- + 2\ H^+ \rightarrow dNDP + H_2O \qquad (1)$$

$$2\ H_2O \rightarrow O_2 + 4\ H^+ + 4\ e^- \qquad (2)$$

1.2 *Types of radical species*

The types of radical species involved in biochemical systems can be subdivided into four main groups: flavin and quinine intermediates, oxygen radicals, radicals on an amino acid, and alkyl radicals (*5*). Flavins and quinines can serve as an electron transfer intermediary and an electron transfer agent, respectively. Oxygen radicals are often involved in monooxygenation and dioxygenation reactions such as the case of cytochrome P450 (*12*). Amino acid radicals are found in the majority of enzymes that use a radical based mechanism, while alkyl radicals can be found in proteins (such as pyruvate formate lyase, and anaerobic RNR) that use a radical centered on the α-carbon of a glycine (*5*).

1.3 *Generation of free radicals*

Free radicals reactions are a special case of oxidation-reduction reactions. They are involved in the transfer of odd numbers of electrons, homolytic bond cleavage and formation, and abstraction of an H atom. This reaction strategy is often used to activate highly stable substrates with no polar bonds such as hydrocarbons. Though free radicals are necessary for certain biochemical reactions, the mechanism in which they are formed needs to be understood. General routes for generating free radicals are: 1) photochemical reactions and 2) thermal decomposition of peroxides, however; these routes are often difficult under biological conditions. Transition metals are found to be the most popular radical generating systems in nature. Their weak M-C bond and variable oxidation states have allowed them to participate in many one-electron transfer reactions. The transition metal cobalt provides one example of how these elements can help generate free radicals. Many enzymes use adenosylcobalamine (AdoCbl) to generate an adenosyl free radical which can abstract a proton from their substrate and initiate subsequent reaction. This is highly favorable because the Co-C bond can be easily broken. The bond dissociation energy for the homolytic cleavage of the Co-C bond in adenosylcobalamine is about 120 kJ/mol (*13*); this

is relatively small compared to the 410 kJ/mol required for a C-C bond cleavage.

The cofactor SAM, analogous to AdoCbl upon one-electron reduction, is a source of a 5'-deoxyadenosyl (5'-dA•) radical, which can initiate many metabolic reactions by hydrogen-atom abstraction. SAM and AdoCbl are both radical initiators and share a common 5'-dA• intermediate. This radical is both highly oxidizing and unstable, preventing its direct observation (*14*). Many SAM-dependent enzymes additionally require an $[4Fe\text{-}4S]^{1+}$ cluster cofactor. The iron-sulfur cluster contains three conserved cysteines, this leaves one unique iron that is not ligated by the protein (*15*). The precise mechanism for the formation of the 5'-dA• radical is still under discussion. However, evidence has shown that the non-ligated iron will directly coordinate to SAM (*15*). The binding of Adomet to the unique iron requires the iron sulfur cluster to be in the $[4Fe\text{-}4S]^{2+}$ state (*15*). By this mechanism, the iron ion is able to form a bridge between SAM and the cluster enabling an injection of one reducing equivalent into SAM facilitating reductive cleave and the generation of the 5'dA• radical.

1.4 *Brief survey of radical enzymes*

1.4.1 *Ribonucleotide Reductase*

To date many radical enzymes have been studied and characterized. Several reviews have been published outlining the work performed in this field (*5, 6, 16-20*). What follows is a brief description of several select enzymes, more detailed information over viewing the field can be found in the references. Ribonucleotide reductase is an enzyme responsible for the synthesis of the deoxyribonucleoside triphosphates (dNTP) (Table 1) and for maintaining the DNA/cell mass ratio in living organisms (*21-33*). This enzyme utilizes a mechanism in which tyrosyl radical is generated in one subunit of the enzyme, and is shuttled to the next subunit as a thiyl radical where it can fulfill its chemical role. There are three

classes of RNR enzymes, classes I, II and III; they all differ slightly on their radical initiation pathways (*28, 31, 34, 35*). There is also a fourth class which includes anaerobic RNR that uses manganese instead of iron as a cofactor to carry out its chemistry (*36*).

1.4.2 *Pyruvate Formate Lyase*

Pyruvate formate lyase (PFL) is an important enzyme utilized in the metabolism of glucose during anaerobic conditions and is responsible for the conversion of pyruvate and CoA to acetylCoA and formate (Table 1) (*37-39*). This enzyme uses a glycyl radical (*40*) in its active form, it should be noted that interconversion between the active and inactive form is a catalytic process mediated by the activating enzyme PFL-AE. There are two proposed mechanism for PFL and in both cases the glycyl radical is converted to a thiyl radical (Cys419). The thiyl radical can then initiate the C-C bond cleavage of pyruvate to generate an acylated-enzyme intermediate (acyl-PFL) and the release of formate. Introduction of HSCoA into the active site sees the release of AcCoA and regeneration of free PFL.

1.4.3 *Photosystem II*

The production of oxygen by photosynthesis is substantial for aerobic life on earth. Lying at the focal point of photosysnthesis are photosystem II (PSII) and photosystem I (PSI); these two systems are responsible for the initial steps in conversion of light energy into biochemically useful products. Photosystem II uses light to oxidize water; water serves as the terminal electron donor producing molecular oxygen (Table 1), and protons (*41-46*). PSII contains two tyrosine species (Y_Z, Y_D) that are able to act as electron donors during the catalytic cycle. Both species are able to generate organic radicals detectable by EPR and have been extensively studied and have been well characterized (*47-51*). Of the two tyrosyl radicals, the role of Y_Z has been determined to function as an oxidizing intermediate in

electron transfer during water oxidation (*52*). It has also been proposed that Y_Z might have the additional role of being able to abstract a proton from water (*6*). The Y_D has been postulated to play redox and electrostatic functions during catalysis (*53*).

1.4.4 *Galactose Oxidase*

From a family of enzymes known as radical-copper oxidases, galactose oxidase (GAO) is one of the most understood members in this large group (*54-58*). The primary function of GAO is the catalysis of a two-electron oxidation of primary alcohols to aldehydes along with a simultaneous reduction of oxygen to hydrogen peroxide (Table 1). Its radical mechanism is well understood, and the identification of the free radical as a tyrosine radical in GAO was done by isotope labeling studies using [*β*,*β*-^{2}H]tyrosine (*59*). The crystal structure of this protein in 1991 revealed a modification of the tyrosine residue where it is covalently bound at the α-position to an adjacent Cys228 (*60*, *61*). Numerous studies have been done on this cofactor showing that it is able to function as a single electron redox center; it does this by switching between the phenoxyl and phenol radical forms during the redox cycle (*59*, *62*, *63*).

Table 1. Reactions of radical enzymes.

Enzyme	Reaction	Radical
Ribonucleotide Reductase (RNR)	$NDP + 2\ e^- + 2\ H^+ \rightarrow dNDP + H_2O$	Tyr122 (*4*)
Pyruvate Formate Lipase (PFL)	Pyruvate → formate + acetyl-CoA	Gly734 (*40*)
Photosystem II (PSII)	$2\ H_2O \rightarrow O_2 + 4\ H^+ + 4\ e^-$	Tyr161 (*64*, *65*), Tyr160 (*66*, *67*)
Galactose Oxidase (GAO)	$RCH_2OH + O_2 \rightarrow RCHO + H_2O_2$	Tyr272 (*59*)

1.5 *Enzymes with radical intermediates*

1.5.1 *Cytochrome c Peroxidase*

Cytochrome *c* peroxidase is a yeast mitochondrial enzyme that catalyzes the reduction of hydrogen peroxide to water by the oxidation of ferrocytochrome *c* to ferricytochrome *c* (Table 2) (*68-71*). The enzyme reacts with H_2O_2 in a two-electron oxidation of the ferric form to form an oxoferryl species (Compound ES) (*72*), this intermediate stores one oxidizing equivalent in the oxyferryl-heme and the second one on a nearby amino acid residue (*73*). This is unlike other peroxidases, where the second oxidizing equivalent is stored locally as a porphyrin radical cation (Compound I) (*74-76*). Studies for this cytochrome *c* peroxidase enzyme have found the second oxidizing radical to be a protonated Trp191 (*73*).

1.5.2 *Isopenicillin N Synthase*

Isopenicillin *N* Synthase (IPNS) is a mononuclear iron enzyme involved in the biosynthesis of penicillin by converting the tripeptide, L-α-aminoadipoyl-L-cysteinyl-L-valine (ACV) to *β*-lactam isopenicillin *N* (*5, 77-79*) (Table 2). IPNS is able to cyclize ACV in an O_2-dependent process forming the bicyclic product; this process has been reviewed by Frey *et al.* Removal of a C3(H) and the peptide-N(H) from the cysteinyl residue leads to formation of the *β*-lactam ring. Removal of the valyl-C3(H) and cysteinyl-S(H) generates the five-membered ring. The reducing equivalents are used to reduce molecular oxygen to water. In the proposed mechanism of IPNS, binding of O_2 to the ferrous heme generates the initial radical in the form of ferric superoxide (Fe(III)-$O_2^{\cdot}$) which can abstract the proton of C3 from the cysteinyl side chain of ACV. This leads to formation of a Fe(II)-O-OH $^{\cdot}$ intermediate, a six-membered cyclic transition state with a thioaldehyde from substrate ligated to the iron. The peroxide can be dehydrated in concert with hydrogen abstraction from cysteinyl-NH generating a ferryl-oxo species. Abstraction of a hydrogen

by the ferryl-oxo from the valyl-C3(H) group generates a tertiary isopropyl radical. The cycle completes when bonding between the tertiary radical and the thiolate ligand on the Fe(III)-OH closes the five-membered ring and reduces iron to Fe(II)-OH.

1.5.3 *Cytochrome P450*

Cytochrome P450 (P450) is versatile enzyme that uses dioxygen and two reducing equivalents to catalyze the regioselective and stereospecific insertion of oxygen into organic compounds (*12, 80-93*) (Table 2). P450 contains a heme cofactor and a ferric ion in the resting state. The cycle of P450 begins upon displacement of a weakly bound water molecule with the substrate. Two reducing equivalents and 2 protons are needed for the release of one water molecule and formation of the reactive oxoferryl species. This intermediate is highly elusive in the P450 enzyme family; however, it is generally accepted to be the active intermediate in oxygen insertion. The P450 mechanism has been fairly well established with many of the key intermediates having been observed (*94*).

1.5.4 *Prostaglandin H Synthase*

Prostaglandin H synthase (PGHS) is an enzyme that catalyzes the conversion of arachadonic acid (AA) and two O_2 to prostaglandin endoperoxide G_2 (PGG_2) (Table 2) as the first and committed step in prostaglandin biosynthesis (*73, 95-98*). This enzyme contains both cyclooxygenase activity and peroxidase activity carried out in two distinct active sites. PGHS generates a tyrosyl radical (*99*) that initiates reaction by abstraction of the *pro*-S hydrogen atom from C12 of AA (*100*). However, studies have shown that PGHS upon reaction with peroxide can generate distinct EPR signals (*98*). Characterization of these radical species by EPR (*101-106*), ENDOR (*107*), and mutagenesis (*106, 108, 109*) have led to the identification of all these species to be tyrosyl radicals from two different residues

(*110*). Research on the Tyr504 radical suggests that this radical helps in maintaining the cyclooxygenase in its activated state (*109*).

1.5.5 *Methylmalonyl-CoA mutase*

As the only AdoCbl-dependent enzyme in mammals (*5*), methylmalonyl-CoA mutase (MCM) catalyzes the interconversion of methylmalonyl-CoA and succinyl-CoA (Table 2). A cyclopropyl intermediate radical is thought to be the key for the rearrangement. Using isotopic substitutions, ^{2}H and ^{13}C of the substrate lead to a narrowing and broadening respectively of the EPR signals (*5*). These changes in the EPR spectra have shown the radical to be derived from the substrate and not from the protein (*111*). Analysis of this species by EPR using freeze trapping techniques shows it to posses characteristics (*g*-tensor and hyperfine tensor) consistent with a strongly coupled, hybrid triplet system (*112*).

1.5.6 *Lysine 2,3-Amino Mutase*

Lysine 2,3-Aminomutase (LAM) is a SAM dependent enzyme that catalyzes the interconversion of L-α-lysine (lysine) and L-*β*-lysine (*β*-lysine) (Table 2). LAM also uses a [4Fe-4S] cluster to generate a radical and mediate hydrogen transfer. The mechanism for LAM has been studied by using EPR spectroscopy and kinetic characterization of the *β*-lysyl radical, analogues of the lysyl radical, and the 5'-deoxyadenosyl radical (*20, 113, 114*). The reaction cycle of LAM starts when lysine binds to the internal aldimine of PLP. Fragmentation of SAM to generate the 5'-deoxyadenosyl radical ([4Fe-4S] dependent process) initiates the radical mechanism. The 3-*pro-R* hydrogen from the lysyl side chain is abstracted and produces 5'-deoxyadenosine and generates a lysyl radical at the active site. This radical isomerizes to the *β*-lysyl radical via a two-step process. The *β*-lysyl radical is the product radical, and hydrogen transfer from the methyl group of 5'-deoxyadenosine quenches this radical and regenerates the 5'-

deoxyadenosyl radical. Transaldimination with Lys337 releases *β*-lysine and restores the internal aldimine for the next cycle.

Table 2. Reactions involving radical intermediates.

Enzyme	Reaction	Radical
Cytochrome c Peroxidase (CcP)	H_2O_2 + 2 Cyt-c(Fe^{II}) + 2 H^+ → 2 H_2O + 2 Cyt-c(Fe^{III})	Trp191 (*73*)
Isopenicillin N Synthase (IPNS)	ACV + O_2 → 2 H_2O + IPN	Fe(III)-$O_2^{\cdot}$
Cytochrome P450	RH + O_2 + 2 H^+ + 2 e^- → ROH + H_2O	Tyr(*115*)
Prostaglandin H synthase (PGHS)	H2O2 + Fe(III) + AA → PGH_2 + H_2O	Tyr385(*116*), Tyr504 (*99*)
Galactose Oxidase (GAO)	RCH_2OH + O_2 → RCHO + H_2O_2	Tyr272 (*59*)
Lysine 2,3-Aminomutase (LAM)	L-α-lysine ↔ L-*β*-lysine	*β*-lysine (*117*)

1.6 *Predicted radical mechanism of pyruvate oxidase*

Pyruvate oxidase (POX) catalyzes the reaction of pyruvate with phosphate and molecular oxygen to form acetyl phosphate, CO_2 and peroxide (*118*). POX is a thiamine pyrophosphate dependent enzyme which is thought to use a radical mechanism. Radical formation in this enzyme would be initiated by electron transfer from an intermediate 2-(α-hydroxyethylidene)-TPP to FAD (*5*). The mechanism of POX occurs by a sequence of steps (eqs 3a-3d).

$$CH_3COCOO^- + E\bullet FAD\bullet TPP + H^+ \leftrightarrow E\bullet FAD\bullet \text{lactyl-TPP} \quad (3a)$$

$$E\bullet FAD\bullet \text{lactyl-TPP} \rightarrow E\bullet FAD\bullet 2\text{-}(\alpha\text{-hydroxyethylidene})\text{-TPP} + CO_2 \quad (3b)$$

$$E\bullet FAD\bullet 2\text{-}(\alpha\text{-hydroxyethylidene})\text{-TPP} + P_i \rightarrow E\bullet FADH_2\bullet TPP + \text{acetyl-P} \quad (3c)$$

$$E\bullet FADH_2\bullet TPP + O_2 \leftrightarrow E\bullet FADH\bullet(O_2^{\cdot-})\bullet TPP + H^+ \quad (3d)$$

$$E\bullet FADH\bullet(O_2^{\cdot-})\bullet TPP + H^+ \rightarrow E\bullet FAD\bullet TPP + H_2O_2 \quad (3e)$$

The first two steps (3a and 3b) occur by polar mechanisms, with the last three steps utilizing free radicals (*119*). $FADH_2$ is oxidized by molecular oxygen in a two step mechanism (*120*). The first step involves an electron transfer from $FADH_2$ leading to formation of superoxide and FAD-semiquinone. Another electron/H+ transfer will produce hydrogen peroxide and FAD. An 2-(α-hydroxyethyl)-TPP radical is assumed to form during the cycle (*5*). However, this has never been spectroscopically observed and has only been inferred from the transient FAD-semiquinone.

1.7 *Radical mechanism of a non-heme based system (Ribonucleotide Reductase)*

Class I RNRs contain two subunits termed R1 and R2. The formation of a radical is oxygen dependent, and exists on the smaller subunit (R2) of the protein as a stable tyrosyl radical. This radical can migrate from R2 to a cysteine residue on the next subunit (R1) generating a thiyl radical upon binding of ribonucletide substrates at the R1 active site. Electrons are provided to the class I group of RNRs by thioredoxin or glutaredoxin (*121*). Class II RNR enzymes differ from class I in that they do not require oxygen to generate their radical and are neither inhibited by its presence. Another difference is that class II RNR contains a single subunit (NrdJ). To generate the substrate activating thiyl radical, class II RNR requires an adenosylcobalamin cofactor (*28, 31, 34*). Thus adenosylcobalamine is able to fulfill the role of the missing R2 subunit found in class I RNR. Additionally, the electron donors utilized by class II RNR is thioredoxin or glutaredoxin which is similar to class I. Class III RNR have several main differentiating properties from the other two. The first being that they are anaerobic enzymes and the presence of oxygen inactivates them. Second, these enzymes have two domains, the large catalytic domain NrdD and the smaller NrdG domain. The NrdG domain uses an iron-sulfur cluster [4Fe-4S], *S*-adenosylmethionine, and reduced flavodoxin to generate a glycyl radical at the NrdD C-terminus. Formate provides the electrons needed to reduce the enzyme (*122, 123*). This glycyl radical is analogous to the tyrosyl radical generated by class I RNRs that is required to generate the thiyl radical needed for

substrate activation. A fourth class, class IV, of RNR has recently been discovered and replaces one of the iron ions with a manganese cofactor (*36*). This new group of RNR contains a Mn^{IV}/Fe^{III} cofactor and has been shown to be able to generate a transient catalytic thiol radical at the active site when the substrate arrives (*36*).

In the catalytic mechanism of RNR, the initial step involves the initial thiyl radical (C439 in *E. coli*) abstracting a proton from the 3'-carbon of the ribose sugar and generating a substrate radical (*124, 125*). In the next step the C2-O bond is cleaved, this is coupled to the formation of a thiyl radical located on the proximal cysteine (C225 in *E. coli* R1) and the protonation of a water molecule. The conserved glutamate (E441 in *E. coli* R1) acts as an active site base, deprotonating the 3'-OH and assisting in the reduction of ribose. Next the 2'-carbon is protonated and a disulphide radical is formed on the protein. In the next step a deoxyribose radical is formed, finally the thiyl radical is regenerated to complete the reaction cycle. The observation and characterization of some of these intermediates has given a lot of support to the proposed mechanism. The thiyl radical which is catalytically competent has been observed in class II RNR (*126*), and substrate and thiol radicals have been observed from mutational studies (*127, 128*).

1.8 *Radical intermediate of a heme-based system (Catalase)*

Catalase is a monofunctional enzyme that is found in many living aerobically respiring organism (*129, 130*). These enzymes prevent cell oxidative damage by catalyze the dismutation of hydrogen peroxide to water: $2\ H_2O_2 \rightarrow 2\ H_2O + O_2$. Catalase enzymes can be divided into three classes of proteins. The first class is composed of monofunctional, heme-containing enzymes, the second class is a group of bifunctional enzymes that possess catalase activity in addition to their native function (*i.e.* catalase-peroxidase). Finally the third class contains the nonheme or Mn-containing catalases (*131*). In addition there are numerous heme proteins that display low levels of catalase activity in the presence of H_2O_2 such

as chloroperoxidase and myoglobin (*129*). Phylogenetic studies of the catalase group of enzymes have resulted in the division of monofunctional catalases into three clades (*132*). Clade 1 catalases are primarily of plant origin; the clade 2 catalases are all large subunit enzymes of bacterial and fungal origin. The clade 3 enzymes are all small subunit enzymes from bacteria, archaebacteria, fungi and other eukaryotes (*131*). Since the discovery of catalase, numerous crystal structures have revealed much about its structure (*133-135*).

Catalase are homotetrameric enzymes with each subunit containing a protopophyrin IX cofactor and Fe(III) (heme *b*). There is also a small group of catalases (clade 3) which possess an additional cofactor, NADPH, with one nucleotide bound per monomer. However, this nucleotide is not a necessary cofactor for catalase activity and its role is currently under investigation (*136, 137*). One role suggested for this cofactor is to prevent the inactivation of catalase by serving as an electron source converting Compound II-catalase (inactive towards H_2O_2) to its resting state (*138*). In the active site are several conserved residues for this group of enzymes: a group of distal residues consisting of histidine, asparagines and serine and a tyrosinate as the proximal heme iron ligand.

The catalytic cycle of catalase can be divided into two stages (reactions 1, 2), in the first stage of the catalase cycle, hydrogen peroxide binds directly to the heme iron(III). The hydroperoxide substrate forms a hydrogen bond with a conserved distal histidine stretching the O-H bond. This allows the second oxygen of peroxide to form a hydrogen bond with the imidazole residue. Subsequently the proton of the iron bound oxygen is transferred via the imidazole to the second oxygen forming a water molecule (*129*). Heterolytic cleavage of the O-O bond releases one water molecule and forms an oxidizing oxene intermediate. The oxene intermediate transforms the heme protein ferric iron to a new oxoferryl intermediate [Fe(IV)=O] and the porphyrin to the corresponding π-cation radical ($Por^{\cdot+}$) (reaction 1). Such an intermediate is known in literature as Compound I. A nearby amino acid such as a tyrosine or

tryptophan can quench the radical and generate an [$aa^{\cdot+}$ Fe(IV)-OH-Por] termed Compound ES. Both of these intermediates are two oxidizing equivalents above the resting state of the enzyme.

The second stage of the catalase cycle, the Compound I intermediate reacts with another equivalent of H_2O_2 to generate water and molecular oxygen (reaction 2). The second H_2O_2 will bind to Compound I where it can form several hydrogen bonding interactions with the distal histidine, an asparagines and the Fe(IV)=O oxygen (*139*). This series of interactions allow one hydrogen from H_2O_2 to be transferred to the imidazole and the second to the Fe(IV)=O. This results in formation of molecular oxygen, the imidazole ring can then transfer a proton to the Fe(IV)=O thus producing a second molecule of water and return the heme to the native ferric form (*140*).

$$\text{Por-Fe(III)} + H_2O_2 \rightarrow \text{Por}^{\cdot+}\text{-Fe(IV)=O} + H_2O_2 \qquad (4)$$

$$\text{Por}^{\cdot+}\text{-Fe(IV)=O} + H_2O_2 \rightarrow \text{Por-Fe(III)} + H_2O + O_2 \qquad (5)$$

1.9 *Protein-based radicals*

Organic radical species used by enzymes have one unpaired electron ($S = 1/2$); since these species are paramagnetic they are very good candidates for electron paramagnetic resonance (EPR) spectroscopy. Enzymes can use these radicals to perform a wide array of chemistry such as activation of C-H bonds for oxygen insertion, oxidation of water, or the reduction of ribonucleotide. Therefore, EPR has proven to be valuable to understanding the chemistry that occurs in these enzymes and the properties of their reactive intermediates. Radicals produced during enzyme catalysis are often centered on the amino acids tyrosine, tryptophan, glycine, or cysteine. Abstraction of a hydrogen atom from any of these amino acids results in the formation of a relatively stable radical species, with the mechanism of abstraction differing for different enzymes. Among the four amino acid radicals the glycyl radicals are unique in that their radicals

are centered on the peptide main chain. These radicals are unstable and are mainly found in enzymes that carry out their process under anaerobic conditions (*141*). X-band EPR studies have shown their spectra to be a doublet (*40*) containing isotropic hyperfine coupling interactions with the α-hydrogen (*142*). Thiyl radicals are postulated intermediates in many enzymatic reactions. These species have a large spin-orbit coupling constant of sulfur, and display an enhanced spin-lattice relaxation that is too fast for detection in solution. Additionally, at higher temperatures thiyl radicals exhibit larger line widths making them no longer detectable; at temperatures lower than 80K they are easily detectible by EPR (*141*).

Tryptophanyl radicals are involved in many enzymatic processes. They possess an X-band EPR signal that is nearly indistinguishable from their tyrosyl counterparts. However high-field EPR (HFEPR) techniques have been used to provide increased resolution when trying to differentiate between tyrosine and tryptophan radicals (*143*). This is because tryptophan radicals have relatively smaller *g*-anisotropy compared to that of tyrosyl radicals. Tryptophan radicals can be either protonated cation or a neutral deprotonated radical (*144*). These different states can have an effect on the localization of the spin density on the aromatic ring. Using the Hückel-McLachlan technique, studies using molecular orbital (MO) calculations have been able to predict the spin density distribution for both tryptophan radicals (Table 3). Their results suggested that the cationic radical was mainly localized on the C2 and C3 positions, while the neutral radical was localized at the C3 and N1 positions (*145*). These calculations have agreed well with experimentally determined values in the case of CcP which contains a cationic tryptophan radical coupled to an oxoferryl intermediate in Compound ES.

Table 3. Spin distribution of select tryptophan radicals

Position	Tryptophan (Neutral) (*145*)	Tryptophan (Cationic) (*145*)	Compound ES (CcP) (Trp cationic radical) (*144*)	RNR (Trp neutral radical) (*146*)
N1	0.30	0.04	0.14	0.2
C2	0.04	0.42	0.35	N/A
C3	0.39	0.39	0.41	0.52
C5	0.09	0.10	N/A	0.17
C6	0.03	-0.04	-0.07	N/A
C7	0.06	0.09	N/A	0.15
C8	0.08	-0.01	N/A	N/A

*N/A. Spin density on these position represent very little of the total spin distribution and is therefore disregarded

Tyrosyl radicals have been detected in numerous enzyme systems. Their principal *g*-tensors can be fully resolved using high-field EPR (HFEPR) techniques. Their spectrum can be characterized by hyperfine coupling to one of the aliphatic β proton (resolved); hyperfine coupling to the other β protons and the aromatic protons can also be seen using ENDOR (typically unresolved). Chemical properties of the tyrosyl radical can be modulated in various enzymes by specific interactions such as hydrogen bonding within the protein (*147*). Additionally as the radical spin is distributed around the aromatic ring, there can be hyperfine couplings between the radical and a nearby proton. These couplings can provide useful information on the spin density. In tyrosine, the radicals can couple with either the *β*-protons or the *α*-protons. Coupling of a tyrosine radical with the *β*-protons causes the EPR radical spectra to form a doublet. This is the case in both tyrosyl (Y_D•, Y_Z•) radicals in PSII, studies on performed on ^{2}H-*β*-tryptophan will remove the doublet splitting that result from hyperfine coupling to the $–CH_2$- protons (*148*). The dihedral angles formed by the two *β*-methylene protons can be determined from the strength of their hyperfine coupling. These couplings can be determined by the extent of interactions between the proton nuclei and the π-electron system on the ring which depend on the spin density on carbon 1 and the dihedral angle formed (*107*). Studies on tyrosine radicals and models show that their spin-density distribution is almost invariant (*149*). A comparison of the spin densities of several tyrosyl radicals presented in Table 4 show this to be the case. Although the environment of different tyrosyl radicals can vary significantly between different enzymes, they can be subdivided into two major groups (*107*). The

first group has a characteristic wide-doublet EPR spectrum and peak-to-trough width of ~33 G; examples include RNR, and GOX. The second group contains a narrower line shape and peak-to-trough width of ~ 24 G; these include PSII, *Salmonella typhimurium* RNR. PGHS is a unique enzyme and contains both types of tyrosyl-radical species (*107*).

Table 4. Spin density distribution of select tyrosine radicals

Position	Tyrosyl model (Solution) (*4*)	RNR (Tyr122) (*4*)	PSII Y_D• (*150*)	PSII Y_Z• (*47*)
O	0.26	0.29	0.26	0.26
C1	0.34	0.38	0.37	0.37
C2	-0.07	-0.08	-0.07	-0.07
C3	0.24	0.25	0.24	0.26
C4	-0.02	-0.05	-0.01	-0.01
C5	0.24	0.25	0.24	0.26
C6	-0.07	-0.08	-0.07	-0.07
$C_{methylene}$	N/A	0.03	N/A	N/A

*N/A. Spin density on these position represent very little of the total spin distribution and is therefore disregarded

1.10 Exchange coupling of radicals and metals

Many metalloproteins that catalyze radical reactions generate a radical that is often localized on the porphyrin for hemoproteins or a nearby amino acid residue. A distance between the radical and metal center of 10 Å or less allows exchange interactions between the radical and other paramagnetic centers (*141*). At distances less than 5 Å these exchange couplings are anisotropic, at larger distances the couplings become isotropic. Interactions as long as 10.6 Å have been observed, as in the case between a flavine mononucleotide radical and an $[4Fe\text{-}4S]^+$ in trimethylamine dehydrogenase (*141*). These interactions can be characterized by EPR by the sign of the parameter J (exchange parameter), and the magnitude of the ratio between the exchange interaction and zero-field splitting parameter (D), $|J|/D$. The spin coupling between two paramagnetic species can be either ferromagnetic ($J < 0$) or antiferromagnetic

($J > 0$). Using EPR characterization of numerous intermediates can reveal the degree to which the metal center can interact with the radical.

Catalase I is a protein-bound system that exhibits ferromagnetic exchange ($J < 0$), with an intermediate strength of $|J|/D = 0.4$ (*75*). APX also has a moderate ferromagnetic exchange ($J < 0$) with $|J|/D = 0.29$ (*76*). Lignin peroxidase I (LiP I) is the third protein with a ferromagnetic exchange coupling of intermediate strength ($|J|/D = 0.29$) (*151*). HRP I has a very weak exchange (*(*$|J|/D < 0.10$) (*152*); simulation of the EPR signal requires that *J/D* be assigned both positive (antiferromagnetic) and negative (ferromagnetic) values (*152*). CPO I exhibits a large antiferromagnetic exchange ($J > 0$), with $|J|/D = 1.02$ (*153*). Finally, the model complexes in the form $[(P)\text{-}Fe{=}O]^{+}$, demonstrate an example of strong ferromagnetic exchange ($J< 0$) and $|J|/D \sim 1$ (*151*). The parameter *D* is positive and varies only over a small range between $D = 22\text{-}35$ cm^{-1}. Thus, changes in $|J|/D$ within this group of Compounds I primarily result from changes in the exchange coupling, *J*. The parameter *J/D* goes from large and negative (ferromagnetic), to near-zero, and then to moderately positive (anitferromagnetic) in the series [(P)Fe=O]+, Cat I, APX I ~ LiP I, HRP I, and CPO I (Table 5), thus showing it to be highly variable.

Variations from ferromagnetic to antiferromagnetic coupling are due to the disruption of the four fold geometry of porphyrin coordination to iron. The two odd electrons in an oxoferryl, $[Fe{=}O]^{2+}$, $S = 1$, moiety reside one each in the two antibonding Fe=O molecular orbitals that have π-symmetry respect to the diatomic axis. In a four-fold symmetric metalloporphyrin, the half-filled orbitals of the $[Fe{=}O]^{2+}$ center, and the π-molecular orbitals of the porphyrin radical are orthogonal in symmetry. In this situation, correlation effects force the spins of the two magnetic subsystems to align parallel with one another, the result is a ferromagnetic exchange, $J_F < 0$. If symmetry is reduced enough that the magnetic orbitals of the metal and the porphyrin are no longer orthogonal, the spins will be subjected to an additional bonding interaction aligning the subsystem spins antiparallel and result in an antiferromagnetic contribution to the

exchange, $J_{AF} > 0$. The observed exchange coupling, *J*, therefore, is a result of the competition between the two opposing configurations. It can be assumed that the major element in this reduction of symmetry for the proteins is π-bonding between the Fe(IV) and the proximal endogenous axial ligand. In CPO I, the axial ligand is a strongly π-bonding cysteinyl thiolate, the symmetry is lowered and the orbital overlap is increased so that antiferromagnetic coupling dominates (*153*). In catalase Compound I, the axial ligand is a phenolate and has a small antiferromagnetic coupling (*154*). HRP I with an imidazole ligand has balanced ferro- and antiferro-magnetic coupling, and the result is $J \sim 0$ (*152*). APX I and LiP I, both also ligated with an imidazolate have small antiferromagnetic coupling and exhibit ferromagnetic exchange between the oxoferryl and porphyrin π-cation radical (*76, 155*). This suggests that the kind of proximal axial ligand and its π-bonding characteristics, possibly influenced by the microenvironment, are important in determining the exchange coupling, *J*.

Table 5. Exchange coupling between radicals and metal center.

Enzyme	*J*	|*J*|/D	Coupling	Ref
[(P)Fe=O]+	< 0	~ 1.0	ferro	(*151*)
LiP I	< 0	0.29	Ferro	(*151*)
CPO I	> 0	1.02	Anti	(*153*)
Catalase I	< 0	0.4	Ferro	(*75*)
APX I	< 0	0.28	Ferro	(*76*)
HRP I	~ 0	< 0.10	Balanced	(*152*)

CHAPTER 2

MATERIALS AND METHODS

Chemicals

L-Trp (99.5%) was purchased from Sigma-Aldrich. $H_2{}^{16}O_2$ (30%, v/v) was obtained from Fisher Scientific. The concentration of H_2O_2 was calculated based on the extinction coefficient of $\varepsilon_{240\ nm} = 43.6\ M^{-1}cm^{-1}$. $H_2{}^{18}O_2$ (2% v/v solution) and $H_2{}^{18}O$ were purchased from Icon Isotopes, New Jersey, at 90.0% and 97.6% isotope enrichment, respectively. All experiments were performed in 50 mM Tris-HCl pH 7.4 buffer unless otherwise specified. ^{57}Fe (95% enrichment) was obtained from Science Engineering & Education Co (Edina, MN).

Overexpression and Purification of TDO

TDO construction of the plasmid encoding full-length *Cupriavidus metallidurans* TDO (*Cm*TDO) has been described elsewhere (*156*). The protein was purified by using a 100 mL HiLoad nickel-affinity column and a Superdex 200 size-exclusion column on an ÅKTA FPLC system as described in an earlier spectroscopic study of the enzyme (*157*). The optical absorption spectrum of the as-isolated TDO used in this work displays a 405/280 nm ($\varepsilon_{Soret} = 130\ mM^1\ cm^{-1}$, $\varepsilon_{280} = 242\ mM^{-1}\ cm^{-1}$) ratio of approximately 1.4 – 1.5:1, corresponding to 60 – 65% heme occupancy based on the determination of protein concentration and iron content using inductively coupled plasma optical emission spectroscopy and EPR spin quantitation technique. The purified enzyme demonstrated a specific activity of 25 μmol/min/mg. The ferrous enzyme used as control samples in the UV-Vis and Mössbauer experiments were obtained by dithionite reduction of ferric enzyme under anaerobic conditions.

Catalase-like activity assay

Oxygen production was measured in a sealed reaction chamber (3 ml) with an integrated oxygen

electrode unit (Oxygraph System, Hansatech Instruments, UK) at 25°C. The oxygraph experiments were initiated in aerated buffer in the absence and presence of L-Trp. The production of oxygen was monitored as a function of time. The kinetic data were fitted to the following equation:

$$v/[E] = k_{cat}[S]^n/(K_m^n + [S]^n) \quad (6)$$

where v is the steady state velocity; [E] is the concentration of TDO; [S] is the concentration of H_2O_2; k_{cat} is the apparent catalytic turnover constant; K_m is the Michaelis-Menten constant and n is the Hill coefficient or cooperativity index. TDO is known to exhibit a homotropic cooperativity during L-Trp binding (*158*).

UV-Vis Spectroscopy

All TDO samples were prepared in 50 mM Tris-HCl pH 7.4. The absorption spectra were obtained by using an Agilent 8453 UV-Vis spectrophotometer at room temperature. The enzyme reactivation by peroxide was performed under anaerobic conditions using a homemade long-arm sealed cuvette (1 ml). All the reagents had been degassed and purged with argon prior to the experiments. L-Trp stock solution was prepared in the reaction buffer in a warm bath (80 ˚C). Both L-Trp and H_2O_2 were freshly prepared in 50 mM Tris-HCl pH 7.4 buffer that had been previously degassed and purged with argon. Unless otherwise stated, the final concentration of TDO in the reaction system was 5 μM. The enzyme was made anaerobic in a vial containing concentrated ferric TDO by repeated evacuation and refilling with argon. A gas-tight microsyringe was used for additions of various amounts of argon-saturated oxygen-free H_2O_2 to the enzyme-substrate complex. NFK concentration was determined by the known extinction coefficient at 321 nm ($\varepsilon_{321\ nm}$ = 3,150 $M^{-1}cm^{-1}$) (*159*). The apparent rates of the dioxygenation reaction were determined from the initial velocity of the NFK formation. The aerobic reaction of H_2O_2 with TDO in presence of L-Trp was performed similarly with exclusion of the steps associated with the oxygen removal.

To test whether the ferric form of TDO can react with H_2O_2 and directly produce NFK through an unknown shunt pathway, we performed the enzyme reactivation in the presence of carbon monoxide (CO). In these experiments, CO was introduced to the reaction system either prior to the reaction or in the middle of the reaction (for comparison) by direct bubbling of CO gas into the reaction solution containing TDO, H_2O_2, and L-Trp.

Mass spectrometry (MS)

All reagents were prepared using anaerobic 50 mM Tris-HCl pH 7.4 buffer which was bubbled and purged with argon prior to the TDO reaction with peroxide experiments. The reactions were performed on ice with stirring using septum-sealed reaction vials. Ferric TDO (100 μM) was allowed to react with H_2O_2 in the presence of L-Trp (5 mM), in which either $H_2{}^{16}O_2$ or $H_2{}^{18}O_2$ was added to a total of 4 mM concentration through a stepwise addition. After reacting for 20 minutes, TDO was removed from the reaction system using a Centriprep-10 at 3000×*g* for 10 min, and the filtrate was collected for electrospray ionization-mass spectrometry (ESI-MS) analysis.

ESI spectrometric analyses were conducted on a Waters ESI-Q-TOF micro mass spectrometer equipped with a Waters alliance 2695 HPLC system (Milford, Massachusetts) in a positive mode. Samples were analyzed through either a direct infusion or through HPLC separation on a Waters 2695 Alliance HPLC system before MS analysis. The TDO reaction samples were mixed with 50% acetonitrile in water containing 0.1% formic acid before analysis. In LC-MS analysis, the collision energy was set to 30 eV. HPLC separation was achieved on a Restek Allure C18 column (100×2 mm i.d. 3 μM). Mobile phase **A** was composed of water and 0.1% formic acid. Mobile phase **B** was composed of acetonitrile and 0.1% formic acid. The elution gradients were performed starting at 100% **A** for 5 min; then falling to 0% **A** over 10 min; staying at 0% **A** for 15 min; then rising to 100% **A** over 20 min at a constant flow rate of 200 μL/min. MassLynx 4.1 software was used for instrument control and data acquisition.

Solvent exchange of the dioxygenation product

^{16}O-NFK was prepared according to the enzyme-based procedures described above. A concentrated sample of ^{16}O-NFK was dissolved in $H_2{}^{18}O$ (75% ^{18}O) to exchange with solvent on ice for 20 min prior to the ESI-MS analysis. In a parallel experiment, a concentrated ^{16}O-NFK sample was first dissolved in $H_2{}^{18}O$ (75% ^{18}O) for 20 min then concentrated again by rapidly evaporating the solvent under a vacuum. Finally it was re-diluted with $H_2{}^{16}O$. The final ratio of $H_2{}^{16}O$:$H_2{}^{18}O$ was determined to be 60:1. This experiment was intended to examine if the solvent exchange would be fully reversible.

Electron Paramagnetic Resonance (EPR) spectroscopy

TDO EPR samples were made in reaction vials containing 50 mM Tris-HCl buffer, pH 7.4 with 10% glycerol, transferred to EPR tubes and quickly frozen in cold isopentane (-140 °C) or liquid nitrogen after the desired reaction time. The 12 and 30 s samples were made in EPR tubes by using a System 1000 rapid-freeze-quenching apparatus (Update Instruments Inc) with a cold isopentane bath (-140 °C). Typically ten EPR samples with 0.15 – 0.50 mM TDO were made in each set of experiments with 1 – 6 equivalents of peroxide in different experiments. Multiple sets of the EPR experiments were conducted to optimize the enzyme/peroxide ratio for production of reactive intermediates while minimizing loss of the heme cofactor. X-band EPR first derivative spectra were recorded in perpendicular mode on a Bruker EMX spectrometer at 100-kHz modulation frequency using a 4119HS resonator. The EPR measurement temperature was maintained with an ESR910 liquid helium cryostat and an ITC503 temperature controller. A calibrated frequency meter was used to aid the *g*-value determination. Spin concentration was determined by double integration of the EPR signals obtained under low microwave power conditions and comparing to that of a copper standard (0.5 mM $CuSO_4$, 5 mM EDTA) obtained under identical conditions.

The relaxation properties of the free radical at different temperatures were analyzed from EPR spectra obtained by varying microwave powers in the range 0.0002 – 200 mW. The values of half-saturation parameter ($P_{1/2}$) were obtained by fitting the data according to Eq. 7:

$$I \propto 1/(1 + P/P_{1/2})^{b/2} \qquad (7)$$

where I is the EPR signal amplitude, b is the inhomogeneous factor, and P is microwave power.

Mössbauer spectroscopy

The ^{57}Fe-enriched protein was obtained by expressing TDO in *Escherichia coli* using ^{57}Fe-enriched culture medium as previously described (24). The Mössbauer samples were prepared from the as-isolated ^{57}Fe(III)-TDO and frozen in liquid nitrogen. In the Fe(II) formation Mössbauer experiments, a final concentration of 1.0 mM (heme concentration) ^{57}Fe-TDO was used. To generate the high-valent Fe intermediate, 1.6 mM (heme concentration) ^{57}Fe-TDO was used to react with six equivalents of H_2O_2 (9.6 mM) and frozen in liquid nitrogen at 20 s or 50 s after reaction. Mössbauer spectra were recorded on a constant acceleration instrument with an available temperature range of 1.5 to 200 K. Isomer shifts are reported relative to Fe metal at 298 K. Least-square fitting of the spectra was performed with the WMOSS software package (WEB Research, Edina, MN). The low-temperature Mössbauer spectra of resting TDO were fit with the standard spin Hamiltonian (Eq. 8):

$$H = g\beta B\cdot S + D[S_z^2 - S(S + 1)/3] + E(S_x^2 - S_y^2) + A_{iso}(S\cdot I) - g_n b_n B\cdot I + (eQV_{zz}/12)\,[3I_z^2 - I(I + 1) + \eta(I_x^2 - I_y^2)] \qquad (8)$$

Computational Modeling

The hybrid functional B3LYP (*160*) with a Wachter's basis (62111111/3311111/3111) for Fe (*161*), 6-311G* for all the other heavy atoms, and 6-31G* for hydrogens was used to predict the values of Mössbauer quadrupole splitting and isomer shift, the same approach used in the previous work for various iron-containing proteins and models (see supporting information for more details) (*162, 163*). In all the investigated models, the heme group is represented by a porphyrin with original β substituent replaced by methyl groups and the axial histidine group is truncated to be 5-methylimidazole. Geometries of all the structural models investigated in this work were optimized with the terminal atoms fixed at the X-ray crystal structure (2nw7.pdb, ref. 12) positions to mimic the protein environment effect, using the density functional theory (DFT) method BPW91 with the above basis set (*164, 165*), which is the same approach used previously to investigate other oxyferryl species (*162, 163*)

CHAPTER 3

ENZYME REACTIVATION BY HYDROGEN PEROXIDE IN HEME-BASED TRYPTOPHAN DIOXYGENASE

3.1 *Introduction*

The work presented here was done in collaboration with Dr. Rong Fu (catalase activity, EPR), Dr. Michael P. Hendrich and Dr. Rupal Gupta (Mössbauer), Jiafeng Geng (CO activity assay), Dr. Siming Wang (MS), and Dr. Yong Zhang (Computational studies).

Hemoproteins perform a wide range of biological functions, including oxygen transport, storage, electron transfer, mono- oxygenation, and reduction of dioxygen. However, they rarely express dioxygenase activity as their native biological function. Tryptophan 2, 3-dioxygenase (TDO) is the first described exception (*166-168*). This enzyme employs a *b*-type ferrous heme prosthetic group to catalyze the oxidative cleavage of the indole ring of L-Trp, converting it to *N*-formylkynurenine (NFK) (Scheme 1). This is the first and rate-limiting step of the kynurenine pathway of L-Trp metabolism, which oxidizes over 99% of L-Trp in mammalian intracellular and extracellular pools (*167*, *169-171*). The kynurenine pathway constitutes the major steps in biosynthesis of NAD, an essential redox cofactor in all living systems (*170*).

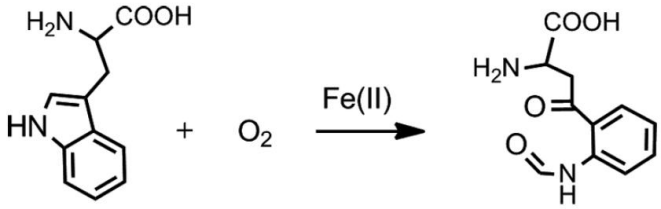

Scheme 1. The chemical reactions catalyzed by TDO

TDO is a hepatic enzyme first discovered in rat liver extracts in 1936 (*166*). An analogous enzyme, indoleamine 2,3-dioxygenase (IDO), was isolated 31 years later from tissues other than the liver (*172*). Although both enzymes catalyze the same reaction, TDO is highly substrate-specific with L-Trp, whereas IDO presents a more relaxed specificity. TDO is a homotetramer with a total mass of ~ 134 kDa, whereas IDO is a monomeric protein. The two enzymes share only 14% sequence identity but conserve similar active site architectures (*156, 173, 174*). In addition to humans, TDO has also been found in other mammals, such as rats and mice, as well as in mosquitoes and bacteria (*167, 170, 175-179*). Recently, a potential heme-dependent dioxygenase enzyme superfamily has been proposed (*180*). Moreover, several other heme-based proteins, such as myoglobin and hemoglobin, express dioxygenase activities from their mutant proteins under certain circumstances (*181, 182*). In general, TDO has been considered as a prototypical member and model system for studying the chemistry of heme-based dioxygenases.

The ferrous heme in TDO is the catalytic center that binds and activates molecular oxygen. Like many other Fe(II)-dependent enzymes, TDO becomes auto-oxidized when its primary substrate is absent. In previous studies, hydrogen peroxide (H_2O_2) was implicated as an activator by the finding that the resting ferric TDO becomes active toward L-Trp after treatment with H_2O_2 (*183*). This was later confirmed by independent optical spectroscopic studies from various laboratories (*175, 178, 184*) and by the observations that the overall enzyme reactivation was inhibited by catalase and that the addition of peroxide relieved the reactivation inhibition (*175*). However, the mechanism by which ferric TDO is reduced to its ferrous form by reacting with H_2O_2 remains elusive after over 60 years.

Here, we provide unequivocal evidence in support of the formation of the ferrous form of the enzyme by reaction of ferric TDO with peroxide and L-Trp. A previously unknown two-phase enzyme reactivation mechanism is proposed based on the chemical identification of nearly all of the intermediates and products. In the first phase, the enzyme is oxidized by peroxide to generate a compound *E*S-type ferryl

intermediate. In the second phase, the ferryl and the protein-based free radical intermediates are each reduced by L-Trp. We further hypothesize that the physiological significance of the peroxide reactivity is to allow for the reactivation of the enzyme in an oxidizing environment.

3.2 *Reaction of oxidized TDO and H_2O_2 in the absence of L-Trp*.

The reaction of ferric TDO with H_2O_2 was examined with an oxygen electrode in a stirred cell at 25°C. Figure 1A shows that the addition of 50 equiv of H_2O_2 to the oxidized protein resulted in an immediate increase in the oxygen concentration of the reaction chamber. Another addition of H_2O_2 in the same amount led to a similar increase in the oxygen concentration, indicating that O_2 generation is reproducible (Fig. 1A). When ferric TDO was added to the buffer containing H_2O_2, similar O_2 production was observed (Fig. 1B), indicating no dependence on the order of additions. In contrast, addition of either the protein or peroxide alone, as shown in Figure 1, did not produce O_2. These results demonstrate that O_2 is produced from H_2O_2, and lead to the conclusion that Fe(III)-TDO possesses a catalase-like activity with H_2O_2 in the absence of L-Trp. The k_{cat}, K_m, and k_{cat}/K_m values of the TDO catalase-like activity determined from steady state analysis according to equation 1 are 13 ± 2 s^{-1}, 16 ± 3 mM, 850 ± 65 $M^{-1}s^{-1}$, respectively (Fig. 2). The kinetic data show no cooperative behavior (n = 1) during O_2 production from H_2O_2.

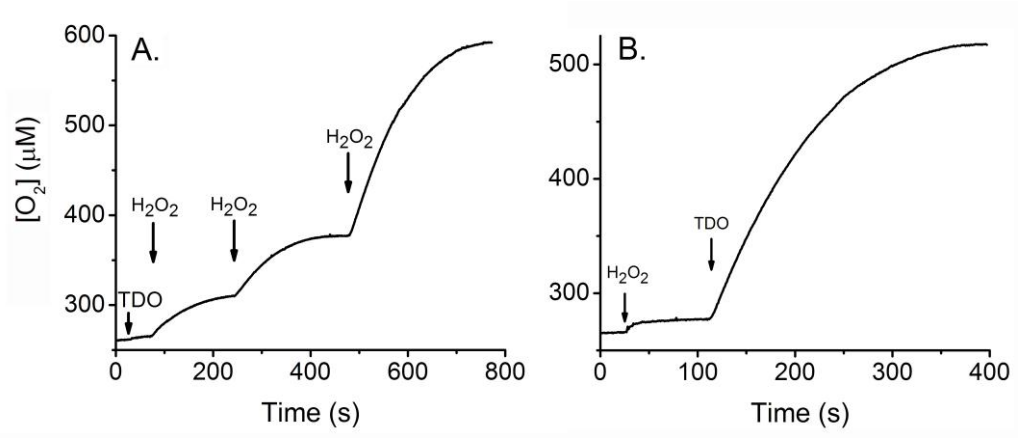

Figure 1. A, H_2O_2 decomposition and O_2 production mediated by Fe(III)-TDO in a stirred O_2-electrode cell in response to discrete additions of H_2O_2. B, reaction initiated by TDO. Arrows indicate the time points in which ferric TDO (5 μM) and H_2O_2 (250 μM or 1 mM in A, and 1 mM in B) were added to the reaction cell.

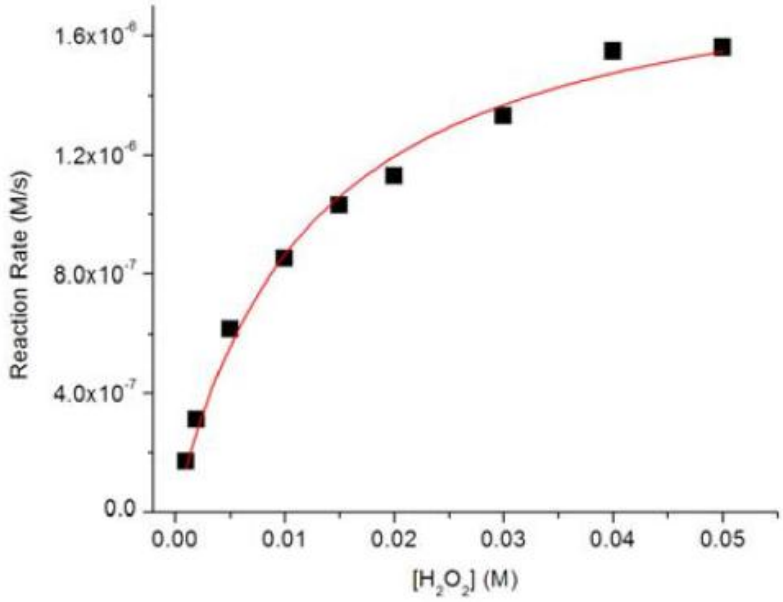

Figure 2. Saturation curve showing the relation between the concentration of H2O2 and rate of the catalase-like activity of ferric TDO. Three repeating experiments were carried out and similar results were observed.

At 4.2 K, the as-isolated ^{57}Fe-TDO shows a six-line magnetic pattern in Mössbauer spectrum (Fig. 3). The simulation overlaid on the experimental data (solid line) is calculated for an S = 5/2 iron site with δ = 0.42 mm/s, ΔE_Q = 1.53 mm/s, D = 13 cm^{-1}, E/D = 0.01, and A_{iso} = 195 kG (Fig. 3B). These values are indicative of a high-spin ferric heme (*157*). Another sample of this protein solution was treated with six equiv of H_2O_2 (20 s reaction plus 10 s frozen time) prior to the spectroscopic characterization (Fig. 3A). The Mössbauer spectrum of this sample is composed of four species. One species is recognized as the high-spin ferric TDO which accounts for 25% of the iron in the sample. Fig. 3C shows the difference spectrum of A - 0.25B. This difference spectrum is composed of three overlapping doublets as indicated on the figure. The fit to the three doublets (solid lines) gives Fe parameters and relative amounts of: (1) δ = 0.055 mm/s, ΔE_Q = 1.755 mm/s, 33%, (2) δ = 0.350 mm/s, ΔE_Q = 0.703 mm/s, 17% (3) δ = 0.585 mm/s, ΔE_Q = 1.5 mm/s, 25%. Species 1 is assigned to an S = 1 Fe(IV) heme, tentatively in the Fe(IV)=O form. The parameter ranges of known S = 1 Fe(IV)-oxo heme species are δ = 0 - 0.1 and ΔE_Q = 1.0 - 2.0 mm/s. The other two species appear to be degradation products of the reaction with peroxide. Species 2 has parameters in the range of high-spin ferric hemes, but the diamagnetic doublet indicates that the hemes are forming μ-oxo bridges (*185*). Species 3 is typical of nondescript Fe(III) formation (*186*), presumably due to loss of iron ion from heme. The same difference spectrum is unchanged in character when recorded at 100 K. Thus, the addition of 6 equiv of H_2O_2, all at once, resulted in a 42% loss of the heme and/or ^{57}Fe from TDO, 25% remained unchanged, and 33% of the iron formed an iron(IV)-oxo heme species. The loss of heme is consistent with the observed tendency of the protein to lose the *b*-type heme cofactor. Similar results were observed for two repeats of the ^{57}Fe-enriched TDO with H_2O_2 and observation with Mössbauer spectroscopy. At longer reaction time (50 s reaction plus 10 s frozen time), species 1 was decreased from 33% to 20%.

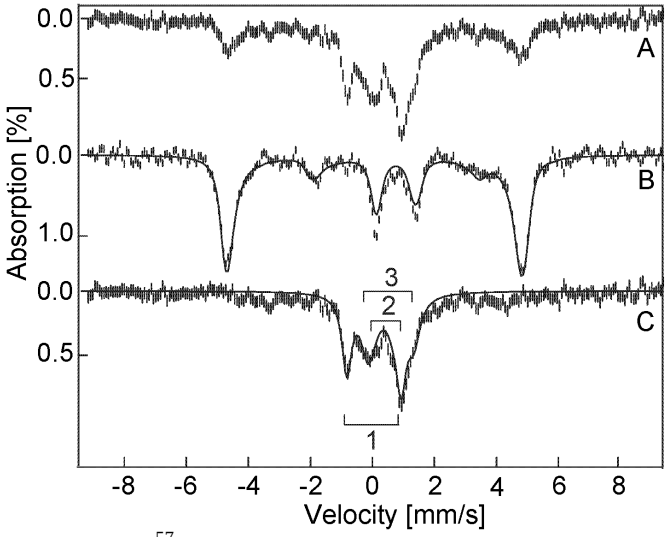

Figure 3. The Mössbauer spectra of ^{57}Fe-TDO. A, Reaction of H_2O_2 (9.6 mM) with TDO (1.6 mM); B, TDO protein in resting state prior to the reaction with H_2O_2 , and C, difference spectrum of A - 0.25B. All spectra were recorded at 4.2 K in an applied field of 45 mT parallel to the direction of the beam of γ rays. The solid lines are least-squares fits with parameters given in the text.

The reaction of TDO with H_2O_2 was also studied by EPR spectroscopy. The as-isolated ferric TDO displays a nearly axial EPR signal at g = 6 **(**Fig. 4**)** and a weak resonance at g = 2 (Fig. 5), typical of a high-spin ferric ion in a heme environment. Fig. 5 shows that this ferric EPR signal decreases in intensity upon addition of H_2O_2, concomitantly with the formation of a g = 2.0028 free radical signal. The amplitude of the EPR signal for the radical is shown on a reduced scale for comparison with the ferric heme signal. At 30 s, the radical species has a spin concentration of 18% of the initial ferric heme concentration. A plot of the concentrations of the high-spin heme and radical species as a function of time is present in Fig. 6. At 12 s, the free radical species has a spin concentration of 40% of the initial iron concentration. The sharp EPR signal of the 12 s sample at g = 2.0028, shown in Fig. 7, is omitted from Figure 5 for clarity. The EPR-active radical intermediate is present in addition to the postulated Fe(IV)-oxo species characterized by Mössbauer spectroscopy.

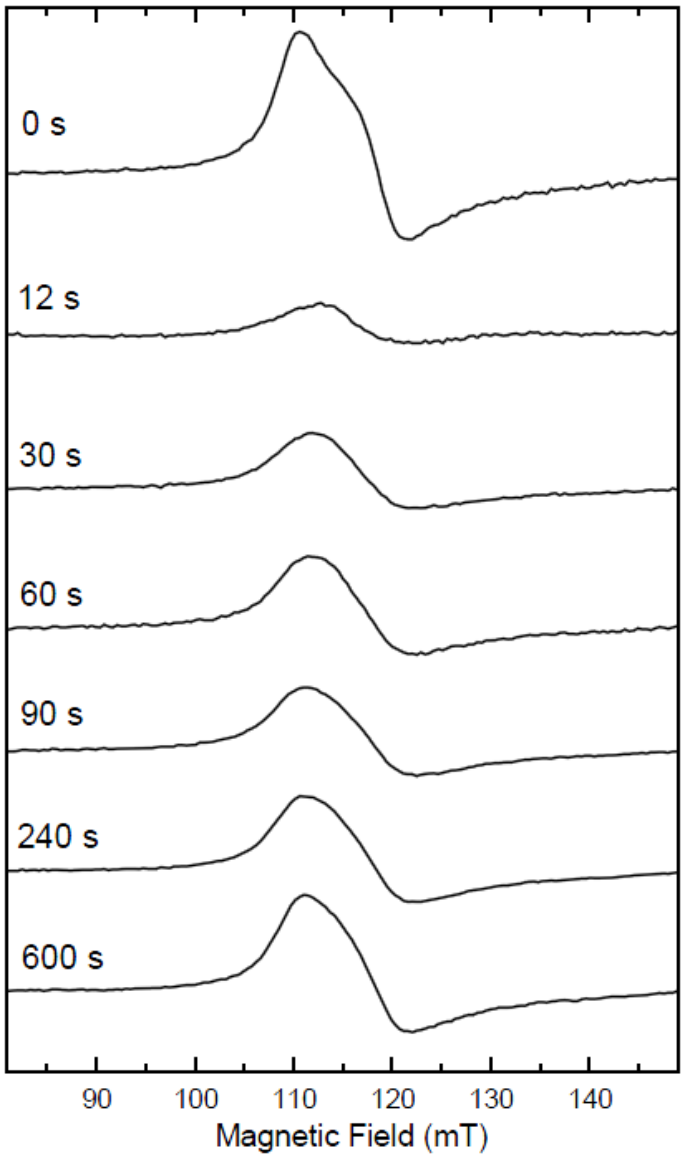

Figure 4. EPR spectra of the high-spin ferric heme (150 μM) taken during the reaction with H2O2 (900 μM). EPR parameters: recording temperature, 10 K; microwave power, 1 mW; microwave frequency, 9.44 GHz; modulation amplitude, 0.8 mT.

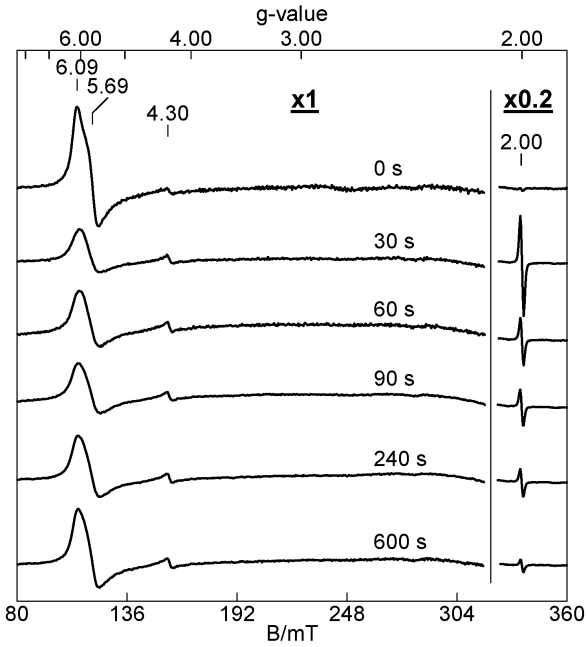

Figure 5. The change in the EPR signals of TDO during the room temperature reaction of TDO (150 µM) with H_2O_2 (900 µM). The times at which the various EPR samples were frozen after addition of H_2O_2 are listed on the figure. The g = 2 signal is 20% of the original experimental data. EPR parameters for obtaining spectra are as follows: temperature, 10 K; microwave frequency, 9.44 GHz; microwave power, 1 mW; and modulation amplitude, 0.8 mT.

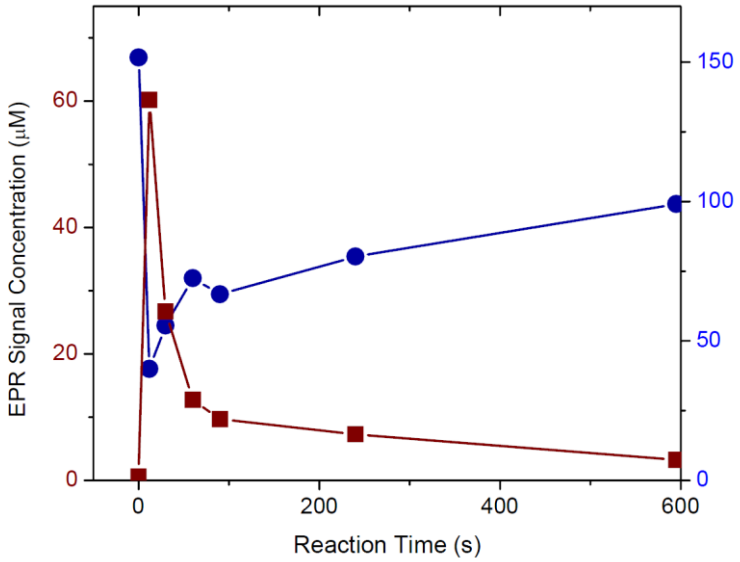

Figure 6. EPR signal intensity as a function of reaction time for the g = 2.0028 (red trace) and g = 6 (navy trace) resonances, respectively. The initial heme concentration was 150 µM.

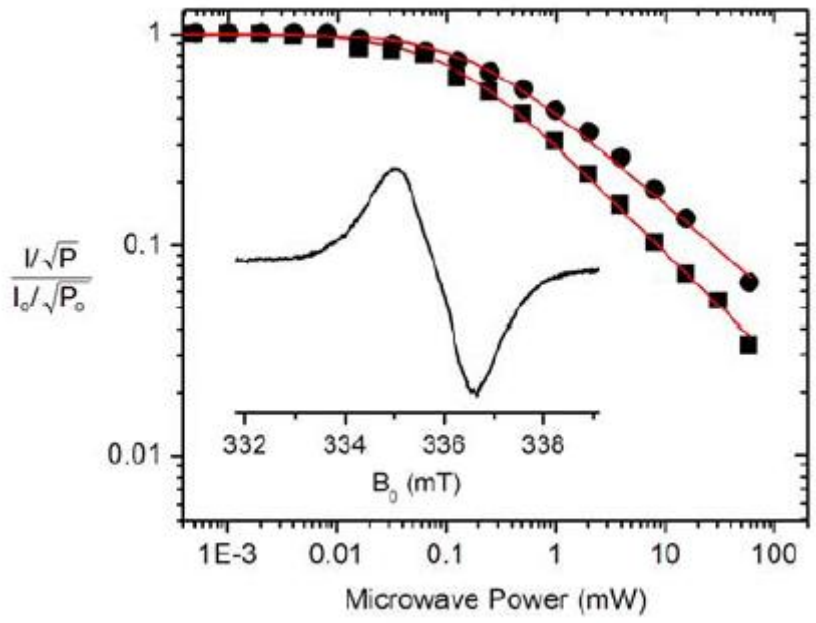

Figure 7. The g = 2.0028 free radical (inset) and its relaxation properties. The power saturation of the 10 K (square) and 100 K (circle) and the fit to Eq. 2 are shown, where I is the EPR signal amplitude and P is the microwave power.

At later reaction times, the radical species decays and the high-spin ferric EPR signal gradually increases in intensity. At 10 minutes, the concentration of the high-spin heme species is about 70% of its initial concentration due to 30% loss of the heme under these conditions. The detected loss of heme in the EPR samples is lower than the ratio obtained by Mössbauer spectroscopy, presumably due to the low concentration of H_2O_2 used in the EPR experiments. During the reaction time of Figure 5, the shape of the high-spin heme EPR signal changed subtlety to a more axial species (Fig. 4), which suggests that the electronic environment of the heme changes during the reaction with peroxide. In the 12 s sample, the ferric heme signal at g = 6 is about 25% of the initial intensity prior to the reaction with H_2O_2 (Fig. 6). This observation suggests that although there are inequivalent hemes in the enzyme they all react with H_2O_2.

The peak-to-peak line width of the radical signal is 1.72 mT (Fig. 7), which is too large for a peroxide-

based free radical (< 1 mT), but typical for a protein-derived aromatic radical (*6*, *187*). The microwave power saturation behavior of the free radical signal at g = 2.0028 was measured at 10 and 100 K, respectively (Fig. 7). The fit to the curves using Eq. 7 led to $P_{1/2}$ values of 0.11 and 1.16 mW for 10 and 100 K, respectively. These values suggest a weak interaction of the protein radical with the Fe ion. At approximately the same reaction time as the Mössbauer sample, the spin concentration of the protein radical is found to be comparable to the concentration of the Fe(IV)=O heme species. Together, these results suggest the formation of an intermediate composed of an Fe(IV)=O heme in close proximity to the free radical, similar to the so-called Compound *E*S (Cpd ES) description based on the initial characterization from cytochrome *c* peroxidase (CcP) (*72*, *188*). The Cpd ES of CcP is a semistable enzyme intermediate that contains an Fe(IV)=O heme and a Trp radical (*73*).

3.3 *Reaction of oxidized TDO and H_2O_2 with L-Trp*

The as-isolated TDO exhibits visible absorbance characteristics of a histidine ligated ferric heme protein with a Soret band at 405 nm (Fig. 8). In the presence of L-Trp, the Soret band shifts to 406 nm (Fig. 9). The intensity of this 406 nm band decreases and new features at 432 and 321 nm develop during the addition of H_2O_2 to a reaction mixture containing ferric TDO and excess (1000 equiv, 5 mM) L-Trp (Fig. 9). The 321 nm spectral feature resembles the optical data for the dioxygenation reaction of ferrous TDO using O_2 as the oxidant and the absorbance in the range of 310 - 330 nm has previously been used to measure the formation of NFK (*167*, *189*). Hence, the absorption at 321 nm is tentatively assigned to NFK production. When H_2O_2 was incubated with L-Trp in the absence of TDO, the development of the 321 nm chromophore did not occur, indicating that NFK formation is an enzymatic process. As shown below, the NFK formation is due to generation of the ferrous form of enzyme. When the peroxide reaction was carried out in the presence of hydroxyurea, a known scavenger of protein-based free radicals, the NFK production in the anaerobic reaction with peroxide was significantly inhibited (Fig. 10),

suggesting the protein radical detected by EPR spectroscopy is indeed an intermediate in enzyme reactivation. In contrast, NFK production in the normal catalytic cycle of Fe(II)-TDO and O_2 is not affected by the presence of hydroxyurea (Fig. 11). The inset (top panel) in Fig. 9C shows a slightly less than 1:2 ratio of [NFK]:[H_2O_2] stoichiometry. When the peroxide reaction was carried out under aerobic conditions, the amount of NFK formed was not associated with the concentration of peroxide because the reaction mediated by the ferrous enzyme had multiple sources of O_2 (Fig. 12).

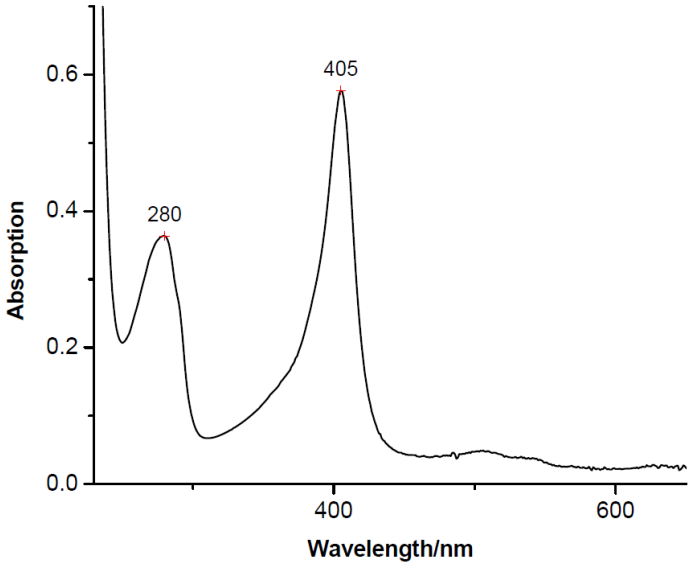

Figure 8. UV-Vis spectrum of as-isolated *Cupriavidus metallidurans* TDO (*Cm*TDO)

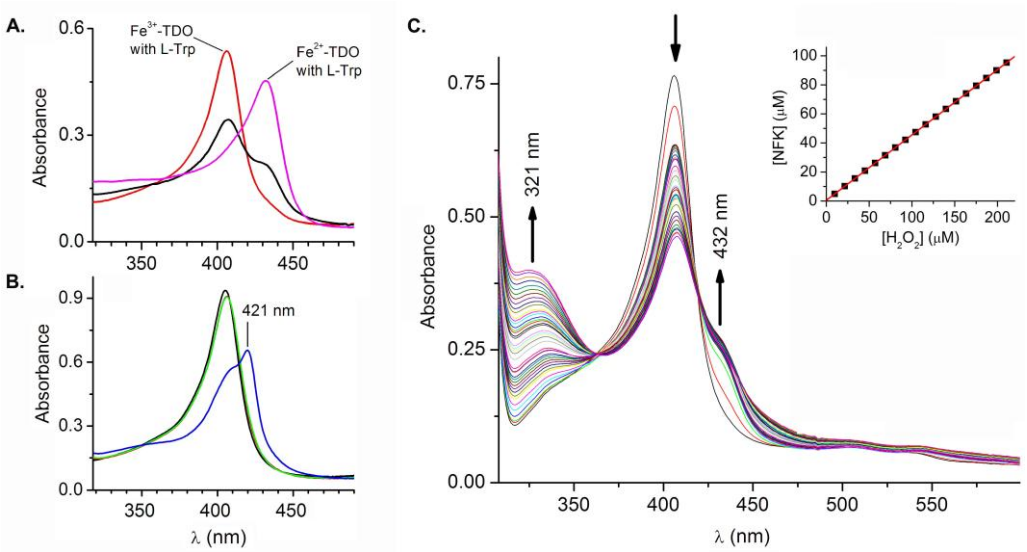

Figure 9. Optical spectra of TDO. (A) The Soret bands of ferric and ferrous *Cm*TDO (5 μM) in the presence of L-Trp (5 mM) are observed at 406 and 432 nm, respectively. The Soret band of the ferric sample splits into two parts 30 s after addition of H_2O_2 (30 μM). (B) ferric TDO (black), after sequential addition of L-Trp (red), CO (green) and H_2O_2 (blue). The red and green traces are nearly identical to each other. (C) Optical spectra of TDO and L-Trp taken from the sequential additions of equal amount of H_2O_2 (see text for experiment details). The inset is the calculated *N*-formylkynurenine (NFK) concentration as a function of the added H_2O_2 under anaerobic conditions. The concentration of H_2O_2 was determined using $\varepsilon_{240\ nm} = 43.6\ M^{-1}cm^{-1}$. NFK concentration was determined using $\varepsilon_{321\ nm} = 3150\ M^{-1}cm^{-1}$ after subtraction of the initial spectrum.

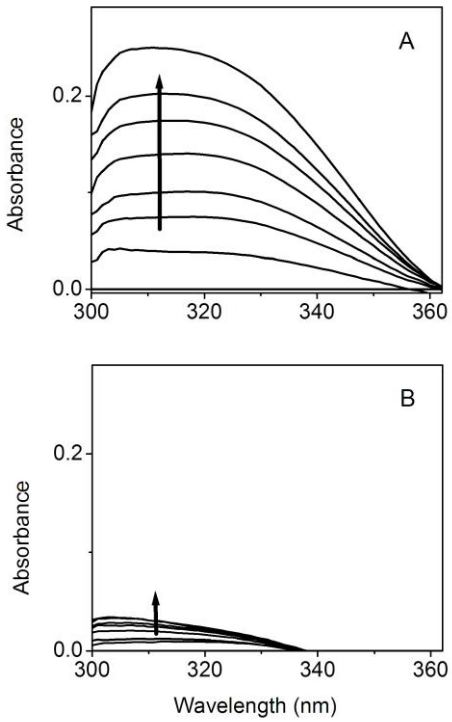

Figure 10. Formation of NFK as a result of the peroxide reaction with ferric TDO (5 μM) and L-Trp (5 mM). The spectra were taken from the anaerobic titration of 35 equiv of H_2O_2 (total 175 μM) in the absence (A) and presence (B) of hydroxyurea (10 mM). Each trace was obtained after the reaction was complete and subtracted against a spectrum of ferric TDO at the same concentration (5 μM).

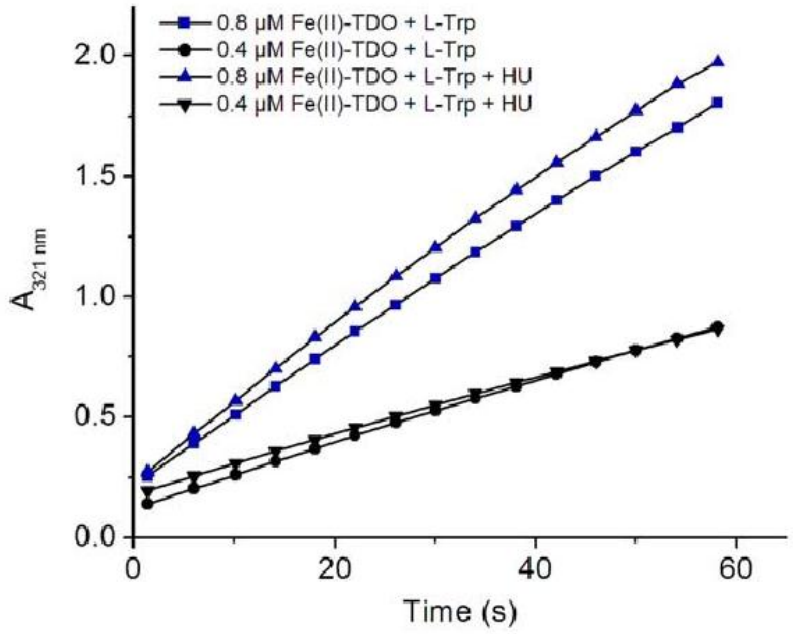

Figure 11. The effect of hydroxyurea (HU) on the enzymatic activity of ferrous TDO. Ferric

TDO was treated with 2 equivalents of sodium dithionite and purged with argon for 15 min under anaerobic conditions. The reactions were conducted in O2-saturated buffer containing 5 mM LTrp in the absence or presence of hydroxyurea (5 mM).

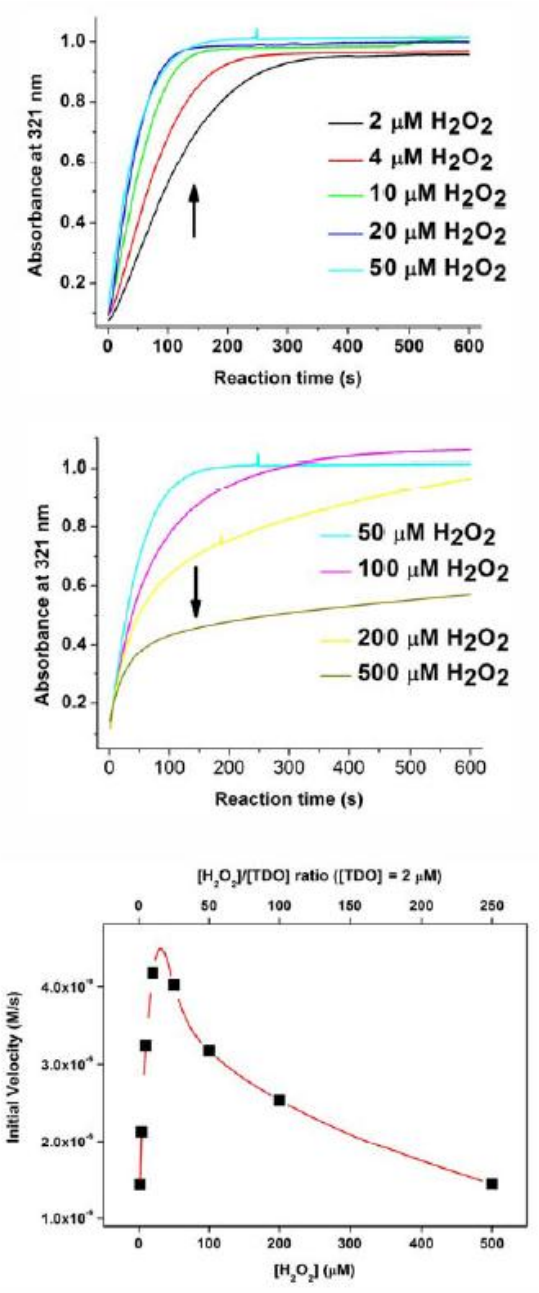

Figure 12. Optical spectra of TDO (2 μM) and L-Trp (5 mM) taken from the reaction with H2O2 (Panel A: 2 – 50 μM, Panel B: 50 – 500 μM) under aerobic conditions. Panel C shows the Initial velocity as a function peroxide concentrations. Initial velocity of each set of experiment was counted within 20 - 40 s. High concentration of peroxide can inhibit the enzyme reactivation due to the oxidation of the newly generated ferrous TDO.

The fully reduced TDO, generated by chemical reduction by dithionite, present a Soret band at 432 nm when L-Trp is bound (Fig. 9). During the course of the reaction of ferric TDO with H_2O_2 and L-Trp, the Soret band decreases while an additional spectral shoulder feature emerges at 432 nm (Fig. 9). The 432 nm chromophore matches the Soret band of ferrous TDO complex with L-Trp, suggesting the formation of the ferrous TDO from a fraction of ferric form of the enzyme. To confirm the formation of Fe(II) heme, CO was introduced to stabilize the presumed ferrous species in a separate test. In our previous study of ferrous TDO, the CO adduct exhibits a Soret band at 421 nm in the presence of L-Trp, and it is stable in the presence of O_2 (24). A similar 421 nm peak has also been reported for the ferrous-CO adduct of human TDO (*190*). When CO was bubbled into a solution containing ferric TDO and L-Trp, the addition of CO does not cause an observable shift of the Soret band. However, upon further addition of H_2O_2, a 421 nm band corresponding to the ferrous-CO adduct of TDO is generated (Fig. 9B).

The formation of active Fe(II) form of TDO from the ferric state by peroxide was further verified by Mössbauer spectroscopy. Fig. 13A shows the Mössbauer spectrum of substrate-bound ferric TDO before addition of CO and peroxide. CO gas was bubbled through an anaerobic sample of ferric TDO with L-Trp for 5 min, after which 2 equiv of H_2O_2 were added and the sample was immediately frozen in liquid nitrogen. The spectrum of the H_2O_2-treated sample is shown in Figure 13B. The difference spectrum (Fig. 13C), generated by subtracting 50% of the unreacted enzyme-substrate complex, shows a doublet indicating a diamagnetic species. The Mössbauer parameters of this species are the same as those of ferrous-CO adduct characterized in our recent work (*157*).

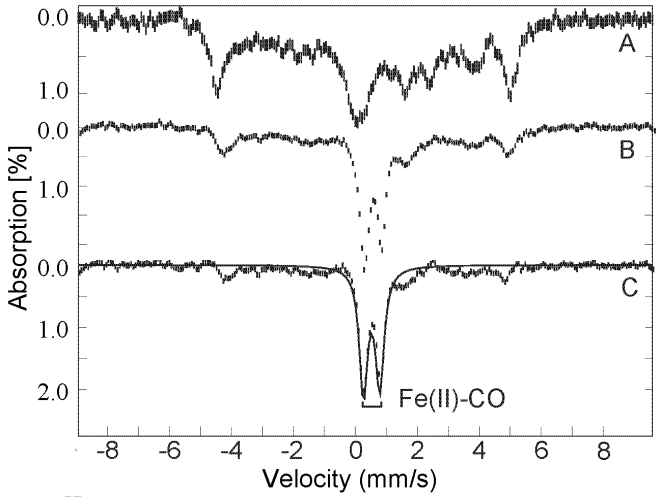

Figure 13. Mössbauer spectra of ^{57}Fe-TDO. (A) Ferric TDO (1 mM) with 50 equiv of L-Trp, (B) after treated with CO and H_2O_2 (2 mM), and (C) difference spectrum of B – 0.5A. All spectra were recorded at 4.2 K in an applied field of 45 mT parallel to the direction of the beam of γ rays. The solid line is the least-squares fits with parameters given in the text.

It is known that CO reacts with the ferrous heme of TDO and that the ferrous-CO complex is catalytically inactive (*190*). Like O_2, CO does not bind to ferric hemoproteins (*191*). With this knowledge in hand, CO was again employed as a probe to test if the ferrous heme generated by addition of H_2O_2 is catalytically active. Fig. 14 shows that the NFK production is inhibited by CO, indicating the dioxygenation product is generated by the Fe(II) heme. When the reaction was initiated by addition of ferric TDO, the initial rate of the CO-treated reaction system dropped by ca. 6.5-fold compared to that of the untreated sample under the same conditions (Fig. 14A). In a separate set of experiments, CO was introduced into the system 15 s after the reaction was initiated. An inhibition of the NFK formation was observed (Fig. 14B), demonstrating depletion of catalytically active Fe(II) enzyme by forming a stable but inactive Fe(II)-CO complex. Before CO was bubbled into the system, the formation of Fe(II) heme was visualized at 432 nm. After a small lag phase upon addition of CO, a sharp decrease of [Fe(II)] was observed (Fig. 14C). The absorbance at 421 nm was concomitantly increased due to the formation of the ferrous-CO adduct (Fig. 14B). These experiments further show that the formation of NFK is catalyzed by ferrous TDO, and an enzyme reactivation mechanism must exist during the reaction with peroxide under appropriate conditions

discussed later.

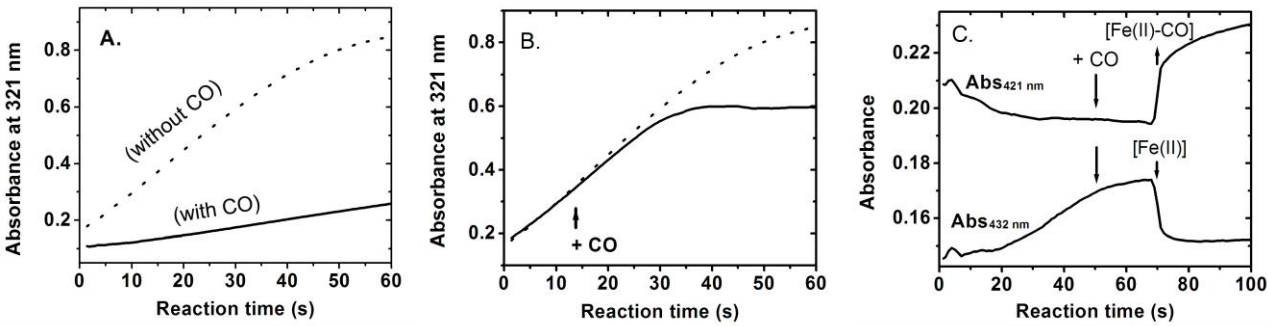

Figure 14. The effect of CO on the enzyme reactivation and formation of NFK. (A) Pre-incubation of CO into a solution of L-Trp (5 mM) and H_2O_2 (10 μM) (solid trace) compared to that in the absence of CO (dotted trace). The reaction was initiated by addition of ferric TDO (1 μM). (B) CO-bubbling 15 s after the reaction, which was initiated by addition of TDO (solid trace). The dotted trace shows a control experiment in the absence of CO. (C) Change of the Soret absorbance as a function of reaction time monitored at 421 nm (corresponding to Fe(II)-CO adduct) and 432 nm (ferrous heme in TDO), respectively. CO gas was bubbled into the solution after 50 s of the reaction. The experiments were carried out under aerobic conditions.

3.4 *Source of oxygen in NFK*

Mass spectrometric analyses of the reaction of ferric TDO and L-Trp with $H_2{}^{16}O_2$ and $H_2{}^{18}O_2$ were conducted. The enzyme was removed by filtration after 5 minutes of reaction with peroxide and prior to the mass spectrometry analysis as described in the experimental section. Fig. 15A shows that the substrate L-Trp presents an ion of mass-to-charge ratio (*m/z*) 205, corresponding to the anticipated $[M+H]^+$ form. The ion at *m/z* 243 in this control sample is tentatively assigned to the dimeric form of Tris (M_r 242). A new major ion at *m/z* 237 is present in the TDO reaction mixture with $H_2{}^{16}O_2$ as the oxidant (Fig. 15B). This new ion is absent in the control sample where TDO was omitted (Fig. 15A). The 32-dalton mass shift of the *m/z* 237 ion compared to the substrate is consistent with production of NFK in which two oxygen atoms have been incorporated into L-Trp. In addition, a peak at *m/z* 409 was observed in the

reaction and is tentatively assigned to an L-Trp dimer (Fig. 16). It was undetectable when either TDO or H_2O_2 was absent, or in the regular dioxygen reaction of ferrous TDO and O_2. The *m/z* 409 ion was invariant when ^{18}O-enriched peroxide was employed in the reaction.

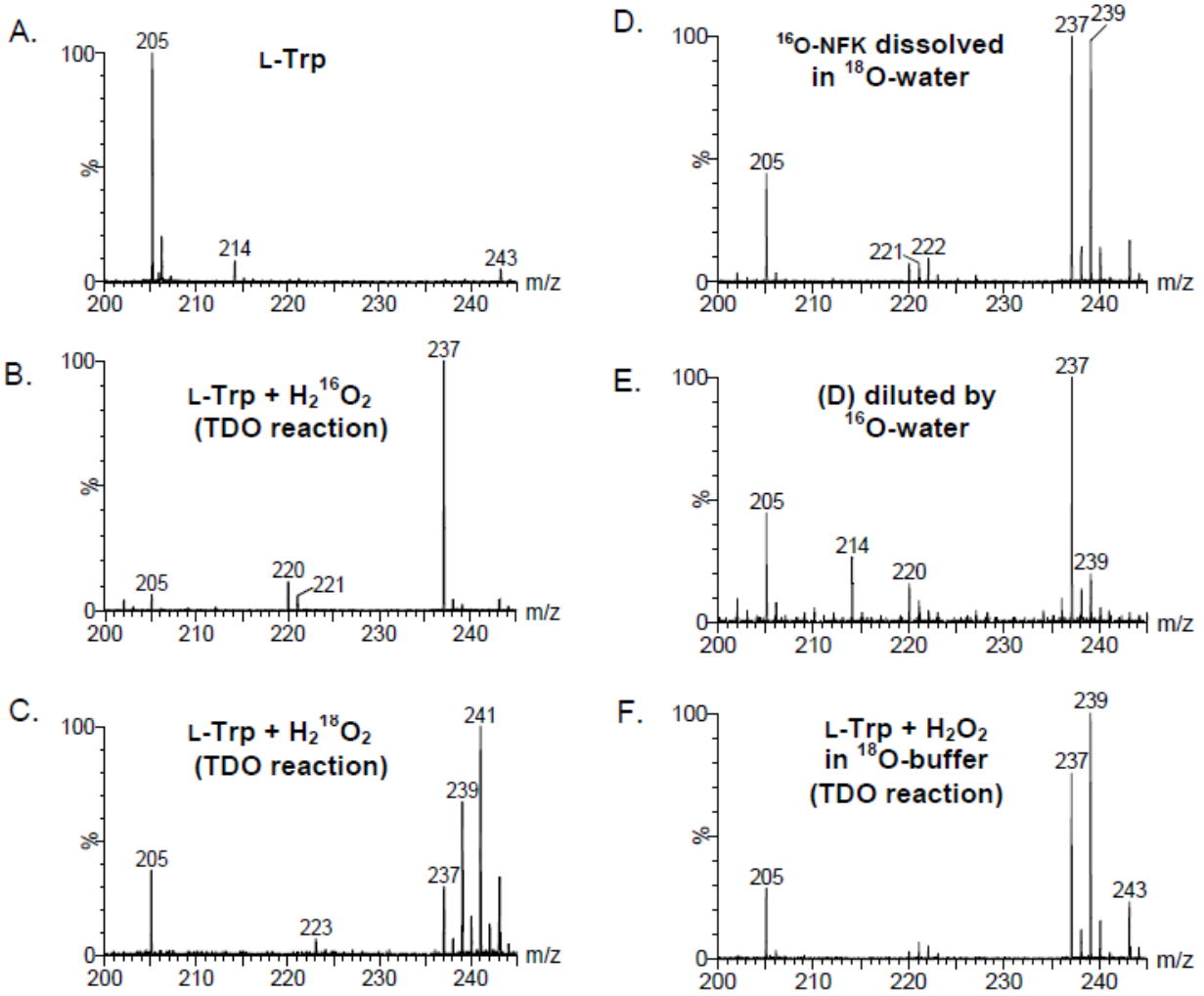

Figure 15. ESI-mass spectrometric characterization of TDO. (A) L-Trp, (B) the reaction product of L-Trp and $H_2{}^{16}O_2$ catalyzed by ferric TDO, (C) the TDO reaction using isotope-labeled $H_2{}^{18}O_2$ as the oxygen donor, (D) A ^{16}O-NFK sample, generated from the TDO reactivation process, was dissolved in an ^{18}O-enriched water (^{16}O :^{18}O ratio of 3:5) after concentrating the reaction solution and removing the enzyme by filtration, (E) A copy of sample (D) was further diluted by ^{16}O-water to reach a final ^{16}O :^{18}O ratio of 60:1 (1.6% ^{18}O), and (F) The TDO reaction carried out in $H_2{}^{18}O$-based Tris-HCl buffer.

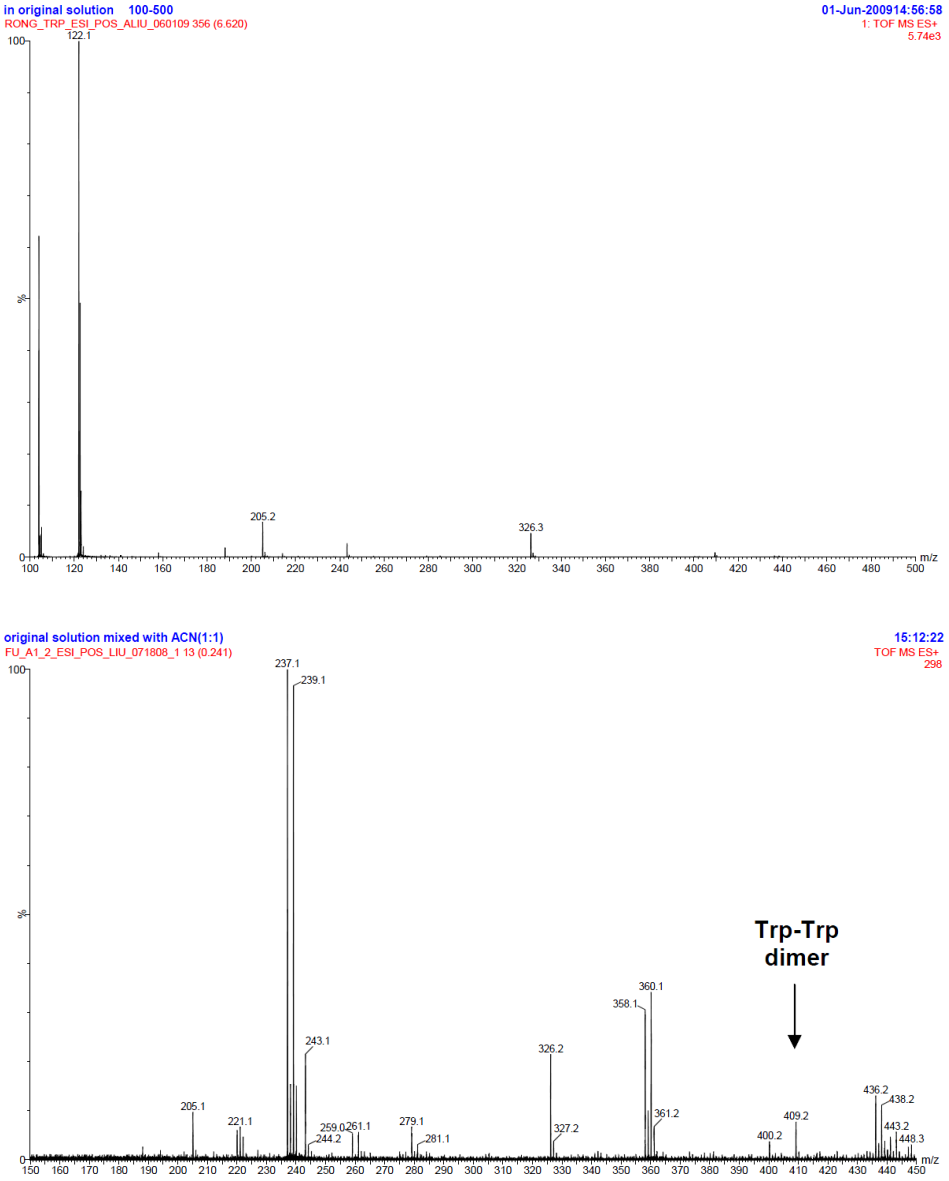

Figure 16. MS of Trp-Trp dimer. (A) 5 mM L-Trp in 50 mM Tris pH 7.4, (B) After reaction with H2O2 (4 mM) in the presence of TDO (100 μM). The experimental details are described below. All the reagents were. prepared using anaerobic 50 mM Tris-HCl pH 7.4 buffer in H_2 ^{18}O (75% ^{18}O) which was bubbled and purged with argon for hours prior to the experiments. The reactions were performed on ice with stirring using septum-sealed reaction vials. Ferric TDO (100 μM) was allowed to react with H_2O_2 in the presence of 5 mM L-Trp, in which H_2 $^{16}O_2$ was added to a total of 4 mM with a stepwise addition. After 20 minutes of reaction, TDO was removed from the reaction system using a Centriprep-10 at 3000×g for 10 min, and the filtrate was collected for electrospray ionization-mass spectrometry (ESI-MS) analysis.

When $H_2{}^{18}O_2$ was used instead of $H_2{}^{16}O_2$, an ion of *m/z* 241 was detected (Fig. 15C). This ion is consistent with the incorporation of two atoms of ^{18}O into the product from $H_2{}^{18}O_2$. An ion at *m/z* 237 was also observed due to the presence of the unlabeled ^{16}O fraction of the peroxide reagent (90% ^{18}O enrichment). Although the experiment was carried out under O_2-free conditions, oxygen leak could occur during the process of filtration to remove enzyme from the reaction system and thus generated a small fraction of NFK by unlabeled oxygen, too. The amplitude of *m/z* 237 ion corresponds to less than 20% of the sum of the total product ions. In Fig. 15C a significant ion of *m/z* 239 is also present, which corresponds to the incorporation of one atom of ^{16}O and one atom of ^{18}O into L-Trp. To investigate the cause of the $^{16}O/^{18}O$ scrambling, a sample of ^{16}O-NFK was prepared which presents the ion of *m/z* 237 of Fig. 15B. The ^{16}O-NFK sample was then re-dissolved in a solvent containing ^{18}O-enriched water (78.1 atom%) with $H_2{}^{16}O$:$H_2{}^{18}O$ ratio of 1:4. The final ^{16}O:^{18}O ratio was approximately 3:5. Fig. 15D shows that a new ion at *m/z* 239 is generated from the non-labeled NFK in a post-enzymatic reaction process in the presence of ^{18}O-enriched water, which indicates that one ^{18}O from solvent is exchanged into ^{16}O-NFK.

The ^{18}O-water exchanged sample containing both the *m/z* 237 and 239 ions was then added to ^{16}O water to reach a $H_2{}^{16}O$:$H_2{}^{18}O$ ratio of 60:1 (1.6% ^{18}O atom), and analyzed again by ESI-MS after a few minutes solvent exchange. Figure 15E shows that the *m/z* 239 peak is substantially reduced while the original *m/z* 237 ion becomes the predominating species, which indicates a reversible solvent exchange for NFK. No *m/z* 241 peak is observed in either of the exchange experiments, indicating that one and only one oxygen site in the product NFK is solvent exchangeable.

A parallel set of experiments was performed using unlabeled H_2O_2 as the oxidant in ^{18}O-based solvent. The *m/z* 237 and 239 ions are present in the $H_2{}^{16}O_2/H_2{}^{18}O$ sample (Fig. 15F), consistent with solvent exchange after the catalytic reaction to form the *m/z* 239 ion. Collectively, these results suggest that the two new oxygen atoms incorporated into NFK are both derived from H_2O_2, and one of the oxygen atoms

is readily exchangeable with solvent.

3.5 *Identification of a minor but reproducible mono-oxygenated tryptophan product.*

In addition to the dioxygenation product NFK, two ions at *m/z* 220 and 221 are observed in the reaction of ferric TDO + L-Trp with unlabeled H_2O_2 (Fig. 15B). As described below, the *m/z* 220 ion is shown in the MS/MS experiments to be a fragment of NFK. The *m/z* 221 ion is, however, 16-Dalton greater than L-Trp, which is consistent with the insertion of one oxygen atom into L-Trp. In the isotope-labeling experiments using $H_2{}^{18}O_2$ as the oxidant, a corresponding *m/z* 223 ion, 18-dalton greater than L-Trp, is observed at the expense of the *m/z* 221 ion (Fig. 15C). The *m/z* 221 ion was not observed in the control mass spectrometry measurements of normal turnover using ferrous TDO, L-Trp and O_2.

Fig. 17 shows the results of an LC-MS experiment using $H_2{}^{16}O_2$ with $H_2{}^{18}O$ solvent to further characterize the two ions at *m/z* 220 and 221. The substrate (*m/z* 205) shows the greatest retention time of 16.6 min. The *m/z* 237 and 239 ions with a retention time of 6.1 min are due to the dioxygenation product NFK (Fig. 17D). The former has two ^{16}O atoms inserted and the latter has a ^{16}O and an ^{18}O atom inserted into the substrate. The *m/z* 243 ion with a 2.9 min retention time is attributed to the Tris-HCl buffer used in the reaction, and the *m/z* 214 ion is a fragment of the Tris-HCl buffer (Fig. 17B). The ions at *m/z* 221 and 223 have a retention time of the 5.3 min (Fig. 17C). It should be noted that the much longer solvent exchange took place in the LC-MS experiments. The observation of the *m/z* 223 ion in $H_2{}^{18}O$ indicates that the presumed monooxygenated byproduct is solvent exchangeable but at a much slower rate. When ^{18}O-enriched peroxide was used in the experiments without LC separations, the *m/z* 223 ion was observed while *m/z* 221 ion was nearly absent (Fig. 17C).

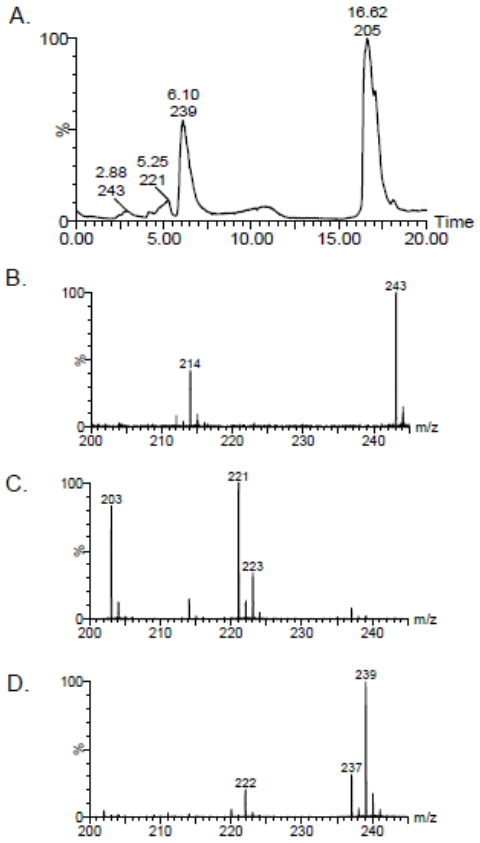

Figure 17. LC-MS characterization of the TDO reaction with H_2O_2 and L-Trp. (A) HPLC chromatography of the reaction product of $H_2{}^{16}O_2$-dependent oxygenation mediated by ferric TDO performed in $H_2{}^{18}O$. MS spectra at retention time of 2.88 (B), 5.25 (C), and 6.10 min (D).

ESI-MS/MS experiments were subsequently conducted to characterize the major products of *m/z* 237 and 239 ions. The Fig. 18 confirms that *m/z* 220 and 222 are the fragments of NFK (*m/z* 237 and 239, respectively), as a consequence of each losing an $-{}^{16}OH$ or $-{}^{18}OH$ group during ionization. The absence of the *m/z* 221 (223 with ^{18}O) ion in the MS/MS spectrum of the *m/z* 237 (239 with ^{18}O) ion is consistent with the LC-MS and isotope-labeling results and thus confirming that the *m/z* 221 ion is not a fragment of the NFK. The presence of the *m/z* 223 ion in the ^{18}O sample suggests an isotope equivalent of the

presumed monooxygenated tryptophan (Trp-O). From these results, it can be concluded that the *m/z* 221 ion (223 with ^{18}O) is arisen from Trp-O. In a post-reaction treatment experiment after removing the enzyme by filtration, the sample containing the Trp-O was incubated with H_2O_2 overnight at 4 ˚C in the absence of TDO. The *m/z* 221 (or 223 with ^{18}O) ion was unchanged in the spectrum after the peroxide treatment.

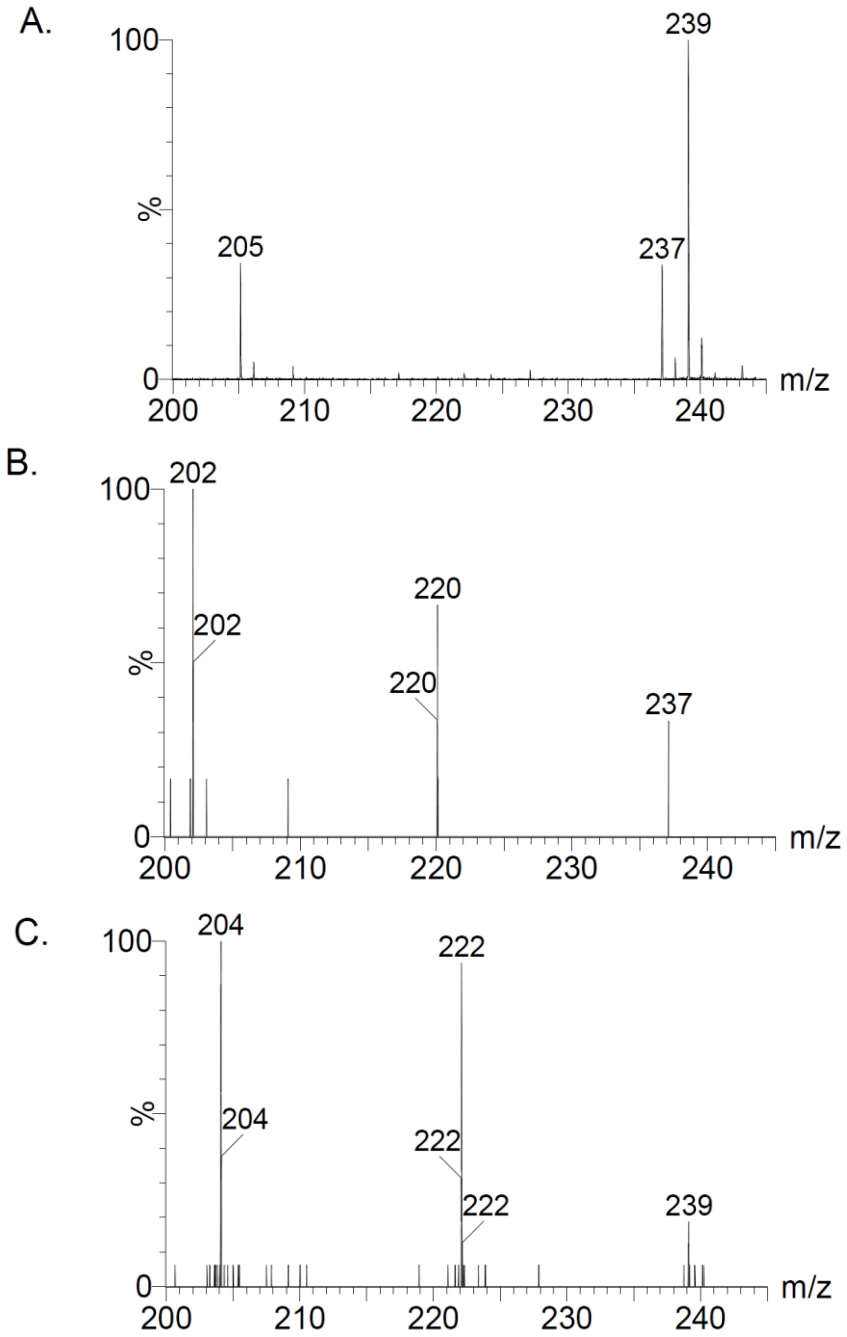

Figure 18. MS/MS analysis of *m/z* 220 and *m/z* 222 ion peaks. (A) ESI-MS spectrum of the TDO reaction in H_2 ^{18}O solvent. MS/MS characterization of ion peaks of *m/z* 237 (B) and *m/z* 239 (C) of the spectrum A, respectively.

3.6 *Modeling study*

The TDO ferryl species observed in our Mössbauer study exhibits an unusually large quadrupole splitting parameter of 1.755 mm/s at the physiologically relevant pH 7.4. This is greater than that of any other reported Fe(IV)-oxo species of hemoproteins, but is smaller than that of protonated Fe(IV)-oxo (see Discussion). Density functional theory calculations on the TDO ferryl intermediate were performed to evaluate the possible structural influences on the Mössbauer parameters, including protonation of the oxo group, hydrogen bonding to the oxo group from a distal histidine and a conserved Ser-Gly pair, and conformational change of the proximal histidine ligand (Table 6). The data presented suggest that the relatively large positive value of quadrupole splitting of parameter is a result of the H-bonding to the oxo group (see section 3.11).

Table 6. Results of various models for TDO ferryl species[a]

	Model	R_{FeO} (Å)	ΔE_Q (mm/s)	δ_{Fe} (mm/s)
TDO	Experimental		1.755	0.055
1A	$Fe^{IV}(Por)^{2-}(His)^{0}(O)^{2-}$	1.654	1.54	0.14
1B	twisted His	1.648	1.97	0.13
2A	$Fe^{IV}(Por)^{2-}(His)^{0}(OH)^{1-}$	1.799	3.02	0.08
2B	twisted His	1.795	3.19	0.11
3A	$Fe^{IV}(Por)^{2-}(His)^{0}(O\cdots HB)^{2-}$	1.663	1.78	0.12
3B	twisted His	1.657	2.20	0.11
4A	$Fe^{IV}(Por)^{2-}(His\cdots H_2O)^{0}(O)^{2-}$	1.656	1.44	0.14
4B	twisted His	1.646	2.14	0.12
5A	$Fe^{IV}(Por)^{2-}(His\cdots H_2O)^{0}(O\cdots HB)^{2-}$	1.665	1.66	0.11
5B	twisted His	1.660	2.11	0.11
6A	$Fe^{IV}(Por)^{2-}(His)^{0}(OH\cdots HB)^{1-}$	1.792	3.07	0.10
7A	$Fe^{IV}(Por)^{2-}(His)^{0}(O\ldots HB)^{2-}$(distalHis)-1	1.664	1.82	0.12
8A	$Fe^{IV}(Por)^{2-}(His)^{0}(O\ldots HB)^{2-}$(distalHis)-2	1.672	1.97	0.09
9A	$Fe^{IV}(Por)^{2-}(His)^{0}(O\ldots HB)^{2-}$(distalHis)-3	1.670	2.01	0.10

[a] HB represents the Ser124-Gly125 residues hydrogen bonded to the oxo group. In **7A**, the terminal atoms in the distal histidine are fixed at X-ray determined positions, while in **8A**, those atoms are allowed to be optimized. In **9A**, all atoms of the HB group (*Cm*TDO Ser124-Gly125) are also allowed to be optimized compared to **8A**.

3.7 *Reactivation of ferric TDO*

This work describes an extensive effort to uncover the long-standing reactivation mystery. Although the activation of ferric TDO by H_2O_2 in the presence of L-Trp has been known since 1950 (*183*), the mechanism of the reactivation was not resolved. The optical and Mössbauer spectroscopic data shown in this work confirms that the addition of H_2O_2 to the ferric form of TDO in the presence of L-Trp results in reduction of the enzyme to produce ferrous heme. The enzyme assay demonstrates that the ferrous enzyme generated by peroxide is catalytically active and is inhibited by CO. A plausible mechanistic model is presented in Scheme 1 that brings together the EPR, Mössbauer, optical, and mass spec data. In order for the model to be correct, ferryl intermediate, protein radical, O_2 production, Trp-dimer, monooxygenated Trp and the normal product NKF must all be observed, and all of them are presented in the results.

In the proposed reactivation model, the first step of the reaction involves a peroxide-dependent process to generate Cpd ES (Scheme 2). The second step involves two branching pathways that deplete Cpd ES: (A) a catalase-like reaction leading to O_2 production, and (B) reduction of the protein radical and Fe(IV)=O species by L-Trp resulting in Trp-O and ferrous TDO. The second branching reactions consume the two oxidizing equivalents stored in the Cpd ES intermediate and, consequently lead to enzyme reactivation and L-Trp dimerization. The reduction of the protein radical by the presence of L-Trp is a necessary step for the Fe(IV)=O to oxidize the substrate and become reduced to ferrous in branch B, because the high-valent Fe ion alone can no longer perform the catalase-like function. We performed a set of experiments in which the protein radical is quenched by a scavenger, such as hydroxyurea, and found that the catalase-like reaction is stalled. Consequently, O_2 production is inhibited, so is the NFK production in the anaerobic experiments (Fig. 10).

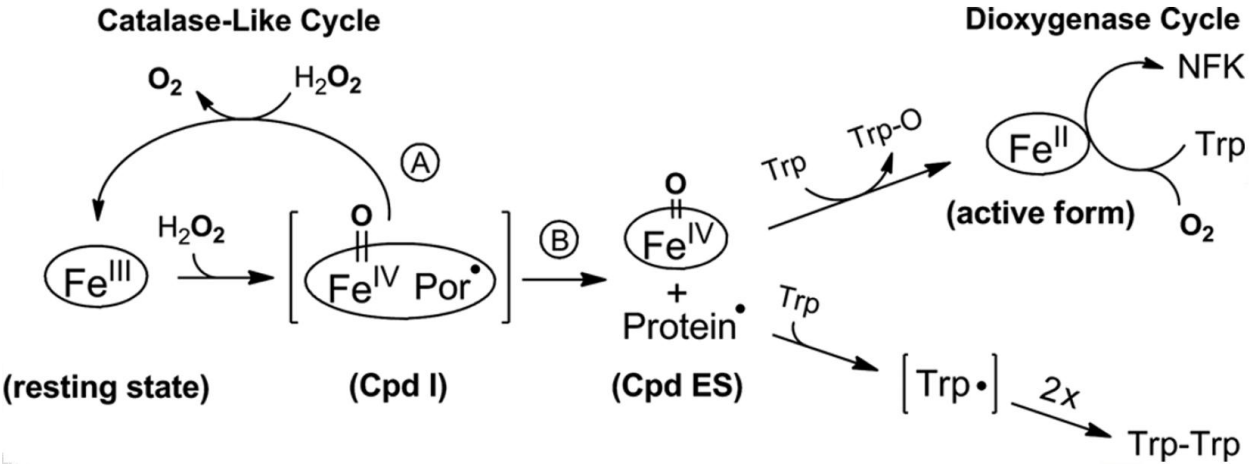

Scheme 2. Mechanism of enzyme reactivation by hydrogen peroxide in tryptophan 2, 3-dioxygenase. The reactivation pathway branches at the Compound ES-type ferryl intermediate. In the absence of L-Trp, a catalase-like activity is present. The enzyme reactivation occurs when the protein radical and the ferryl species are each reduced by L-Trp. Intermediates shown in brackets are predicted but not detected experimentally.

The reactivated enzyme turns over L-Trp with O_2 to produce NFK, which is observed both optically and with mass spectrometry. Under anaerobic conditions, the source of oxygen for the Fe(II)-dependent dioxygenation reaction arises solely from the catalase-like catalytic cycle. While under aerobic conditions, oxygen is not limited to that produced by the catalase-like activity. L-Trp is quickly converted to NFK under aerobic conditions. High concentration of peroxide can inhibit the enzyme reactivation in the aerobic experiments. This is due to the depletion of L-Trp and oxidation of the newly generated ferrous TDO (Fig. 12).

Although the presence of both H_2O_2 and L-Trp will cause TDO reactivation, there are two prerequisites for spectral detection of Fe(II) heme from the ferric enzyme: (1) L-Trp must be present in large excess relative to enzyme, and (2) L-Trp/H_2O_2 ratio must be greater than 2. The branched pathways shown in Scheme 2 are the competing reactions. Branch A is [H_2O_2]-dependent, while it is independent of [L-Trp]. Branch B, on the other hand, is [L-Trp]-dependent. H_2O_2 is also required for branch B to take place, so it is not independent of [H_2O_2]. A large excess of L-Trp must be present for branch B to effectively compete with branch A. The branched pathways are also internally connected. When the concentration of H_2O_2 is

increased, the rate of O_2 formation increases; at the same time, the NFK formation should decrease as branch A competes with branch B. However, the O_2 generated from branch A would become substrate of the dioxygenase reaction in branch B, hence masking this effect. O_2 production was also detected in the reaction of TDO and H_2O_2 in the presence of L-Trp, but at a much slower and variable rate depending on the reaction conditions, *e.g.*, the concentration and ratio of H_2O_2 and L-Trp. Because the Fe(II)-TDO consumes O_2, the change of O_2 concentration is a net effect of the catalase-like activity and the NFK formation. Thus, the classic kinetic measurements would not be very informative unless the exact concentration of the ferrous enzyme is characterized by spectroscopic methods at all times and under each of those conditions. Nevertheless, the observation of O_2 production in the presence of L-Trp suggests that the catalase-like reaction is not affected by the presence of the enzyme-bound L-Trp. Hence the catalase-like activity is probably an intrinsic property of TDO.

An intriguing aspect of the TDO reactivation is that the reduction of Fe(III) to Fe(II) heme in the absence of a reducing agent. H_2O_2 is a common oxidant with a standard reduction potential 1.32 V for the couple $H_2O_2/2H_2O$ at pH 7.0 (*192*), which is significantly higher than that of IDO (-30 mV) (*193*), and is also expected to be much higher than that of *Cm*TDO based on the reported data of *Xanthomonas campestris* TDO (< +150 mV) (*174*). Scheme 2 reveals that the reducing power in the TDO reactivation is ultimately derived from L-Trp.

A full conversion of Fe(III) to Fe(II) in TDO reactivation was never observed in this work. We believe this is due to the presence of competing reactions and because the ferrous heme can be re-oxidized. The amount of ferrous heme generated by this method depends on the concentrations of peroxide and L-Trp. In the presence of CO, the ferrous heme is stabilized against oxidation. The presence of CO also inhibits the production of NFK, indicating that the formation of NFK is through the normal enzyme cycle catalyzed by ferrous TDO and O_2 rather than a short circuit or peroxide shunt described for cytochrome

P450 enzymes (*194-197*). The experimental results presented here do not include evidence for a ferryl intermediate in the presence of L-Trp, but the observation of the ferryl intermediate in the absence of L-Trp suggests that the protein active site is capable of forming the ferryl intermediate. Previously, high-valent ferryl intermediate has never been trapped in TDO. Hence, it is likely that the decay rate of the high-valent Fe intermediate is greater than the formation rate when the primary substrate L-Trp is available. The Fe(IV)-oxo intermediate would thus never accumulate in the presence of L-Trp.

3.8 *Potential physiological relevance*

H_2O_2 is naturally produced by enzymes such as oxidases in organisms as a byproduct of aerobic respiration. Basal levels of H_2O_2 are present in most cells. In healthy individuals, H_2O_2 is produced in sufficient quantity to counteract unwanted bacterial invaders (*198*). During oxidative stress of the organism, reactive oxygen species, including H_2O_2, may be overproduced (*199*). In this work, we show the first clear spectroscopic observation that H_2O_2 is able to react with ferric TDO and L-Trp to produce the catalytically active form of the enzyme. The H_2O_2-based mechanism of enzyme reactivation may be physiologically important because TDO is a hepatic enzyme, and hepatocytes are known to be an oxidizing environment that may cause inactivation of TDO by oxidation of iron ion. In contrast, the catalytic activity of IDO is known to be inhibited by H_2O_2 (*200*). It is worth noting that IDO exists in tissues other than the liver and is unlikely to become oxidized under normal cellular conditions, suggesting that the H_2O_2-triggered reactivation mechanism found in TDO would not be necessary for IDO. Under normal physiological conditions H_2O_2 is present at low levels in cells. However, we find that a small amount of peroxide is sufficient to cause enzyme reactivation under aerobic conditions and when the primary substrate L-Trp is present. This is significant as amino acids are neither stored nor excreted in the human body. They have to be degraded. TDO is the key enzyme responsible for tryptophan degradation. In general, the discovery of such an enzyme reactivation mechanism by peroxide is

important for understanding strategies how a ferrous enzyme maintains its catalytic activity in an oxidizing environment.

3.9 *Byproducts of the enzyme reactivation*

Two minor byproducts were detected after enzyme reactivation: a Trp-Trp dimer and a Trp-O species. A *m/z* of 409 ion corresponding to the L-Trp dimer, is observed in our mass spectrometric study, which is absent in the control samples described in the results section. The dimerization of L-Trp is tentatively attributed to the result of reduction of the protein radical by L-Trp. Our isotope-labeling analyses show that the Trp-Trp dimer is insensitive to ^{18}O-enriched peroxide. Thus, its formation is not linked with the oxo group of the ferryl intermediate. The Fe(IV)-oxo intermediate oxidizes an enzyme-bound L-Trp to generate a monooxygenated product via a two electron oxidation. This monooxygenated product is experimentally detected by mass spectrometry (*m/z* 221). An ^{18}O enriched form (*m/z* 223) is also observed. LC-MS experiments provided further evidence for the presence of a monooxygenated product. The minor Trp-O product is a byproduct of reactivation and is expected to be only equivalent to the ferrous heme concentration. Due to the limitation of L-Trp solubility, one cannot increase the enzyme concentration to the millimolar range. The yield of Trp-O is unfortunately insufficient for further structural characterizations by other means such as NMR spectroscopy. Thus, its precise chemical structure is presently unknown. The most likely candidate is an epoxide, derived from O-insertion of the indole. An alternative candidate is 6-hydroxytryptophan, which is observed in the reaction of L-Trp, H_2O_2 and a triple mutant of myoglobin (*201*). The Trp-O byproduct survives during the enzyme reactivation. A similar Trp-O product was not observed in the dioxygenase cycle of the ferrous TDO reaction with O_2 as the oxidant, nor is shown in the reaction of peroxide with ferrous TDO. The structure of Trp-O is probably insignificant in this work because this minor product is not generated from the ferrous heme-dependent catalytic cycle of dioxygenase reaction. Nonetheless, the finding of the Trp-O byproduct has

helped us understand how the reactivation proceeds through the involvement of L-Trp.

3.10 *Catalase activity of TDO*

We have identified a previously unknown catalase-like activity for TDO by two sets of experiments. The first entails direct observation of O_2 formation from H_2O_2, and the second is the spectroscopic study of an Fe(IV)=O species necessary for a catalase-like catalytic mechanism. Similar to other heme enzymes for which this catalase-like function is not native, the data presented here indicate that this activity is detrimental to the function of the enzyme. The addition of concentrated peroxide without L-Trp results in radical formation and irreversible partial loss of enzymatic activity as shown by the loss of heme and iron from the enzyme in our Mössbauer experiments. It has been shown that the heme-based catalases and the enzymes with a promiscuous catalase-like catalytic activity have a wide range of catalytic efficiencies (Table 7). The catalase-like activity observed from TDO, at 13 s^{-1}, is significantly below those found in native catalases or bifunctional catalase-peroxidases KatG. However, it is appreciable in comparison to the catalase activities of other hemoproteins whose primary biological activities are not catalase (Table 7). Whether the catalase-like activity has a physiological role *in vivo* is speculative. However, the reactivity of TDO with H_2O_2 is important for enzyme reactivation when the primary substrate is present.

In the mechanism of catalase, the ferric heme reacts with the first peroxide molecule to produce a reactive oxoferryl and a π-cationic porphyrin radical, which subsequently reacts with a second peroxide to produce an O_2 molecule and water (*202, 203*). Our observation of an approximate ratio of 1:2 ratio of [NFK]:[H_2O_2] stoichiometry under anaerobic conditions (Figure 9, inset) is consistent with the catalase mechanism. The observed NFK/H_2O_2 ratio is slightly under 1:2 which is puzzling. This deviation may be explained by the nonproductive consumption of peroxide in the following processes: 1) the small amount of peroxide used to generate ferrous heme, 2) peroxide-induced heme degradation observed in our Mössbauer study, and 3) oxidation of the newly generated ferrous heme. The last of which is

inconsequential when O_2 is the limiting reagent.

Table 7. The kinetic properties of catalase activity in hemeoproteins.

Protein	k_{cat} (s^{-1})	K_m (mM)	k_{cat}/K_m ($M^{-1}s^{-1}$)
Horse liver catalase (*204*)	3.8×10^7	1100	3.5×10^7
E. coli catalase-peroxidase (*205*)	1.6×10^4	3.9	4.1×10^6
M. tuberculosis KatG (*206*) Recombinant KatG (*204*)	1.0×10^4 2.3×10^3	5.2 30	1.9×10^6 7.7×10^4
Periplasmic catalase–peroxidase (KatP) (*207*)	1.8×10^4	27	6.4×10^5
Nα-acetylated microperoxidase-8 (*208*)	4.1	40.9	100.2
Catecol oxidase (*209*)	0.063	1.2	63
Hemoglobin (*Bovin*) (*210*)	1.92	24	80
TDO (this work)	13	16	850

3.11 *Ferryl intermediate of TDO*

We present clear spectroscopic evidence for the first experimental observation of a high-valent Fe species in TDO. The detection of a monooxygenated product is consistent with the recent successful detection of an oxoferryl intermediate in the orthologous enzyme IDO by resonance Raman spectroscopy (*211*). Such a high-valent Fe intermediate was expected to exist in the enzyme mechanism in a recent ONIOM study (*212*).

We show that the addition of H_2O_2 to ferric TDO, in the absence of L-Trp, generates an Fe(IV)-oxo species and a protein-based radical with a concomitant decrease in ferric TDO concentration. At approximately the same reaction time, the concentrations of the Fe(IV)-oxo and radical species are comparable. Thus, the generation of the Fe(IV)-oxo and radical species in nearly equal amounts is consistent with formation of a Cpd ES-type intermediate, rather than an Fe(IV)-oxo/porphyrin cation intermediate (Cpd I) observed in catalases. The presence of a Cpd ES species, which may be derived from

a Cpd I-type intermediate in this case, may be critical for the subsequent enzyme reactivation to occur, because the Fe(IV)=O species and radical intermediate will have to be reduced by L-Trp through separate reactions.

The observed radical species has properties in common with those of protein-based aromatic radicals. The $P_{1/2}$ value of the observed radical in TDO (1.2 mW at 100 K) is significantly higher than that of isolated free radicals (*187*), for example, 0.07 mW at 90 K (*213*), indicating the presence of a relaxation mechanism. The $P_{1/2}$ value for the protein-based Trp radical of Compound ES species of cytochrome *c* peroxidase is 1.5 mW at 100 K (*145*), and the Tyr radical of P450-ES is 1 mW at 70 K (*214*). These higher $P_{1/2}$ values have all been attributed to relaxation of the radical by the adjacent heme iron. The $P_{1/2}$ value of the TDO radical is indicative of its close proximity to the metal center. The site of the radical in TDO is to be determined by future study. There are at least four tyrosine and tryptophan residues in the immediate vicinity of the enzyme active site. The identification of the radical site is challenging because a mutation of a tyrosine/tryptophan (fated to be a free radical) can result in the radical moving to a nearby tyrosine/tryptophan, as demonstrated in other heme-based enzymes such as prostaglandin H synthase (*110*).

Recent experimental studies and density functional theory calculations suggest that the ΔE_Q value might correlate with the protonation state of some heme-based ferryl species (*215, 216*). The parameter range for protonated Fe(IV)-OH species is 2.00 – 2.5 mm/s (*217*), while the range for unprotonated Fe(IV)=O is 1.0 – 1.6 mm/s (*215-219*). The ΔE_Q of the TDO Fe(IV)-oxo intermediate (1.755 mm/s determined at the physiologically relevant pH 7.4) lies between these ranges (Table 8). The quadrupole splitting parameter of the TDO intermediate is noticeably greater than those of any other heme-based ferryl species but much smaller than those of protonated basic ferryl species. The nearest value is found in MauG, another enzyme that oxidizes L-Trp inside a protein (*220*). A *bis*-Fe(IV) intermediate has been trapped from MauG and

one of the hemes is described as an oxyferryl species with ΔE_Q value of 1.70 mm/s (*220*).

Table 8. Comparison of the Mössbauer parameters of TDO Fe(IV) intermediate with known heme-based ferryl moieties [a].

Intermediate	Iron Species	Trans Ligand	Spin	δ (mm/s)	ΔE_Q (mm/s)	Refs
CcP-ES	$[Fe^{4+}=O^{2-}]^{\bullet+}$	histidine	$S = 1$	0.05	1.55	(*72*)
HRP-I	$[Fe^{4+}=O^{2-}]^{\bullet+}$	histidine	$S = 1$	0.08	1.25	(*221, 222*)
HRP-II	$Fe^{4+}=O^{2-}$	histidine	$S = 1$	0.03	1.61	(*222*)
Mb-II	$Fe^{4+}=O^{2-}$	histidine	$S = 1$	0.09	1.43	(*223*)
JRP-I	$[Fe^{4+}=O^{2-}]^{\bullet+}$	histidine	$S = 1$	0.10	1.33	(*224*)
JRP-II	$Fe^{4+}=O^{2-}$	histidine	$S = 1$	0.03	1.59	(*223*)
Mb (annealed)	$Fe^{4+}=O^{2-}$	histidine	$S = 1$	0.10	1.49	(*225*)
CPO-I CPO-II	$[Fe^{4+}=O^{2-}]^{\bullet+}$ $Fe^{4+}=O^{2-}$	cysteine cysteine	$S = 1$ $S = 1$	0.13 0.11(3)	0.96 1.59	(*153*),76 (*216*)
P450-I	$[Fe^{4+}=O^{2-}]^{\bullet+}$	cysteine	$S = 1$	0.11	0.90	(*226*)
TDO	$Fe^{4+}=O^{2-}$	histidine	$S = 1$	0.055	1.755	This work
MauG	$Fe^{4+}=O^{2-}$ (heme site 1)	histidine	$S = 1$	0.06	1.70	(*220*)
Basic CPO-II	$[Fe^{4+}=O^{2-}]H^{+}$	cysteine	$S = 1$	0.10(3)	2.06(3)	(*216*)
Basic $P450_{BM3}$	$[Fe^{4+}=O^{2-}]H^{+}$	cysteine	$S = 1$	0.13	2.16	(*215*)
Basic $P450_{cam}$	$[Fe^{4+}=O^{2-}]H^{+}$	cysteine	$S = 1$	0.14	2.06	(*215*)

[a] Abbreviations used in this table are: CcP, cytochrome *c* peroxidase; HRP, horseradish peroxidase; Mb, myoglobin; JRP, Japanese radish peroxidase. P450-I was trapped and characterized from CYP119, the thermophilic P450 from *Sulfolobus acidocaldarius* (*226*).

Protein environments can conceivably provide a range of proton interactions with the oxyferryl heme. A possible interpretation of the atypical quadrupole splitting value was examined in this work by DFT calculations performed on fourteen structural models (not shown). Since the iron equatorial heme ligands

in TDO are the same as those found with other heme proteins that display typical Mössbauer ΔE_Q values for Fe(IV)=O species, these models were used to evaluate the structural contributions that can directly affect the iron axial ligands: 1) protonation of the oxo group, 2) hydrogen bonding to the oxo group, 3) hydrogen bonding to the proximal His, and 4) conformation of the proximal His. All the models were generated on the basis of the X-ray crystal structure of the substrate-free TDO (PDB ID: 2NW7). Geometries of the models (see Table S1-14 for the optimized coordinates) were optimized using the method developed previously for defining other oxoferryl species (*163*) with the terminal atoms fixed at the X-ray crystal structure positions to mimic the protein environment effect. Both the Mössbauer quadrupole splitting and isomer shift parameters for these models were calculated using the DFT method, which enabled accurate predictions of these two properties in various iron proteins and models covering all iron spin states and coordination states (*162, 163*).

As shown in Table 6, the predicted Mössbauer isomer shift (δ) of these models are all close to the experimental value with no significant difference, indicating its insensitivity to the secondary structural changes along the axial positions. In contrast, the predicted Mössbauer quadrupole splittings (ΔE_Q) display a large range from 1.44 mm/s to 3.19 mm/s, suggesting its role as a sensitive structural probe. The best agreement with the experimental value was found by incorporation of the nearby hydrogen bonding residues Ser124-Gly125 (these two residues are fixed at their X-ray positions except for the peptide bond atoms CONH, which were allowed to be optimized). The predicted ΔE_Q value of 1.78 mm/s for model **3A** (*i.e.*, $Fe^{IV}(Por)^{2-}(His)^{0}(O^{\cdots}HB)^{2-}$, Table S5) is in excellent agreement with the experimental measurement of 1.755 mm/s described in this work. These calculations suggest that the ΔE_Q value of the TDO ferryl species originates from the hydrogen bonding interaction provided by the unique protein environment, similar to the computational results obtained for the MauG Fe(IV) species (*162*).

An examination of the high-resolution crystal structures of TDO from both *Cupriavidus metallidurans*

and *Xanthomonas campestris* (PDB codes: 2NW7, 2NW8, and 2NW9) (*174*) suggests that the conserved active site residues at the distal pocket, His72 and Gly125 (*Cm*TDO numbering system) are ideal candidates for hydrogen bonding with the Fe-bound oxo group. These residues are also conserved in the human enzyme. The role of these two residues has already been investigated in recent experimental and computational studies (*158, 211, 227, 228*) by several laboratories. The consensus is that the heme site in the dioxygenase can indeed generate a high-valent Fe(IV)-oxo species under appropriate conditions and that the protein microenvironment is critical to dictating the chemical and physical property of the intermediate.

3.12 *Oxygen exchange with solvent in NFK*

An unexpected minor finding of this study is that one of the oxygen atoms in the reaction product NFK is exchangeable with water in the time frame of minutes. Based on the well-known ketonic oxygen exchange with water, and the fact that both the carboxylate oxygen and the amide group of NH-COOH can exchange with a buffered solvent slower than a ketone (*229-231*), we propose that the ketone carbonyl group exchanges its oxygen with solvent via a diol-intermediate mechanism. Scheme 3 depicts a plausible mechanism for the solvent exchange. The nucleophilic attack at the ketone carbon by water generates a diol-intermediate. This is facilitated by a transient state with a six-member ring structure. The finding of NFK solvent exchange may become important in the mechanistic studies of the enzyme with ^{18}O. A previous ^{18}O-study was carried out by Hayaishi et al. in the absence of the knowledge of solvent exchange described in this work. The less than theoretical ^{18}O content was found in kynurenine, the hydrolysis product of NFK, and the exact contents vary in different sets of experiments (*232*). Furthermore, the results of $^{18}O_2$ and ^{18}O-water are not mutually consistent. This was thought to be caused by either an exchange reaction during the isolation procedure or by preferential utilization of ^{16}O over ^{18}O by TDO (*232*). The previous observations can be fully explained by our proposed ^{18}O-exchange

mechanism. It is the ketonic oxygen exchange that causes less than one atom of ^{18}O in kynurenine, rather than the preference of ^{16}O over ^{18}O hypothesized in the previous study. The exact ^{18}O content in NFK and kynurenine is dependent on the sample preparation procedures, i.e., the longer solvent exchange time lowers ^{18}O content.

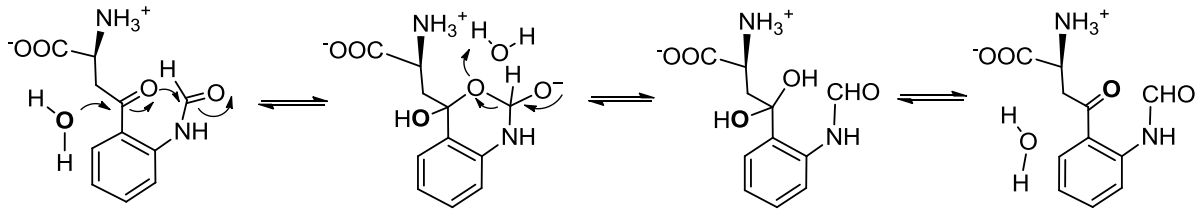

Scheme 3. Proposed solvent exchange mechanism on the carbonyl group of NFK.

CHAPTER 4

Nature's Strategy for Oxidizing Tryptophan: EPR and Mössbauer Characterization of the Unusual High-Valent Heme Fe Intermediates

4.1 *Two Oxidizing Equivalents Stored at a Ferric Heme*

Heme (iron protoporphyrin IX) proteins play important roles in a wide array of biological functions, including single electron transfer mediators, oxygen transport and storage, redox reactions, detoxification, and transcription regulations. Heme proteins are also known to play a key role in many metabolic processes involving oxidation reactions to satisfy the needs required for sustaining life. Redox reactions involve the transfer of electrons to and from a heme and thus produce heme intermediates with distinct oxidation states of the iron ion, some of which are high-valent Fe intermediates. The term "high-valent" is defined here as the iron ion with an oxidation state exceeding III. The most common heme Fe oxidation states found in biological chemical reactions are the ferrous, ferric, and ferryl species (*233-236*). Mössbauer spectroscopy, which can detect and characterize Fe species in all forms, is thus an indispensable tool for understanding the fundamental aspects of heme chemistry in enzymology. In the past decades, the high-valent Fe chemistry developed from biochemical, spectroscopic, and modeling studies has provided key insight into numerous essential biological processes that involve enzymes with Fe cofactors (*197*). Thus, the importance of high-valent Fe intermediates in heme and nonheme systems has become widely appreciated.

Since the oxidation or oxygenation reactions involving molecular oxygen are generally two- or four-electron processes, an important piece of chemistry is to understand how the metal centers store and, stabile, the oxidizing equivalents. When two oxidizing equivalents are stored at a heme center, the most common form of the heme intermediate is known as Compound I (cpd I), which is a classical intermediate

with a ferry1 ion, *i.e*., Fe(IV)=O, coupled with a π-cation radical located on the porphyrin ring (Por) (Fig. 19). Such a heme Fe intermediate transiently stabilizes two oxidizing equivalents above the resting Fe(III), and it is chemically equivalent to an Fe(V) species. Until now, Fe(V) intermediates have not yet been observed in any biological reactions. Compound I appears to be the most popular natural evolution of strategy for storing oxidizing power on a heme moiety. Similar to an Fe(V) species, the two oxidizing equivalents in cpd I are stored in the heme cofactor. However, cpd I is an easily modifiable system compared to Fe(V) due to its higher chemical stability gained from the charge distribution to the porphyrin ring. This is a great advantage for promoting biological reactions because the organic substrates need to bind to the enzyme active site and orientate properly. At the same time, the enzyme active site often needs reorganization and conformational changes in order to activate substrates or stabilize transient intermediates. The oxidative heme intermediate should not be too reactive to accommodate the required substrate orientation and active site reorganization. Another common form of the high-valent Fe species in heme proteins is Compound ES (cpd ES), which is composed of an Fe(IV)=O heme and amino acid-based cation radical in close proximity to the high-valent heme. The Compound ES description is based on the initial characterization from cytochrome *c* peroxidase (*237*). In cytochrome *c* peroxidase, Compound ES is derived from the transfer of the porphyrin cation radical of a Compound I-type intermediate to a nearby tryptophan (Trp) residue. Likewise, cpd ES is also an intermediate state with two oxidizing equivalents above the original ferric state. In what follows, we will review in this chapter the discovery of a third high-valent Fe heme intermediate termed Compound G (cpd G), which carries the two oxidizing equivalents in two discrete hemes and presents a *bis*-Fe(IV) intermediate (Figure 19). Cpd G is an unprecedented Fe species. This intermediate was found from a diheme enzyme that oxidizes tryptophan residues in the substrate protein. The spatial separation of the two oxidizing equivalents found in cpd G results in unique consequences in stability and chemical properties of the intermediate. This chapter will review its discovery and discuss its biological and general chemical significance.

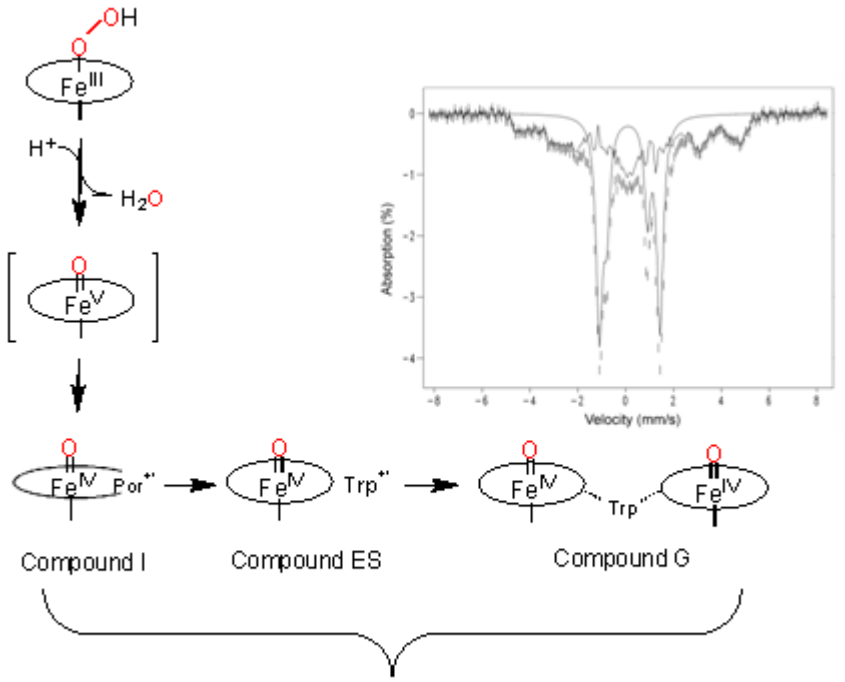

Figure 19. Strategies to store two oxidizing equivalents in heme proteins. The inset shows a Mössbauer spectrum of a *bis*-Fe(IV) intermediate in MauG (*220*). The hashed marks are the experimental data of diferric MauG reacts with one equiv of H_2O_2 for 45 s. The noisy line indicates the contribution of ferric heme (~34% of total Fe). The simulated smooth solid line represents two Fe(IV) species. See text for details.

4.2 *Oxidation of L-Tryptophan by Heme-Based Enzymes*

L-Tryptophan (Trp) is an essential amino acid for humans. The majority of the dietary supply of Trp is metabolized in the kynurenine pathway in which tryptophan 2,3-dioxygenase (TDO), the enzyme that converts Trp to *N*-formylkynurenine, catalyzes the first and committed step. In addition to being an important metabolite, Trp is also involved in various biochemical activities. When cross-linked and oxygenated, two Trp residues can serve as a cofactor for amine oxidations in several enzymes (*238, 239*). Furthermore, Trp plays many indirect biologically significant roles. In the kynurenine pathway, several metabolites generated from Trp oxidation is known to display neuroactive properties (*169, 171*). Kynurenic acid is a neuroprotectant and endogenous antagonist at *N*-methyl-D-aspartic acid (NMDA)

receptors while quinolinic acid is an agonist of these receptors. L-Tryptophan is also an endogenous source of NAD production, and the kynurenine pathway constitutes the major part of the *de novo* biosynthetic route of NAD (*169-171*). The oxidation of the amino acid tryptophan is thus an important biological event.

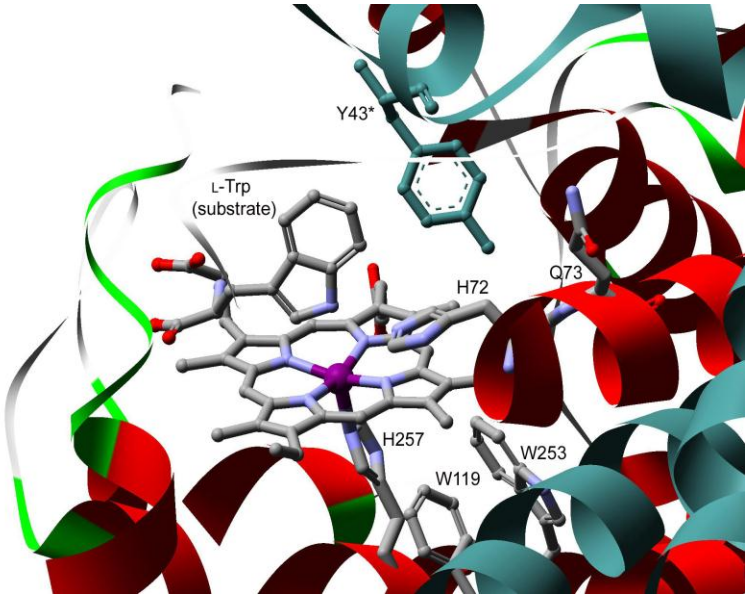

Figure 20. The ligand-bound structure of tryptophan 2,3-dioxygenase
PDB: 2NW7, Forouhar et al., 2006, *PNAS*, 104, 473-478

Recent reports have linked the oxidation/oxygenation of free and protein-bound Trp to heme-based proteins, *i.e*. TDO (Fig. 20) and MauG (Fig. 21), respectively. The oxidation of free Trp is carried out by TDO, which inserts two oxygen atoms into Trp in a four electron oxidizing process by utilizing a *b*-type heme cofactor (Fig. 22).

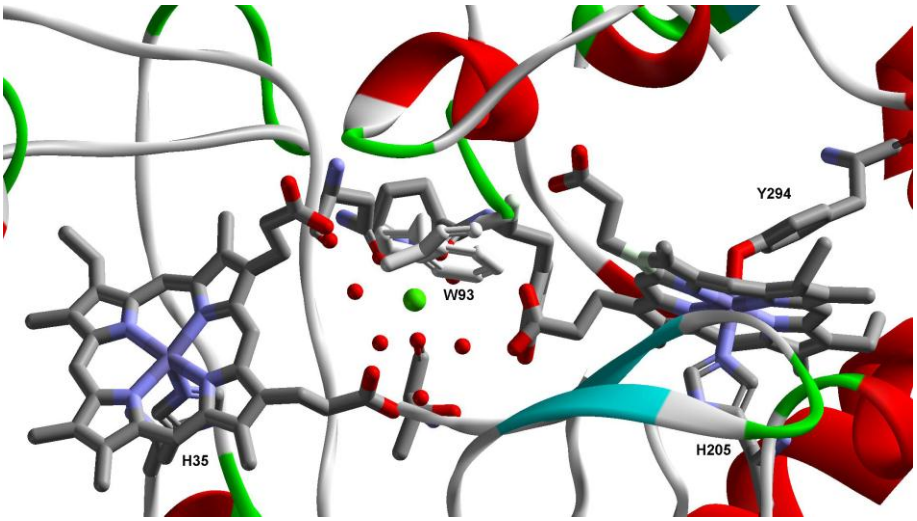

Figure 21. The structure of the di-heme cofactor in MauG (PDB code: 3L4M)
PDB: 2NW7, Jensen et al., 2010, Science, 327, 1392-1394

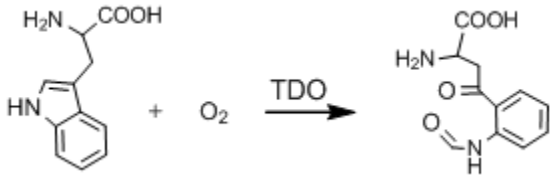

Figure 22. The chemical reactions catalyzed by TDO

This enzyme is representative of a potentially new hemoprotein dioxygenase superfamily whose oxygenase mechanism remains poorly understood. It should be noted that dioxygenase activity is typically accomplished by nonheme metalloenzymes. The non-heme iron active sites generally have two histidines, one carboxylate and two or three solvent-derived metal ligands, which allow simultaneous binding of both substrate and dioxygen by replacing the solvent-derived labile ligands. The primary substrate and O_2 bind to a nonheme metal ion and thus both become activated. The metal ion functions as a conduit so that the electrons of the primary substrate move to O_2 through the metal ion. In some cases, such as α-ketoglutarate-depedent dioxygenases, a co-substrate is needed for production of an oxygenated intermediate followed by attack of the primary substrate. In contrast, the heme cofactor does not allow

binding of the primary substrate and O_2 because porphyrin and the proximal ligand are not labile. In TDO, after binding of O_2 the heme Fe becomes coordination saturated, therefore, the primary substrate must bind to a pocket adjacent to the Fe ion (*174*). Thus, the Fe ion cannot function as a bridge in between the primary substrate and O_2. The oxygen activation and insertion of TDO must proceed with a distinct mechanism relative to the well-characterized nonheme Fe-dependent dioxygenase enzymes. The oxidation of protein-bound Trp residues is catalyzed by a novel enzyme MauG, which utilizes two *c*-type hemes to catalyze a posttranslational modification of a 119 kDa protein is an example of an enzyme that oxidizes protein-bound tryptophan residues. The reaction is a six-electron oxidation, and the utilization of two *c*-type hemes by MauG to perform the hydroxylation and subsequent oxidation reactions is unprecedented (Fig. 21).

4.3 *The Chemical Reaction Catalyzed by MauG*

While tryptophan 2,3-dioxygenase (TDO) oxidizes free Trp in a fast reaction, MauG oxidizes specific tryptophan residues within a large protein in a relatively slower catalytic process (*240*). In methylamine dehydrogenase (MADH) from *Paracoccus denitrificans*, the catalytic center is a tryptophan tryptophylquinone (TTQ) cofactor, presented on each β subunit of the 119 kDa heterotetrameric $\alpha_2\beta_2$ protein (*241, 242*). The TTQ cofactor is derived from Trp57 and Trp108 in a posttranslational process. The biogenesis of TTQ requires incorporation of two oxygen atoms into Trp57 and a cross-linking of the indole rings of Trp57 and Trp108 of the β subunits (Fig. 23) (*243*). Such a biosynthesis is, however, not a self-processing event but an enzyme-mediated posttranslational process that requires the action of at least one processing enzyme encoded in the methylamine utilization (*mau*) gene cluster (*244*, *245*). It has been shown that MauG, the 42.3 kDa *mauG* gene product, is the crucial enzyme for TTQ biogenesis (*246, 247*). MauG catalyzes the second oxygenation (at C6 of the Trp57 phenyl ring), the cross-linking of the two tryptophan residues (Trp57 and Trp108), and the oxidation of the semiquinone intermediate during

the TTQ biogenesis (*248*). Deletion of *mauG* in the *mau* gene cluster causes an accumulation of a 119 kDa biosynthetic precursor of MADH in which Trp57 is mono-hydroxylated at C7 and the cross-link is absent (*249*). This 119 kDa protein precursor of MADH is the natural substrate of MauG. The TTQ-biosynthesis from the precursor is achievable *in vitro* using either O_2 plus electrons from an external donor or H_2O_2.

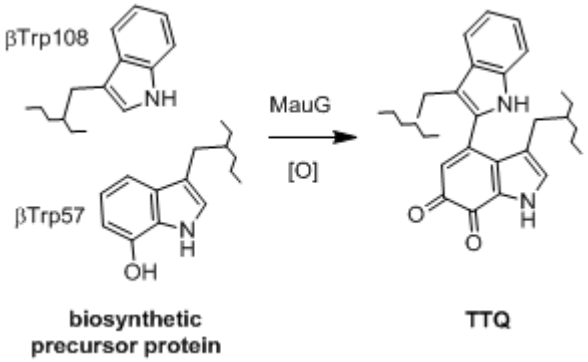

Figure 23. The chemical reactions catalyzed by MauG.

MauG is the first enzyme described that utilizes *c*-type hemes to carry out oxygenase activity (Figure 21). This enzyme exhibits sequence homology to bacterial di-heme cytochrome *c* peroxidase, but it possesses negligible peroxidase activity (*247*). The initial characterization of MauG by EPR spectroscopy suggests that this diheme enzyme is similar to heme-based oxygenase enzymes such as heme oxygenase (HO) and P450 with bound inhibitors (*247*). Subsequent biochemical and mass spectrometry studies establish that MauG performs an unusual six-electron oxidation reaction, presumably two per step in three successive steps, to insert an oxygen atom to a Trp residue on the substrate protein and remove four protons from the oxygenated Trp and another adjacent Trp residue to produce a cross-linked tryptophan tryptophylquinone (TTQ) cofactor on the substrate protein (Figure 23). Such a quinone cofactor is the catalytic center for methylamine dehydrogenase (MADH). The MauG-mediated reaction is essentially the terminal step of

the MADH cofactor biogenesis.

The unique utilization of two *c*-type hemes to perform oxygenation and subsequent oxidation reactions contrasts other hemoproteins that generally utilize *b*-type hemes, such as P450 (*196, 197, 250*), for their oxygenase activity. Most recently, a few additional enzymes have also been found to utilize *c*-type hemes to perform similar reactions. For instance, RoxA is a rubber oxygenase that utilizes two *c*-type hemes for an oxidative cleavage of poly(cis-1,4-isoprene) (*251*). As the best characterized protein in this potential new group of hemoproteins, MauG is an ideal model or studying the catalytic mechanisms of those covalently bound *c*-type heme cofactors. Another special aspect of MauG is that its substrate is a pair of protein-bound tryptophan residues inside a protein, which is about 3-fold larger in size than the enzyme itself. The characterization of MauG-catalyzed TTQ biosynthesis is carried out with the expectation to expand the existing knowledge about protein evolution, protein structure-function relationships, and protein engineering strategies for introducing new functional groups into proteins.

Sequence alignment, biochemical and EPR study of MauG reveals that the two ferric hemes are present in a distinct spin state (*247*). The high-spin ferric heme is ligated with a histidine (His35) ligand. The low-spin ferric heme is six-coordinate with two protein ligands, one of which is His205 (*247*). The two His ligands, one for each heme, are confirmed to provide the proximal axial heme ligands by the X-ray structural study of the enzyme (*252*). The EPR and intrinsic oxidation-reduction midpoint potential studies of MauG reveal a redox cooperativity, *i.e*. facile equilibration of electrons, between the two hemes (*253, 254*). However, EPR studies show that the two hemes are not spin-coupled (*220*) (*247*). Therefore, the two hemes must be distantly located even though they efficiently share electrons. The physical separation of the two hemes was later verified by the crystal structure of the enzyme in complex with its substrate protein at 2.1 Å resolution (*252*). The two Fe ions are ~ 21 Å apart although the heme edges are within 10 Å of each other and are connected through H-bonds by Trp93 (*252*). A recent spectroscopic

study also shows that the His-Tyr ligation remain unchanged at the fully reduced diferrous state (*254*). At both the diferrous and diferric oxidation states, only the five-coordinate heme reacts with exogenous molecules such as and O_2 and nitric oxide (NO). The six-coordinate heme does not directly react with exogenous molecules. The distal Tyr ligand appears to remain bound to the heme during the chemical reaction of the five-coordinate heme (*254*).

4.4 *A High-Valent bis-Fe(IV) Intermediate in MauG*

Upon mixing MauG with stoichiometric amounts of H_2O_2 a new intermediate is formed. This species is stable and is characterized in UV-Vis by a Soret peak shift from 405 to 407 nm. The X-band EPR spectrum of MauG displays two heme signals, a high-spin (g = 5.57, 1.99) and low-spin (g = 2.54, 2.19, 1.87). After mixing with H_2O_2 both high and low spin signals disappear and a new radical signal can be observed at g = 2.003 with a peak-to-peak width of 1.3 millitesla (*220*). The EPR characterization of the g = 2.003 radical suggests that it is an organic free radical. However, quantitation from spin double integration is that the radical signal represents 1% of the protein and cannot compensate for the loss of the two ferric heme EPR signals.

When ^{57}Fe-labeled MauG is treated with H_2O_2 the resultant Mössbauer spectra shows two sharp lines (intermediate) and an addition broad, magnetically split feature associated with ferric heme (*220*). Upon subtraction of the ferric species, the resulting spectrum is fitted by two quadrupole doublets with the following parameters: (δ_1) of 0.06 mm/s and quadrupole splitting parameter (ΔE_{Q1}) of 1.70 mm/s and δ_2 = 0.17 mm/s and ΔE_{Q2} = 2.54 mm/s (Fig. 19 inset). The isomer shift values are typical of Fe(IV) (*255*) species and the quadrupole splitting parameter of Species 1 is in the range typically observed for ferryl and protonated ferryl species (*216*). The quadrupole splitting parameter of Species 2 is unusually large (ΔE_{Q2} = 2.54 mm/s) and is likely due to the proposed six-coordinate heme with two axial amino acid

ligands. The detailed spectral characterization of this intermediate is reported in reference (*220*). A recent quantum chemical study found that the unusual Mössbauer properties of both Fe(IV) species originated from novel structural features of the enzyme (*162*).

To our knowledge, the spin-uncoupled *bis*-Fe(IV) species found in MauG is an unprecedented Fe intermediate that represents a novel natural strategy to oxidize a large substrate. We therefore named it cpd G. This species is analogous to the *bis*-ligated high-valent inorganic porphyrin model compounds that were generated previously. In all such cases only a small isomer shift (δ) and large quadruple splitting (ΔE_Q) parameter were observed from those model compounds (*256*) (*257*). Compound G also contains a six-coordinate Fe(IV) heme species with two axial amino acid ligands in protein. In the previous Fe(IV) intermediates characterized, an exogenous oxygen is attached to the Fe(IV) ion as an oxo ligand to effectively stabilize the high-valent charge. In contrast, this role is fulfilled by the distal Tyr ligand and a Trp residue rests in between the two hemes.

4.5 *High-Valent Fe Intermediate of Tryptophan 2,3-Dioxygenase*

While hemoproteins perform a wide range of biological functions, they rarely express a dioxygenase activity as the native biological function. TDO is the first enzyme known to utilize a heme cofactor to express dioxygenase activity (*166*). TDO catalyzes the oxidative cleavage of the indole ring of L-tryptophan, converting it to *N*-formylkynurenine (NFK) in the absence of a coenzyme or an external electron donor (Figure 22). This activity is the initiating and the committing step for Trp to enter into the kynurenine pathway (*170*). In mammals, TDO is responsible for oxidizing over 99% of the free Trp in intracellular and extracellular pools of this amino acid, hence it is a biologically significant enzyme (*169*). TDO is a tetramer composed of identical subunits with a total mass of 134 kDa. Each subunit contains a *b*-type heme cofactor. However, the four heme cofactors display two types of spectroscopic properties

upon substrate binding despite the α_4 subunit structure (*157*). The discovery of the inequivalent hemes in the enzyme-substrate complex is consistent with the cooperative binding of substrate (*158*).

The high-valent Fe(IV) intermediate of TDO has been proposed in computational studies but has not yet been directly observed in the catalytic cycle (*212*). However, such a high-valent Fe(IV) heme has been observed by stopped-flow resonance Raman spectroscopy in its sister enzyme, indoleamine 2,3-dioxygenase (IDO) (*211*). IDO and TDO are evolutionally related enzymes that catalyze the same chemical reaction. IDO is a monomeric protein existing in all human tissues except the liver. The lack of substrate binding cooperativity in IDO results in a slower chemical reaction and thus affords a great opportunity to directly trap the reactive intermediates. The IDO Fe(IV)=O intermediate is shown to display a characteristic 799 cm^{-1} for ν_{Fe}=O stretching mode with histidine as a proximal ligand of the heme (*211*).

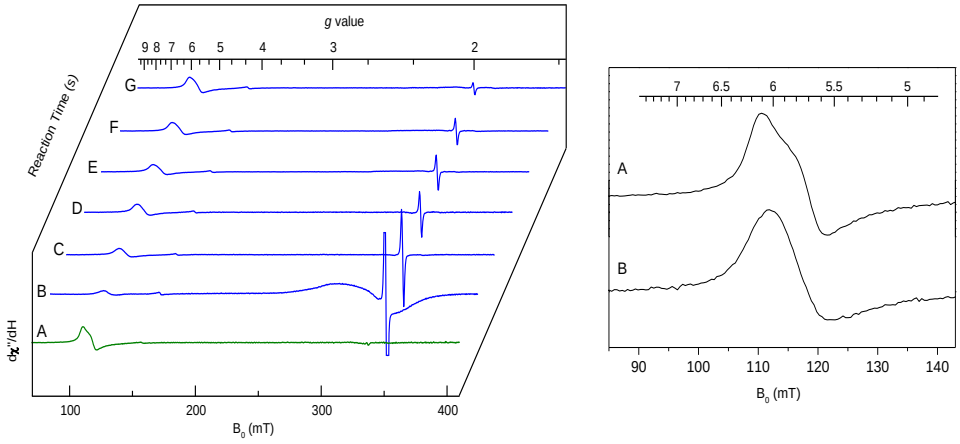

Figure 24. The formation and decay of the Compound I-type ferryl intermediate in the reaction of 150 μM tryptophan 2.3-dioxygenase with 900 μM hydrogen peroxide monitored by EPR spectroscopy at 10 K. (a) Seven representative EPR spectra (traces A to G) are shown in a 2D plot for the reaction of 0, 12, 30, 60, 90, 240, and 600 s in the parallel samples. (b) The high spin EPR signal of TDO (A), H_2O_2 treated TDO at 30 s (B).

Although a similar Fe(IV)=O intermediate of IDO has not yet been directly observed in the catalytic cycle of TDO, it has been trapped and characterized in the enzyme reactivation study. The ferric form of TDO can be reactivated by H_2O_2 in the presence of Trp through a complex mechanism (*258*). When Fe(III)-TDO reacts with H_2O_2 in the absence of Trp, the Fe ion become EPR-silent and a protein-based radical is observed (Figure 24). The free radical decays over time while the EPR signal of the high-spin ferric heme restores. The ferric ion is shown by Mössbauer spectroscopy to become a ferryl intermediate (*258*). The Mössbauer parameters of the Fe(IV)=O intermediate are nearly identical to those found for the Fe(IV)=O heme in cpd G (Table 8). The similar Fe(IV)=O intermediates exhibited by two structurally diverse heme-containing enzymes are intriguing. Given the similarity of the catalytic function of the two enzymes, *i.e.*, oxidizing either free- or protein-bound tryptophan, the striking similarity in the key intermediates is not very surprising.

The proposed protonated state of heme-based ferryl species has been studied in systems such as chloroperoxidase (CPO), cytochrome c peroxidase (CCP), cytochrome P450, catalase, horseradish peroxidase (HRP), myoglobin (Mb) and is still under investigation (*236*). Indeed, both cysteine and tyrosine (donating anionic ligands) are able to stabilize multiple forms of a ferryl species. In both cases, the equilibrium between the two seems to favor the deprotonated forms at physiologically relevant pH (*216*) (*259*). Additionally, the presented histidine ligated ferryls have a quadrupole splitting value of which is far less than the anticipated value for a protonated ferryl species (> 2 mm/s) (*219*). Thus if the values of the quadrupole splitting parameter of TDO and MauG do represent protonated species, then there must be other contributing factors that can lower the value for these intermediates. Due to the nature of the reaction it is possible that these enzymes are using secondary ligands to fine-tune the properties of the high-valent Fe intermediates. This can already be seen in the DFT calculations that predicted hydrogen bonding interactions from secondary ligands in the enzyme active site (*162*).

CHAPTER 5

Concluding Remarks

The molecular biochemistry exhibited by two structurally diverse heme-containing enzymes that oxidize either free tryptophan or protein-bound tryptophan residues is fascinating. Mono- and *bis*-Fe(IV) intermediates have been trapped and characterized by EPR and Mössbauer spectroscopy from these enzymes (*220, 258*). In particularly, the *bis*-Fe(IV) intermediate (cpd G) found in MauG is unprecedented. The target Trp residues of substrate is remotely located from the hemes, ~ 40 A from the heme that reacts with exogenous molecules. Thus, a long-range remote catalysis must take place in MauG. Recently, the co-crystal structure of MauG and its substrate protein preMADH is reported. When the crystal is soaked in a solution containing H_2O_2, the TTQ product is formed in the substrate protein (*252*). Thus, the proposed long-range remote catalysis is validated (*260*). It should be noted that one of the indelible stories about spatial separation of the catalytic center and the site that stores oxidizing equivalent(s) is described in ribonucleotide reductase (*261*). In that case, the catalytic center is located in the R1 subunit, while the oxidizing power, a protein-bound Tyr radical, is generated and stabilized by a metal center in the R2 subunit. When the substrate is loaded properly in the active site of R1 subunit, a long-range radical transfer takes place and a thiol-based transient radical is generated at the expanse of the Tyr radical for the nucleotide reduction. The chemistry found in MauG is much like that found in ribonucleotide reductase and is more straightforward in terms of the nature of remote catalysis (*260*). The di-heme cofactor in MauG reacts with exogenous oxidants, generates high-valent Fe intermediate, and then transmits oxidizing equivalents to the substrate protein. Unquestionably cpd G or, *bis*-Fe(IV), is a new natural strategy discovered thus far for harnessing the problem of substrates way too large for an enzyme to accommodate. In this case, a remote catalysis must take place. Thus, the unprecedented *bis*-Fe(IV) intermediate found in MauG occupies an entry position for future study of long-range remote catalysis by

metalloenzymes.

After the discovery and identification of the tyrosyl radical in ribonucleotide reductase, numerous other protein radicals have been characterized and shown to play essential roles in enzyme mechanisms and in enzymes involved in many different metabolic pathways. The common feature among this group is that their activities metal-mediated involving Co, Cu, Fe, and Mn. In some cases additional protein factors and small molecules are required. These include flavins, heme, pterins, adenosylcobalamin, *S*-adenosylmethionine, and [4Fe-4S] clusters to name a few. Reactions catalyzed by radical-dependent proteins are very diverse and span a wide range of chemical transformations. These reactions include: reduction, electron transfer, carbon-carbon bond cleaving, O_2 evolution, and lyases. Additionally, free radicals are also involved in many biological processes such as: amino acid, carbohydrate, and hydrocarbon metabolism; coenzyme and cofactor biosynthesis; DNA biosynthesis and repair; and antibiotic biosynthesis. Even with recent understandings of radical mechanisms in enzymology, there are still many questions left unanswered including energetic of radical initiation but most are poorly understood from the standpoint of the energetics of radical initiation. With the high interest in free radical mechanisms in enzymology displayed today, these remaining questions will hopefully be answered.

REFERENCES

1. Gomberg, M. (1900) An instance of trivalent carbon: Triphenylmethyl. *J. Am. Chem. Soc. 22*, 757-771.
2. Wentrup, C. (2002) From Reactive Intermediates to Stable Compounds. *Science. 295*, 1846-1847.
3. Ehrenberg, A., and Reichard, P. (1972) Electron Spin Resonance of the Iron-containing Protein B2 from Ribonucleotide Reductase. *J. Biol. Chem. 247*, 3485-3488.
4. Hoganson, C. W., Sahlin, M., Sjöberg, B.-M., and Babcock, G. T. (1996) Electron Magnetic Resonance of the Tyrosyl Radical in Ribonucleotide Reductase from *Escherichia coli*. *J. Am. Chem. Soc. 118*, 4672-4679.
5. Frey, P. A., Hegeman, A. D., and Reed, G. H. (2006) Free Radical Mechanisms in Enzymology. *Chem. Rev. 106*, 3302-3316.
6. Stubbe, J., and van Der Donk, W. A. (1998) Protein Radicals in Enzyme Catalysis. *Chem. Rev. 98*, 705-762.
7. Reichard, P., and Ehrenberg, A. (1983) Ribonucleotide Reductase--A Radical Enzyme. *Science. 221*, 514-519.
8. Cheek, J., and Broderick, J. B. (2001) Adenosylmethionine-dependent iron-sulfur enzymes: versatile clusters in a radical new role. *J. Biol. Inorg. Chem. 6*, 209-226.
9. Layer, G., Verfurth, K., Mahlitz, E., and Jahn, D. (2002) Oxygen-Independent Coproporphyrinogen-III Oxidase HemN from *Escherichia coli*. *J. Biol. Chem. 277*, 34136-34142.
10. Kulzer, R., Pils, T., Kappl, R., Huttermann, J., and Knappe, J. (1998) Reconstitution and Characterization of the Polynuclear Iron-Sulfur Cluster in Pyruvate Formate-Lyase-Activating Enzyme - Molecular Properties of the Holoenzyme form. *J. Biol. Chem. 273*, 4897-4903.
11. Tamarit, J., Gerez, C., Meier, C., Mulliez, E., Trautwein, A., and Fontecave, M. (2000) The

Activating Component of the Anaerobic Ribonucleotide Reductase from *Escherichia coli* - An iron-sulfur center with only three cysteine. *J. Biol. Chem. 275*, 15669-15675.

12. de Montellano, P. R. O., and De Voss, J. J. (2002) Oxidizing species in the mechanism of cytochrome P450. *Nat. Prod. Rep. 19*, 477-493.
13. Tsou, T. T., Loots, M., and Halpern, J. (1982) Kinetic Determination of Transition Metal-Alkyl Bond Dissociation Energies: Application to Organocobalt Compounds Related to B12 Coenzymes. *J. Am. Chem. Soc. 104*, 623-624.
14. Vey, J. L., and Drennan, C. L. (2011) Structural Insights into Radical Generation by the Radical SAM Superfamily. *Chem. Rev. 111*, 2487-2506.
15. Krebs, C., Broderick, W. E., Henshaw, T. F., Broderick, J. B., and Huynh, B. H. (2002) Coordination of Adenosylmethionine to a Unique Iron Site of the [4Fe-4S] of Pyruvate Formate-Lyase Activating Enzyme: A Mössbauer Spectroscopic Study. *J. Am. Chem. Soc. 124*, 912-913.
16. Grillo, M. A., and Colombatto, S. (2007) S-adenosylmethionine and radical-based catalysis. *Amino Acids. 32*, 197-202.
17. Selmer, T., Pierik, A. J., and Heider, J. (2005) New glycyl radical enzymes catalysing key. metabolic steps in anaerobic bacteria. *Biol. Chem. 386*, 981-988.
18. Buckel, W., and Golding, B. T. (2006) Radical Enzymes in Anaerobes. *Annu. Rev. Microbiol. 60*, 27-49.
19. Wei, C. C., Crane, B. R., and Stuehr, D. J. (2003) Tetrahydrobiopterin Radical Enzymology. *Chem. Rev. 103*, 2365-2383.
20. Frey, P. A. (2001) Radical Mechanisms of Enzymatic Catalysis. *Annu. Rev. Biochem. 70*, 121-148.
21. Herrick, J., and Sclavi, B. (2007) Ribonucleotide Reductase and the Regulation of DNA Replication: An Old Story and an Ancient Heritage. *Mol. Microbiol. 63*, 22-34.
22. Reichard, P. (2002) Ribonucleotide reductases: The evolution of allosteric regulation. *Arch.*

Biochem. Biophys. 397, 149-155.

23. Eklund, H., Uhlin, U., Farnegardh, M., Logan, D. T., and Nordlund, P. (2001) Structure and function of the radical enzyme ribonucleotide reductase. *Prog. Biophys. Mol. Biol. 77*, 177-268.

24. Fontecave, M., and Gerez, C. (2002) Tyrosyl radicals and ribonucleotide reductase, In *Protein Sensors and Reactive Oxygen Species, Pt B, Thiol Enzymes and Proteins*, pp 21-30, Academic Press Inc, San Diego.

25. Sjoberg, B. M., and Sahlin, M. (2002) Thiols in redox mechanism of ribonucleotide reductase, In *Protein Sensors and Reactive Oxygen Species, Pt B, Thiol Enzymes and Proteins*, pp 1-21, Academic Press Inc, San Diego.

26. Fontecave, M., Mulliez, E., and Logan, D. T. (2002) Deoxyribonucleotide synthesis in anaerobic microorganisms: The class III ribonucleotide reductase, In *Progress in Nucleic Acid Research and Molecular Biology, Vol 72*, pp 95-127, Academic Press Inc, San Diego.

27. Graslund, A. (2002) Ribonucleotide reductase: Kinetic methods for demonstrating radical transfer pathway in protein R2 of mouse enzyme in generation of tyrosyl free radical, In *Enzyme Kinetics and Mechanism, Pt F: Detection and Characterization of Enzyme Reaction Intermediates*, pp 399-414, Academic Press Inc, San Diego.

28. Kolberg, M., Strand, K. R., Graff, P., and Andersson, K. K. (2004) Structure, function, and mechanism of ribonucleotide reductases. *Biochim. Biophys. Acta. 1699*, 1-34.

29. Cerqueira, N., Pereira, S., Fernandes, P. A., and Ramos, M. J. (2005) Overview of ribonucleotide reductase inhibitors: An appealing target in anti-tumour therapy. *Curr. Med. Chem. 12*, 1283-1294.

30. Han, W. G., Liu, T. Q., Lovell, T., and Noodleman, L. (2006) Seven clues to the origin and structure of class-I ribonucleotide reductase intermediate X. *J. Inorg. Biochem. 100*, 771-779.

31. Nordlund, N., and Reichard, P. (2006) Ribonucleotide Reductases. *Annu. Rev. Biochem. 75*, 681-

706.

32. Holmgren, A., and Sengupta, R. (2010) The use of thiols by ribonucleotide reductase. *Free Radic. Biol. Med. 49*, 1617-1628.

33. Hogbom, M. (2011) Metal use in ribonucleotide reductase R2, di-iron, di-manganese and heterodinuclear-an intricate bioinorganic workaround to use different metals for the same reaction. *Metallomics 3*, 110-120.

34. Jordan, A., and Reichard, P. (1998) Ribonucleotide Reductases. *Annu. Rev. Biochem. 67*, 71-98.

35. Reichard, P. (1993) From RNA to DNA, Why So Many Ribonucleotide Reductases? *Science. 260*, 1773-1777.

36. Jiang, W., Yun, D., Saleh, L., Barr, E. W., Xing, G., Hoffart, L. M., Maslak, M.-A., Krebs, C., and Bollinger, J. M. (2007) A Manganese(IV)/Iron(III) Cofactor in *Chlamydia trachomatis* Ribonucleotide Reductase. *Science. 316*, 1188-1191.

37. Knappe, J., and Sawers, G. (1990) A radical-chemical route to acetyl-CoA: the anaerobically induced pyruvate formate-lyase system of *Escherichia coli*. *FEMS. Microbiol. Rev. 75*, 383-398.

38. Buis, J. M., and Broderick, J. B. (2005) Pyruvate formate-lyase activating enzyme: elucidation of a novel mechanism for glycyl radical formation. *Arch. Biochem. Biophys. 433*, 288-296.

39. Knappe, J., and Volker Wagner, A. F. (2001) Stable glycyl radical from pyruvate formate-lyase and ribonucleotide reductase (III), In *Adv. Protein. Chem.* (Judith P. Klinman, J. E. D., Ed.), pp 277-315, Academic Press.

40. Wagner, A. F. V., Frey, M., Neugebauer, F. A., Schafer, W., and Knappe, J. (1992) The free radical in pyruvate formate-lyase is located on glycine-734. *Proc. Natl. Acad. Sci. U.S.A. 89*, 996-1000.

41. Debus, R. J. (1992) The manganese and calcium ions of photosynthetic oxygen evolution. *Biochim. Biophys. Acta. 1102*, 269-352.

42. Williamson, A., Conlan, B., Hillier, W., and Wydrzynski, T. (2011) The evolution of Photosystem II:

insights into the past and future. *Photosynthesis Research 107*, 71-86.

43. Guskov, A., Gabdulkhakov, A., Broser, M., Glöckner, C., Hellmich, J., Kern, J., Frank, J., Müh, F., Saenger, W., and Zouni, A. (2010) Recent progress in the crystallographic studies of photosystem II. *ChemPhysChem 11*, 1160-1171.

44. Siegbahn, P. E. M. (2009) Structures and energetics for O2 formation in photosystem II. *Accounts of Chemical Research 42*, 1871-1880.

45. Pospísil, P. (2009) Production of reactive oxygen species by photosystem II. *Biochim. Biophys. Acta. 1787*, 1151-1160.

46. Fromme, P., Yu, H., DeRuyter, Y. S., Jolley, C., Chauhan, D. K., Melkozernov, A., and Grotjohann, I. (2006) Structure of photosystems I and II. *Comptes Rendus Chimie 9*, 188-200.

47. Tommos, C., Tang, X.-S., Warncke, K., Hoganson, C. W., Styring, S., McCracken, J., Diner, B. A., and Babcock, G. T. (1995) Spin-Density Distribution, Conformation, and Hydrogen Bonding of the Redox-Active Tyrosine YZ in Photosystem II from Multiple-Electron Magnetic-Resonance Spectroscopies: Implications for Photosynthetic Oxygen Evolution. *J. Am. Chem. Soc. 117*, 10325-10335.

48. Faller, P., Debus, R. J., Brettel, K., Sugiura, M., Rutherford, A. W., and Boussac, A. (2001) Rapid formation of the stable tyrosyl radical in photosystem II. *Proc. Natl. Acad. Sci. U.S.A. 98*, 14368-14373.

49. Diner, B. A. (2001) Amino acid residues involved in the coordination and assembly of the manganese cluster of photosystem II. Proton-coupled electron transport of the redox-active tyrosines and its relationship to water oxidation. *Biochim. Biophys. Acta. 1503*, 147-163.

50. Dorlet, P., Rutherford, A. W., and Un, S. (2000) Orientation of the Tyrosyl D, Pheophytin Anion, and Semiquinone QA•- Radicals in Photosystem II Determined by High-Field Electron Paramagnetic Resonance. *Biochemistry. 39*, 7826-7834.

51. Un, S., Tang, X.-S., and Diner, B. A. (1996) 245 GHz high-field EPR study of tyrosine-D° and tyrosine-Z° in mutants of photosystem II. *Biochemistry. 35*, 679-684.

52. Babcock, G. T., Barry, B. A., Debus, R. J., Hoganson, C. W., Atamian, M., McIntosh, L., Sithole, I., and Yocum, C. F. (1989) Water oxidation in photosystem II: From radical chemistry to multielectron chemistry. *Biochemistry. 28*, 9557-9565.

53. Rutherford, A. W., Boussac, A., and Faller, P. (2004) The stable tyrosyl radical in photosystem II: Why D? *Biochim. Biophys. Acta. 1655*, 222-230.

54. Whittaker, J. W. (2005) The radical chemistry of galactose oxidase. *Arch. Biochem. Biophys. 433*, 227-239.

55. Whittaker, J. W. (2003) Free Radical Catalysis by Galactose Oxidase. *Chem. Inform. 34*, no-no.

56. Whittaker, J. (2002) Galactose oxidase. *Adv. Protein. Chem. 60*, 1.

57. Branchaud, B. P., and Turner, B. E. (2002) Galactose oxidase: Probing radical mechanism with ultrafast radical probe, In *Methods. Enzymol.* (Daniel, L. P., Ed.), pp 415-425, Academic Press.

58. Jazdzewski, B. A., and Tolman, W. B. (2000) Understanding the copper-phenoxyl radical array in galactose oxidase: contributions from synthetic modeling studies. *Coord. Chem. Rev. 200-202*, 633-685.

59. Whittaker, M. M., and Whittaker, J. W. (1990) A Tyrosine-Derived Free Radical in Apogalactose Oxidase. *J. Biol. Chem. 265*, 9610-9613.

60. Ito, N., Phillips, S. E. V., Stevens, C., Ogel, Z. B., McPherson, M. J., Keen, J. N., Yadav, K. D. S., and Knowles, P. F. (1991) Novel thioether bond revealed by a 1.7 Å crystal structure of galactose oxidase. *Nature. 350*, 87-90.

61. Ito, N., Phillips, S. E. V., Yadav, K. D. S., and Knowles, P. F. (1994) Crystal Structure of a Free Radical Enzyme, Galactose Oxidase. *J. Mol. Biol. 238*, 704-814.

62. Whittaker, M. M., and Whittaker, J. W. (1988) The Active Site of Galactose Oxidase. *J. Biol.*

Chem. 263, 6074-6080.

63. Whittaker, M. M., DeVito, V. L., Asher, S. A., and Whittaker, J. W. (1989) Resonance Raman Evidence for Tyrosine Involvement in the Radical Site of Galactose Oxidase. *J. Biol. Chem. 264*, 7104-7106.

64. Debus, R. J., Barry, B. A., Sithole, I., Babcock, G. T., and McIntosh, L. (1988) Directed Mutagenesis Indicates That the Donor to P^{+680} in Photosystem II is Tyrosine-161 of the D1 Polypeptide. *Biochemistry. 27*, 9071-9074.

65. Metz, J. G., Nixon, P. J., Rogner, M., Brudvig, G. W., and Diner, B. A. (1989) Directed alteration of the D1 Polypeptide of Potosystem II: Evidence that Tyrosine-161 is the Redox Component, Z, Connecting the Oxygen-Evolving Complex to the Primary Electron Donor, P680. *Biochemistry. 28*, 6960-6969.

66. Debus, R. J., Barry, B. A., Babcock, G. T., and McIntosh, L. (1988) Site-directed mutagenesis identifies a tyrosine radical involved in the photosynthetic oxygen-evolving system. *Proc. Natl. Acad. Sci. U.S.A. 85*, 427-430.

67. Vermass, W. F. J., Rutherford, A. W., and Hansson, Ö. (1988) Site-directed mutagenesis in photosystem II of the cyanobacterium Synechocystis sp. PCC 6803: Donor D is a tyrosine residue in the D2 protein. *Proc. Natl. Acad. Sci. U.S.A. 85*, 8477-8481.

68. Poulos, T. L. (2010) Thirty years of heme peroxidase structural biology. *Arch. Biochem. Biophys. 500*, 3-12.

69. Atack, J. M., and Kelly, D. J. (2006) Structure, Mechanism and Physiological Roles of Bacterial Cytochrome c Peroxidases, In *Adv. Microb. Physiol.* (Robert, K. P., Ed.), pp 73-106, Academic Press.

70. Bonagura, C. A., Bhaskar, B., Shimizu, H., Li, H., Sundaramoorthy, M., McRee, D. E., Goodin, D. B., and Poulos, T. L. (2003) High-Resolution Crystal Structures and Spectroscopy of Native and

Compound I Cytochrome *c* Peroxidase. *Biochemistry. 42*, 5600-5608.

71. Erman, J. E., and Vitello, L. B. (2002) Yeast cytochrome c peroxidase: mechanistic studies via protein engineering. *Biochim. Biophys. Acta. 1597*, 193-220.

72. Lang, G., Spartalian, K., and Yonetani, T. (1976) Mössbauer Spectroscopic Study of Compound ES of Cytochrome *c* Peroxidase. *Biochim. Biophys. Acta. 451*, 250-258.

73. Sivaraja, M., Goodin, D., Smith, M., and Hoffman, B. (1989) Identification by ENDOR of Trp191 as the free-radical site in cytochrome c peroxidase compound ES. *Science. 245*, 738-740.

74. Dolphin, D., Forman, A., Borg, D. C., Fajer, J., and Felton, R. H. (1971) Compounds I of Catalase and Horse Radish Peroxidase: π-Cation Radicals. *Proc. Natl. Acad. Sci. U.S.A. 68*, 614-618.

75. Benecky, M. J., Frew, J. E., Scowen, N., Jones, P., and Hoffman, B. M. (1993) EPR and ENDOR Detection of Compound I from *Micrococcus lysodeikticus* Catalase. *Biochemistry. 32*, 11929-11933.

76. Patterson, W. R., Poulos, T. L., and Goodin, D. B. (1995) Identification of a Porphyrin π Cation Radical in Ascorbate Peroxidase Compound I. *Biochemistry. 34*, 4342-4345.

77. Schenk, W. A. (2000) Isopenicillin N Synthase: An Enzyme at Work. *Angew. Chem. Int. Ed. Engl. 39*, 3409-3411.

78. Baldwin, J. E., and Bradley, M. (1990) Isopenicillin N synthase: mechanistic studies. *Chem. Rev. 90*, 1079-1088.

79. Sim, T. S., and Loke, P. (2000) Molecular studies on isopenicillin N synthases. *Appl. Micriobiol. Biotech. 54*, 1-8.

80. Mizutani, M., and Sato, F. (2011) Unusual P450 reactions in plant secondary metabolism. *Arch. Biochem. Biophys. 507*, 194-203.

81. Guengerich, F. P., Sohl, C. D., and Chowdhury, G. (2011) Multi-step oxidations catalyzed by cytochrome P450 enzymes: Processive vs. distributive kinetics and the issue of carbonyl

oxidation in chemical mechanisms. *Arch. Biochem. Biophys. 507*, 126-134.

82. de Montellano, P. R. O., and Nelson, S. D. (2011) Rearrangement reactions catalyzed by cytochrome P450s. *Arch. Biochem. Biophys. 507*, 95-110.

83. Conner, K. P., Woods, C. M., and Atkins, W. M. (2011) Interactions of cytochrome P450s with their ligands. *Arch. Biochem. Biophys. 507*, 56-65.

84. Jung, C., de Vries, S., and Schunemann, V. (2011) Spectroscopic characterization of cytochrome P450 Compound I. *Arch. Biochem. Biophys. 507*, 44-55.

85. Jung, C. (2011) The mystery of cytochrome P450 Compound I: A mini-review dedicated to Klaus Ruckpaul. *Biochim. Biophys. Acta. 1814*, 46-57.

86. Omura, T. (2010) Structural diversity of cytochrome P450 enzyme system. *J. Biochem. 147*, 297-306.

87. Makris, T. M., von Koenig, K., Schlichting, I., and Sligar, S. G. (2006) The status of high-valent metal oxo complexes in the P450 cytochromes. *J. Inorg. Biochem. 100*, 507-518.

88. Cojocaru, V., Winn, P. J., and Wade, R. C. (2007) The ins and outs of cytochrome P450s. *Biochim. Biophys. Acta. 1770*, 390-401.

89. Isin, E. M., and Guengerich, F. P. (2007) Complex reactions catalyzed by cytochrome P450 enzymes. *Biochim. Biophys. Acta. 1770*, 314-329.

90. Green, M. T. (2009) C-H bond activation in heme proteins: the role of thiolate ligation in cytochrome P450. *Curr. Opin. Chem. Biol. 13*, 84-88.

91. Guengerich, F. P. (2001) Uncommon P450-catalyzed reactions. *Curr. Drug. Metab. 2*, 93-115.

92. Guengerich, F. P. (2002) Rate-limiting steps in cytochrome P450 catalysis. *Biol. Chem. 383*, 1553-1564.

93. Newcomb, M., and Chandrasena, R. E. P. (2005) Highly reactive electrophilic oxidants in cytochrome P450 catalysis. *Biochem. Biophys. Res. Commun. 338*, 394-403.

94. Meunier, B., de Visser, S. P., and Shaik, S. (2004) Mechanism of Oxidation Reactions Catalyzed by Cytochrome P450 Enzymes. *Chem. Rev. 104*, 3947-3980.

95. Smith, W. L., and Marnett, L. J. (1991) Prostaglandin endoperoxide synthase: Structure and catalysis. *Biochim. Biophys. Acta. 1083*, 1-17.

96. Helliwell, R. J. A., Adams, L. F., and Mitchell, M. D. (2004) Prostaglandin synthases: recent developments and a novel hypothesis. *Prostaglandins, Leukotrienes and Essential Fatty Acids 70*, 101-113.

97. Kulmacz, R. J., van der Donk, W. A., and Tsai, A.-L. (2003) Comparison of the properties of prostaglandin H synthase-1 and -2. *Prog. Lipid. Res. 42*, 377-404.

98. Tsai, A.-L., and Kulmacz, R. J. (2000) Tyrosyl Radicals in Prostaglandin H Synthase-1 and -2. *Prostag. Oth. Lipid. M. 62*, 231-254.

99. Karthein, R., Dietz, R., Nastainczyk, W., and Ruf, H. H. (1988) Higher oxidation states of prostaglandin H synthase. *Eur. J Biochem. 171*, 313-320.

100. Rouzer, C. A., and Marnett, L. J. (2003) Mechanism of Free Radical Oxygenation of Polyunsaturated Fatty Acids by Cyclooxygenases. *Chem. Rev. 103*, 2239-2304.

101. Kulmacz, R. J., Ren, Y., Tsai, A. L., and Palmer, G. (1990) Prostaglandin H Synthase: Spectroscopic Studies of the Interaction With Hydroperoxides and With Indomethacin. *Biochemistry. 29*, 8760-8771.

102. Tsai, A.-l., Wu, G., Palmer, G., Bambai, B., Koehn, J. A., Marshall, P. J., and Kulmacz, R. J. (1999) Rapid Kinetics of Tyrosyl Radical Formation and Heme Redox State Changes in Prostaglandin H Synthase-1 and -2. *J. Biol. Chem. 274*, 21695-21700.

103. Kulmacz, R. J., and Lands, W. E. (1985) Stoichiometry and Kinetics of the Interaction of Prostaglandin H Synthase with Anti-Inflammatory Agents. *J. Biol. Chem. 260*, 12572-12578.

104. DeGray, J. A., Lassmann, G., Curtis, J. F., Kennedy, T. A., Marnett, L. J., Eling, T. E., and Mason, R.

P. (1992) Spectral Analysis of the Protein-Derived Tyrosyl Radicals from Prostaglandin H Synthase. *J. Biol. Chem. 267*, 23583-23588.

105. Tsai, A. L., Palmer, G., and Kulmacz, R. J. (1992) Prostaglandin H Synthase. Kinetics of Ttyrosyl Radical Formation and of Cyclooxygenase Catalysis. *J. Biol. Chem. 267*, 17753-17759.

106. Tsai, A., Hsi, L. C., Kulmacz, R. J., Palmer, G., and Smith, W. L. (1994) Characterization of the Tyrosyl Radicals in Ovine Prostaglandin H Synthase-1 by Isotope Replacement and Site-directed Mutagenesis. *J. Biol. Chem. 269*, 5085-5091.

107. Shi, W., Hoganson, C. W., Espe, M., Bender, C. J., Babcock, G. T., Palmer, G., Kulmacz, R. J., and Tsai, A.-l. (2000) Electron Paramagnetic Resonance and Electron Nuclear Double Resonance Spectroscopic Identification and Characterization of the Tyrosyl Radicals in Prostaglandin H Synthase 1. *Biochemistry. 39*, 4112-4121.

108. Rogge, C. E., Liu, W., Wu, G., Wang, L.-H., Kulmacz, R. J., and Tsai, A.-L. (2004) Identification of Tyr504 as an Alternative Tyrosyl Radical Site in Human Prostaglandin H Synthase-2. *Biochemistry. 43*, 1560-1568.

109. Rogge, C. E., Liu, W., Kulmacz, R. J., and Tsai, A.-L. (2009) Peroxide-induced radical formation at TYR385 and TYR504 in human PGHS-1. *J. Inorg. Biochem. 103*, 912-922.

110. Tsai, A.-L., and Kulmacz, R. J. (2010) Prostaglandin H synthase: Resolved and unresolved mechanistic issues. *Arch. Biochem. Biophys. 493*, 103-124.

111. Mansoorabadi, S. O., Padmakumar, R., Fazliddinova, N., Vlasie, M., Banerjee, R., and Reed, G. H. (2005) Characterization of a Succinyl-CoA Radical−Cob(II)alamin Spin Triplet Intermediate in the Reaction Catalyzed by Adenosylcobalamin-Dependent Methylmalonyl-CoA Mutase†. *Biochemistry. 44*, 3153-3158.

112. Padmakumar, R., and Banerjee, R. (1995) Evidence from Electron Paramagnetic Resonance Spectroscopy of the Participation of Radical Intermediates in the Reaction Catalyzed by

Methylmalonyl-coenzyme A Mutase. *J. Biol. Chem. 270*, 9295-9300.

113. Frey, P. A., and Booker, S. J. (2001) Radical Mechanisms of S-Adenosylmethionine-Dependent Enzymes, In *Adv. Protein. Chem.* (Judith P. Klinman, J. E. D., Ed.), pp 1-45, Academic Press.

114. Frey, P. A., and Magnusson, O. T. (2003) S-Adenosylmethionine: A Wolf in Sheep's Clothing, or a Rich Man's Adenosylcobalamin? *Chem. Rev. 103*, 2129-2148.

115. Spolitak, T., Dawson, J. H., and Ballou, D. P. (2005) Reaction of Ferric Cytochrome P450cam with Peracids. *J. Biol. Chem. 280*, 20300-20309.

116. Dorlet, P., Seibold, S. A., Babcock, G. T., Gerfen, G. J., Smith, W. L., Tsai, A.-l., and Un, S. (2002) High-Field EPR Study of Tyrosyl Radicals in Prostaglandin H2 Synthase-1. *Biochemistry. 41*, 6107-6114.

117. Lieder, K. W., Booker, S., Ruzicka, F. J., Beinert, H., Reed, G. H., and Frey, P. A. (1998) S-Adenosylmethionine-Dependent Reduction of Lysine 2,3-Aminomutase and Observation of the Catalytically Functional Iron−Sulfur Centers by Electron Paramagnetic Resonance. *Biochemistry. 37*, 2578-2585.

118. Tittmann, K., and Wille, G. (2009) X-Ray crystallographic snapshots of reaction intermediates in pyruvate oxidase and transketolase illustrate common themes in thiamin catalysis. *J. Mol. Catal. B. Enzym. 61*, 93-99.

119. Tittmann, K., Wille, G., Golbik, R., Weidner, A., Ghisla, S., and Hübner, G. (2005) Radical Phosphate Transfer Mechanism for the Thiamin Diphosphate- and FAD-Dependent Pyruvate Oxidase from *Lactobacillus plantarum*. Kinetic Coupling of Intercofactor Electron Transfer with Phosphate Transfer to Acetyl-thiamin Diphosphate via a Transient FAD Semiquinone/Hydroxyethyl-ThDP Radical Pair. *Biochemistry. 44*, 13291-13303.

120. Tittmann, K., Golbik, R., Ghisla, S., and Hübner, G. (2000) Mechanism of Elementary Catalytic Steps of Pyruvate Oxidase from Lactobacillus plantarum. *Biochemistry. 39*, 10747-10754.

121. Jordan, A., Pontis, E., Aslund, F., Hellman, U., Gibert, I., and Reichard, P. (1996) The Ribonucleotide Reductase System of *Lactococcus lactis* - Characterization of an NrdEF enzyme and a new electron transport protein. *J. Biol. Chem. 271*, 8779-8785.

122. Bianchi, V., Eliasson, R., Fontecave, M., Mulliez, E., Hoover, D. M., Matthews, R. G., and Reichard, P. (1993) Flavodoxin Is Required for the Activation of the Anaerobic Ribonucleotide Reductase. *Biochem. Biophys. Res. Commun. 197*, 792-797.

123. Bianchi, V., Reichard, P., Eliasson, R., Pontis, E., Krook, M., Jornvall, H., and Haggardljungouist, E. (1993) *Escherichia coli* Ferredoxin NADP+ Reductase: Activation of *E. coli* Anaerobic Ribonucleotide Reduction, Cloning of the Gene (fpr), and Overexpression of the Protein. *J. Bacteriol. 175*, 1590-1595.

124. Stubbe, J., Ator, M., and Krenitsky, T. (1983) Mechanism of Ribonucleoside Diphosphate Reductase from *Escherichia coli*. Evidence for 3'-C--H Bond Cleavage. *J. Biol. Chem. 258*, 1625-1631.

125. Stubbe, J. (2003) Di-iron-tyrosyl radical ribonucleotide reductases. *Curr. Opin. Chem. Biol. 7*, 183-188.

126. Licht, S., Gerfen, G. J., and Stubbe, J. (1996) Thiyl Radicals in Ribonucleotide Reductases. *Science. 271*, 477-481.

127. Sahlin, M., and SjΛberg, B.-M. (2002) Ribonucleotide Reductase A Virtual Playground for Electron Transfer Reactions, In *Enzyme-Catalyzed Electron and Radical Transfer* (Holzenburg, A., and Scrutton, N., Eds.), pp 405-443, Springer US.

128. Persson, A. L., Sahlin, M., and Sjöberg, B.-M. (1998) Cysteinyl and Substrate Radical Formation in Active Site Mutant E441Q of *Escherichia coli* Class I Ribonucleotide Reductase. *J. Biol. Chem. 273*, 31016-31020.

129. Nicholls, P., Fita, I., and Loewen, P. C. (2001) Enzymology and structure of catalases, In *Advances*

in Inorganic Chemistry, Vol 51, pp 51-106, Academic Press Inc, San Diego.

130. Kirkman, H. N., and Gaetani, G. F. (2007) Mammalian catalase: A venerable enzyme with new mysteries. *Trends. Biochem. Sci. 32*, 44-50.

131. Chelikani, P., Fita, I., and Loewen, P. C. (2004) Diversity of Structures and Properties Among Catalases. *Cell. Mol. Life. Sci. 61*, 192-208.

132. Klotz, M. G., and Loewen, P. C. (2003) The Molecular Evolution of Catalatic Hydroperoxidases: Evidence for Multiple Lateral Transfer of Genes Between Prokaryota and from Bacteria into Eukaryota. *Mol. Biol. Evol. 20*, 1098-1112.

133. Alfonso-Prieto, M., Borovik, A., Carpena, X., Murshudov, G., Melik-Adamyan, W., Fita, I., Rovira, C., and Loewen, P. C. (2007) The Structures and Electronic Con**fig**uration of Compound I Intermediates of Helicobacter pylori and Penicillium vitale Catalases Determined by X-Ray Crystallography and QM/MM Density Functional Theory Calculations. *J. Am. Chem. Soc. 129*, 4193-4205.

134. Maté, M. J., Zamocky, M., Nykyri, L. M., Herzog, C., Alzari, P. M., Betzel, C., Koller, F., and Fita, I. (1999) Structure of catalase-A from *Saccharomyces cerevisiae*. *J. Mol. Biol. 286*, 135-149.

135. Putnam, C. D., Arvai, A. S., Bourne, Y., and Tainer, J. A. (2000) Active and inhibited human catalase structures: ligand and NADPH binding and catalytic mechanism. *J. Mol. Biol. 296*, 295-309.

136. Kirkman, H. N., Galiano, S., and Gaetani, G. F. (1987) The Function of Catalase-bound NADPH. *J. Biol. Chem. 262*, 660-666.

137. Almarsson, O., Sinha, A., Gopinath, E., and Bruice, T. C. (1993) Mechanism of One-electron Oxidation of NAD(P)H and Function of NADPH Bound to Catalase. *J. Am. Chem. Soc. 115*, 7093-7102.

138. Hillar, A., Nicholls, P., Switala, J., and Loewen, P. C. (1994) NADPH binding and control of

catalase Compound II formation: Comparison of bovine, yeast, and *Escherichia coli* enzymes. *Biochem. J. 300*, 531-539.

139. Fita, I., and Rossmann, M. G. (1985) The Active Center of Catalase. *J. Mol. Biol. 185*, 21-37.

140. Murshudov, G. N., Melik-Adamyan, W. R., Grebenko, A. I., Barynin, V. V., Vagin, A. A., Vainshtein, B. K., Dauter, Z., and Wilson, K. S. (1992) Three-dimensional structure of catalase from *Micrococcus lysodeikticus* at 1.5 Å resolution. *FEBS. Lett. 312*, 127-131.

141. Jeschke, G. (2005) EPR techniques for studying radical enzymes. *Biochim. Biophys. Acta. 1707*, 91-102.

142. Duboc-Toia, C., Hassan, A. K., Mulliez, E., Ollagnier-de Choudens, S., Fontecave, M., Leutwein, C., and Heider, J. (2002) Very High-Field EPR Study of Glycyl Radical Enzymes. *J. Am. Chem. Soc. 125*, 38-39.

143. Bleifuss, G., Kolberg, M., Pötsch, S., Hofbauer, W., Bittl, R., Lubitz, W., Gräslund, A., Lassmann, G., and Lendzian, F. (2001) Tryptophan and Tyrosine Radicals in Ribonucleotide Reductase: A Comparative High-Field EPR Study at 94 GHz. *Biochemistry. 40*, 15362-15368.

144. Huyett, J. E., Doan, P. E., Gurbiel, R., Houseman, A. L. P., Sivaraja, M., Goodin, D. B., and Hoffman, B. M. (1995) Compound ES of Cytochrome c Peroxidase Contains a Trp π-Cation Radical: Characterization by CW and Pulsed Q-Band ENDOR Spectroscopy. *J. Am. Chem. Soc. 117*, 9033-9041.

145. Hoffman, B. M., Roberts, J. E., Kang, C. H., and Margoliash, E. (1981) Electron Paramagnetic and Electron Nuclear Double Resonance of the Hydrogen Peroxide Compound of Cytochrome *c* Peroxidase. *J. Biol. Chem. 256*, 6556-6564.

146. Lendzian, F., Sahlin, M., MacMillan, F., Bittl, R., Fiege, R., Pötsch, S., Sjöberg, B.-M., Gräslund, A., Lubitz, W., and Lassmann, G. (1996) Electronic Structure of Neutral Tryptophan Radicals in Ribonucleotide Reductase Studied by EPR and ENDOR Spectroscopy. *J. Am. Chem. Soc. 118*,

8111-8120.

147. Hoganson, C. W., and Babcock, G. T. (1992) Protein-Tyrosyl Radical Interactions in Photosystem II Studied by Electron Spin Resonance and Electron Nuclear Double Resonance Spectroscopy: Comparison with Ribonucleotide Reductase and in Vitro Tyrosine. *Biochemistry. 31*, 11874-11880.

148. Barry, B. A., el-Deeb, M. K., Sandusky, P. O., and Babcock, G. T. (1990) Tyrosine radicals in photosystem II and related model compounds. Characterization by isotopic labeling and EPR spectroscopy. *J. Biol. Chem. 265*, 20139-20143.

149. Babcock, G. T., Espe, M., Hoganson, C. W., McCracken, J., Styring, S., Tommos, C., and Warncke, K. (1997) Tyrosyl Radicals in Enzyme Catalysis: Some Properties and a Focus on Photosynthetic Water Oxidation. *Acta. Chem. Scand. 51*, 533.

150. Warncke, K., McCracken, J., and Babcock, G. T. (1994) Structure of the Y_D Tyrosine Radical in Photosystem II as Revealed by ^2H Electron Spin Echo Envelope Modulation (ESEEM) Spectroscopic Analysis of Hydrogen Hyperfine Interactions. *J. Am. Chem. Soc. 116*, 7332-7340.

151. Khindaria, A., and Aust, S. D. (1996) EPR Detection and Characterization of Lignin Peroxidase Porphyrin π-Cation Radical. *Biochemistry. 35*, 13107-13111.

152. Schulz, C. E., Devaney, P. W., Winkler, H., Debrunner, P. G., Doan, N., Chiang, R., Rutter, R., and Hager, L. P. (1979) Horseradish peroxidase Compound I: Evidence for spin coupling between the heme iron and a "Free" radical. *FEBS. Lett. 103*, 102-105.

153. Rutter, R., Hager, L. P., Dhonau, H., Hendrich, M., Valentine, M., and Debrunner, P. (1984) Chloroperoxidase Compound I: Electron Paramagnetic Resonance and Mössbauer Studies. *Biochemistry. 23*, 6809-6816.

154. Hu, S. H., and Kincaid, J. R. (1992) Resonance Raman studies of the carbonmonoxy form of catalase: Evidence for and effects of phenolate ligation. *FEBS. Lett. 314*, 293-296.

155. Poulos, T. L., Edwards, S. L., Wariishi, H., and Gold, M. H. (1993) Crystallographic Refinement of Lignin Peroxidase at 2 Å. *J. Biol. Chem. 268*, 4429-4440.

156. Zhang, Y., Kang, S. A., Mukherjee, T., Bale, S., Crane, B. R., Begley, T. P., and Ealick, S. E. (2007) Crystal Structure and Mechanism of Tryptophan 2,3-Dioxygenase, a Heme Enzyme Involved in Tryptophan Catabolism and in Quinolinate Biosynthesis. *Biochemistry. 46*, 145-155.

157. Gupta, R., Fu, R., Liu, A., and Hendrich, M. P. (2010) EPR and Mössbauer Spectroscopy Show Inequivalent Hemes in Tryptophan Dioxygenase. *J. Am. Chem. Soc. 132*, 1098-1109.

158. Fukumura, E., Sugimoto, H., Misumi, Y., Ogura, T., and Shiro, Y. (2009) Cooperative binding of L-Trp to human tryptophan 2,3-dioxygenase: resonance Raman spectroscopic analysis. *J. Biochem. 145*, 505-515.

159. Ishimura, Y., Nozaki, M., Hayaishi, O., Nakamura, T., Tamura, M., and Yamazaki, I. (1970) The Oxygenated Form of L-Tryptophan 2,3-Dioxygenase as Reaction Intermediate. *J. Biol. Chem. 245*, 3593-3602.

160. Becke, A. D. (1993) Density-Functional Thermochemistry. III. The role of exact exchange. *J. Chem. Phys. 98*, 5648-5652.

161. Wachters, A. J. (1970) Gaussian Basis Set for Molecular Wavefunctions Containing Third-Row Atoms. *J. Chem. Phys. 52*, 1033-1036.

162. Ling, Y., Davidson, V. L., and Zhang, Y. (2010) Unprecedented Fe(IV) Species in A Diheme Protein MauG: A Quantum Chemical Investigation on the Unusual Mössbauer Spectroscopic Properties. *J. Phys. Chem. Lett. 1*, 2936-2939.

163. Zhang, Y., and Oldfield, E. (2004) Cytochrome P450: An investigation of the Mössbauer spectra of a reaction intermediate and an Fe(IV)=O model system. *J. Am. Chem. Soc. 126*, 4470-4471.

164. Becke, A. D. (1988) Density-functional exchange-energy approximation with correct asymptotic behavior. *Phys. Rev. A. 38*, 3098-3100.

165. Perdew, J. P., Burke, K., and Wang, Y. (1996) Generalized gradient approximation for the exchange-correlation hole of a many-electron system. *Phys. Rev. B 54*, 16533-16539.

166. Kotake, Y., and Masayama, I. (1936) The intermediary metabolism of tryptophan. XVIII. The mechanism of formation of kynurenine from tryptophan. *Hoppe. Seylers. Z. Physiol. Chem. 243*, 237-244.

167. Yamamoto, S., and Hayaishi, O. (1970) Tryptophan 2,3-dioxygenase (Tryptophan Pyrrolase) (Rabit Inestine). *Methods Enzymol. 17*, 434-438.

168. Feigelson, P., and Greengard, O. (1961) The isolation of the apoprotein of the heme enzyme tryptophan pyrrolase. *Biochim. Biophys. Acta. 50*, 200-202.

169. Stone, T. W., and Darlington, L. G. (2002) Endogenous kynurenines as targets for drug discovery and development. *Nat. Rev. Drug. Discov. 1*, 609-620.

170. Kurnasov, O., Goral, V., Colabroy, K., Gerdes, S., Anantha, S., Osterman, A., and Begley, T. P. (2003) NAD biosynthesis: Identification of the Tryptophan to Quinolinate Pathway in Bacteria. *Chem. Biol. 10*, 1195-1204.

171. Schwarcz, R. (2004) The kynurenine pathway of tryptophan degradation as a drug target. *Curr. Opin. Pharmacol. 4*, 12-17.

172. Hayaishi, O. (1993) MY Life With Tryptophan - Never a dull moment. *Protein. Sci. 2*, 472-475.

173. Sugimoto, H., Oda, S. I., Otsuki, T., Hino, T., Yoshida, T., and Shiro, Y. (2006) Crystal structure of human indoleamine 2,3-dioxygenase: Catalytic mechanism of O-2 incorporation by a heme-containing dioxygenase. *Proc. Natl. Acad. Sci. U.S.A. 103*, 2611-2616.

174. Forouhar, F., Anderson, J. L., Mowat, C. G., Vorobiev, S. M., Hussain, A., Abashidze, M., Bruckmann, C., Thackray, S. J., Seetharaman, J., Tucker, T., Xiao, R., Ma, L. C., Zhao, L., Acton, T. B., Montelione, G. T., Chapman, S. K., and Tong, L. (2007) Molecular Insights into Substrate Recognition and Catalysis by Tryptophan 2,3-Dioxygenase. *Proc. Natl. Acad. Sci. U.S.A. 104*, 473-

478.

175. Tanaka, T., and Knox, W. E. (1959) The Nature and Mechanism of the Tryptophan Pyrrolase (Peroxidase-Oxidase) Reaction of Pseudomonas and of Rat Liver. *J. Biol. Chem. 234*, 1162-1170.

176. Takikawa, O. (2005) Biochemical and medical aspects of the indoleamine 2,3-dioxygenase-initiated l-tryptophan metabolism. *Biochem. Biophys. Res. Commun. 338*, 12-19.

177. Paglino, A., Lombardo, F., Arcà, B., Rizzi, M., and Rossi, F. (2008) Purification and biochemical characterization of a recombinant *Anopheles gambiae* tryptophan 2,3-dioxygenase expressed in Escherichia coli. *Insect Biochemistry and Molecular Biology 38*, 871-876.

178. Li, J. S., Han, Q., Fang, J., Rizzi, M., James, A. A., and Li, J. (2007) Biochemical mechanisms leading to tryptophan 2,3-dioxygenase activation. *Arch. Insect. Biochem. Physiol. 64*, 74-87.

179. Colabroy, K. L., and Begley, T. P. (2005) Tryptophan Catabolism: Identification and Characterization of a New Degradative Pathway. *J. Bacteriol. 187*, 7866-7869.

180. De Laurentis, W., Khim, L., Anderson, J. L. R., Adam, A., Phillips, R. S., Chapman, S. K., van Pee, K.-H., and Naismith, J. H. (2007) The Second Enzyme in Pyrrolnitrin Biosynthetic Pathway Is Related to the Heme-Dependent Dioxygenase Superfamily. *Biochemistry. 46*, 12393-12404.

181. KÜHn, H., GÖTze, R., Schewe, T., and Rapoport, S. M. (1981) Quasi-Lipoxygenase Activity of Haemoglobin. *Eur. J Biochem. 120*, 161-168.

182. Rao, S. I., Wilks, A., Hamberg, M., and Ortiz de Montellano, P. R. (1994) The lipoxygenase activity of myoglobin. Oxidation of linoleic acid by the ferryl oxygen rather than protein radical. *J. Biol. Chem. 269*, 7210-7216.

183. Knox, W. E., and Mehler, A. H. (1950) The Conversion of Tryptophan to Kynurenine in Liver. I. The coupled tryptophan peroxidase-oxidase system forming formylkynurenine. *J. Biol. Chem. 187*, 419-430.

184. Brady, F. O., Forman, H. J., and Feigelson, P. (1971) The Role of Superoxide and Hydroperoxide in

the Reductive Activation of Tryptophan-2,3-dioxygenase. *J. Biol. Chem. 246*, 7119-7124.

185. Debrunner, P. G. (1989) *Iron Porphyrins*, Vol. III, VCH, New York.

186. Münck, E. (2000) *Aspects of 57-Fe Mössbauer Spectroscopy*, University Science Books, Saussalito, CA.

187. Liu, A. (2009) Electron Paramagnetic Resonance (EPR) in Enzymology. *Wiley Encycl. Chem. Biol. 1*, 591-601.

188. Yonetani, T. (1965) Studies on Cytochrome *c* Peroxidase. *J. Biol. Chem. 240*, 4509-4514.

189. Mehler, A. H., and Knox, W. E. (1950) The Conversion of Tryptophan to Kynurenine in Liver. II. The enzymatic hydrolysis of formyl kynurenine. *J. Biol. Chem. 187*, 431-438.

190. Basran, J., Rafice, S. A., Chauhan, N., Efimov, I., Cheesman, M. R., Ghamsari, L., and Lloyd Raven, E. (2008) A Kinetic, Spectroscopic, and Redox Study of Human Tryptophan 2,3-Dioxygenase. *Biochemistry. 47*, 4752-4760.

191. Dalosto, S. D., Vanderkooi, J. M., and Sharp, K. A. (2004) Vibrational Stark Effects on Carbonyl, Nitrile, and Nitrosyl Compounds Including Heme Ligands, CO, CN, and NO, Studied With Density Functional Theory. *J. Phys. Chem. B. 108*, 6450-6457.

192. Koppenol, W. H. (1987) Thermodynamics of Reactions Involving Oxyradicals and Hydrogen Peroxide. *Bioelectrochem. Bioenerg. 18*, 3-11.

193. Papadopoulou, N. D., Mewies, M., McLean, K. J., Seward, H. E., Svistunenko, D. A., Munro, A. W., and Raven, E. L. (2005) Redox and Spectroscopic Properties of Human Indoleamine 2,3-Dioxygenase and a His303Ala Variant: Implications for Catalysis. *Biochemistry. 44*, 14318-14328.

194. Porter, T. D., and Coon, M. J. (1991) Cytochrome P-450. Multiplicity of isoforms, substrates, and catalytic and regulatory mechanisms. *J. Biol. Chem. 266*, 13469-13472.

195. White, R. E., and Coon, M. J. (1980) Oxygen Activation By Cytochrome P-450. *Annu. Rev. Biochem. 49*, 315-356.

196. Ortiz de Montellano, P. R. (1995) *Cytochrome P450: Structure, Mechanism, and Biochemistry*, 2nd ed., Plenum, New York.

197. Sono, M., Roach, M. P., Coulter, E. D., and Dawson, J. H. (1996) Heme-Containing Oxygenases. *Chem. Rev. 96*, 2841-2888.

198. Van de Bittner, G. C., Dubikovskaya, E. A., Bertozzi, C. R., and Chang, C. J. (2010) In vivo imaging of hydrogen peroxide production in a murine tumor model with a chemoselective bioluminescent reporter. *Proc. Natl. Acad. Sci. U.S.A. 107*, 21316-21321.

199. Rana, S. V. S. (1997) Oxidative Stress and Liver Injury by Environmental Xenobiotics. *Liver. Environ. Xenobiot.*, 114-134.

200. Poljak, A., Grant, R., Austin, C. J. D., Jamie, J. F., Willows, R. D., Takikawa, O., Littlejohn, T. K., Truscott, R. J. W., Walker, M. J., Sachdev, P., and Smythe, G. A. (2006) Inhibition of indoleamine 2,3 dioxygenase activity by H_2O_2. *Arch. Biochem. Biophys. 450*, 9-19.

201. Pfister, T. D., Ohki, T., Ueno, T., Hara, I., Adachi, S., Makino, Y., Ueyama, N., Lu, Y., and Watanabe, Y. (2005) Monooxygenation of an Aromatic Ring by F43W/H64D/V68I Myoglobin Mutant and Hydrogen Peroxide. *J. Biol. Chem. 280*, 12858-12866.

202. Deisseroth, A., and Dounce, A. L. (1970) Catalase: physical and chemical properties, mechanism of catalysis, and physiological role. *Physiol. Rev. 50*, 319-375.

203. Gouet, P., Jouve, H. M., Williams, P. A., Andersson, I., Andreoletti, P., Nussaume, L., and Hajdu, J. (1996) Ferryl intermediates of catalase captured by time-resolved Weissenberg crystallography and UV-VIS spectroscopy. *Nat. Struct. Biol. 3*, 951-956.

204. Nagy, J. M., Cass, A. E. G., and Brown, K. A. (1997) Purification and Characterization of Recombinant Catalase-Peroxidase, Which Confers Isoniazid Sensitivity in *Mycobacterium tuberculosis*. *J. Biol. Chem. 272*, 31265-31271.

205. Claiborne, A., and Fridovich, I. (1979) Purification of the o-Dianisidine Peroxidase from

Escherichia coli B: Physicochemical characterization and analysis of its dual catalitic and peroxidatic activities. *J. Biol. Chem. 254*, 4245-4252.

206. Johnsson, K., Froland, W. A., and Schultz, P. G. (1997) Overexpression, Purification, and Characterization of the Catalase-Peroxidase KatG from *Mycobacterium tuberculosis*. *J. Biol. Chem. 272*, 2834-2840.

207. Varnado, C. L., Hertwig, K. M., Thomas, R., Roberts, J. K., and Goodwin, D. C. (2004) Properties of a novel periplasmic catalase-peroxidase from *Escherichia coli* O157:H7. *Arch. Biochem. Biophys. 421*, 166-174.

208. Jeng, W. Y., Tsai, Y. H., and Chuang, W. J. (2004) The catalase activity of N^{α}-acetyl-microperoxidase-8. *J. Pept. Res. 64*, 104-109.

209. Gerdemann, C., Eicken, C., Magrini, A., Meyer, H. E., Rompel, A., Spener, F., and Krebs, B. (2001) Isozymes of *Ipomoea batatas* catechol oxidase differ in catalase-like activity. *Biochim. Biophys. Acta. 1548*, 94-105.

210. Paco, L., Galarneau, A., Drone, J., Fajula, F., Bailly, C., Pulvin, S., and Thomas, D. (2009) Catalase-like activity of bovine met-hemoglobin: Interaction with the pseudo-catalytic peroxidation of anthracene traces in aqueous medium. *Biotechnol. J. 4*, 1460-1470.

211. Lewis-Ballester, A., Batabyal, D., Egawa, T., Lu, C., Lin, Y., Marti, M. A., Capece, L., Estrin, D. A., and Yeh, S.-R. (2009) Evidence for a ferryl intermediate in a heme-based dioxygenase. *Proc. Natl. Acad. Sci. U.S.A. 106*, 17371-17376.

212. Chung, L. W., Li, X., Sugimoto, H., Shiro, Y., and Morokuma, K. (2010) ONIOM Study on a Missing Piece in our Understanding of Heme Chemistry: Bacterial Tryptophan 2,3-Dioxygenase With Dual Oxidants. *J. Am. Chem. Soc. 132*, 11993-12005.

213. Schünemann, V., Jung, C., Trautwein, A. X., Mandon, D., and Weiss, R. (2000) Intermediates in the reaction of substrate-free cytochrome P450cam with peroxy acetic acid. *FEBS Lett. 479*, 149-

154.

214. Schünemann, V., Lendzian, F., Jung, C., Contzen, J., Barra, A.-L., Sligar, S. G., and Trautwein, A. X. (2004) Tyrosine Radical Formation in the Reaction of Wild Type and Mutant Cytochrome P450cam with Peroxy Acids: A MULTIFREQUENCY EPR STUDY OF INTERMEDIATES ON THE MILLISECOND TIME SCALE. *J. Biol. Chem. 279*, 10919-10930.

215. Behan, R. K., Hoffart, L. M., Stone, K. L., Krebs, C., and Green, M. T. (2006) Evidence for basic ferryls in cytochromes P450. *J. Am. Chem. Soc. 128*, 11471-11474.

216. Stone, K. L., Hoffart, L. M., Behan, R. K., Krebs, C., and Green, M. T. (2006) Evidence for Two Ferryl Species in Chloroperoxidase Compound II. *J. Am. Chem. Soc. 128*, 6147-6153.

217. Green, M. T., Dawson, J. H., and Gray, H. B. (2004) Oxoiron(IV) in Chloroperoxidase Compound II Is Basic: Implications for P450 Chemistry. *Science. 304*, 1653-1656.

218. Horner, O., Mouesca, J. M., Solari, P. L., Orio, M., Oddou, J. L., Bonville, P., and Jouve, H. M. (2007) Spectroscopic description of an unusual protonated ferryl species in the catalase from Proteus mirabilis and density functional theory calculations on related models. Consequences for the ferryl protonation state in catalase, peroxidase and chloroperoxidase. *J Biol Inorg Chem 12*, 509-525.

219. Behan, R. K., and Green, M. T. (2006) On the status of ferryl protonation. *J Inorg Biochem 100*, 448-459.

220. Li, X., Fu, R., Lee, S., Krebs, C., Davidson, V. L., and Liu, A. (2008) A catalytic di-heme *bis*-Fe(IV) intermediate, alternative to an Fe(IV)=O porphyrin radical. *Proc. Natl. Acad. Sci. U.S.A. 105*, 8597-8600.

221. Schulz, C., Chiang, R., and Debrunner, P. G. (1979) Mössbauer Parameters of Iron(4+) Heme Proteins of Spin *S* = 1. *J. Phys., Colloq.*, 534-536.

222. Schulz, C. E., Rutter, R., Sage, J. T., Debrunner, P. G., and Hager, L. P. (1984) Mössbauer and

Electron Paramagnetic Resonance Studies of Horseradish Peroxidase and Its Catalytic Intermediates. *Biochemistry. 23*, 4743-4754.

223. Harami, T., Maeda, Y., Morita, Y., Trautwein, A., and Gonser, U. (1977) Mössbauer spectroscopic determination of the electronic structure of highly oxidized iron in hemoproteins. *J. Chem. Phys. 67*, 1164-1169.

224. Maeda, Y., Higashimura, T., and Morita, Y. (1967) Mössbauer effect in peroxidase. *Biochem. Biophys. Res. Commun. 29*, 362-367.

225. Garcia-Serres, R., Davydov, R. M., Matsui, T., Ikeda-Saito, M., Hoffman, B. M., and Huynh, B. H. (2007) Distinct Reaction Pathways Followed Upon Reduction of Oxy-heme Oxygenase and Oxy-myoglobin As Characterized by Mössbauer Spectroscopy. *J. Am. Chem. Soc. 129*, 1402-1412.

226. Rittle, J., and Green, M. T. (2010) Cytochrome P450 compound I: Capture, Characterization, and C-H bond Activation Kinetics. *Science. 330*, 933-937.

227. Batabyal, D., and Yeh, S.-R. (2009) Substrate-Protein Interaction in Human Tryptophan Dioxygenase: The Critical Role of H76. *J. Am. Chem. Soc. 131*, 3260-3270.

228. Thackray, S. J., Bruckmann, C., Anderson, J. L. R., Campbell, L. P., Xiao, R., Zhao, L., Mowat, C. G., Forouhar, F., Tong, L., and Chapman, S. K. (2008) Histidine 55 of Tryptophan 2,3-Dioxygenase Is Not an Active Site Base but Regulates Catalysis by Controlling Substrate Binding. *Biochemistry. 47*, 10677-10684.

229. Bender, M. L., and Kemp, K. C. (1957) Kinetics of the α-Chymotrypsin-Catalyzed Oxygen Exchange of Carboxylic Acids. *J. Am. Chem. Soc. 79*, 116-120.

230. Ronsein, G. E., Oliveira, M. C., Miyamoto, S., Medeiros, M. H., and Di Mascio, P. (2008) Tryptophan oxidation by singlet molecular oxygen [O_2 ($^1\Delta_g$)]: mechanistic studies using 18O-labeled hydroperoxides, mass spectrometry, and light emission measurements. *Chem. Res. Toxicol. 21*, 1271-1283.

231. Byrn, M., and Calvin, M. (1965) Oxygen-18 Exchange Reatcions of Aldehydes and Ketones. *Lawrence Berkeley National Laboratory UCRL-16571*, 1-26.

232. Hayaishi, O., Rothberg, S., Mehler, A. H., and Saito, Y. (1957) Study on Oxygenases - Enzymatic Formation of Kynurenine from Tryptophan. *J. Biol. Chem. 229*, 889-896.

233. Fujii, H. (2002) Electronic structure and reactivity of high-valent oxo iron porphyrins. *Coord. Chem. Rev. 226*, 51-60.

234. Harris, D. L. (2001) High-valent intermediates of heme proteins and model compounds. *Curr. Opin. Chem. Biol. 5*, 724-735.

235. Watanabe, Y. (2000) High-valent Intermediates. *Porphyrin Handbook. 4*, 97-117.

236. Gumiero, A., Metcalfe, C. L., Pearson, A. R., Raven, E. L., and Moody, P. C. E. (2011) Nature of the Ferryl Heme in Compounds I and II. *J. Biol. Chem. 286*, 1260-1268.

237. Lang, G., Spartalian, K., and Yonetani, T. (1976) Mössbauer spectroscopic study of Compound ES of cytochrome *c* peroxidase. *Biochim. Biophys. Acta 451*, 250-258.

238. McIntire, W. S., Wemmer, D. E., Chistoserdov, A., and Lidstrom, M. E. (1991) A new cofactor in a prokaryotic enzyme: Tryptophan tryptophylquinone as the redox prosthetic group in methylamine dehydrogenase. *Science. 252*, 817-824.

239. Okeley, N. M., and van der Donk, W. A. (2000) Novel cofactors via post-translational modifications of enzyme active sites. *Chem. Biol. 7*, R159-171.

240. Lee, S., Shin, S., Li, X., and Davidson, V. L. (2009) Kinetic Mechanism for the Initial Steps in MauG-Dependent Tryptophan Tryptophylquinone Biosynthesis. *Biochemistry. 48*, 2442-2447.

241. Chen, L., Durley, R. C., Mathews, F. S., and Davidson, V. L. (1994) Structure of an Electron Transfer Complex: Methylamine Dehydrogenase, Amicyanin, and Cytochrome c551i. *Science. 264*, 86-90.

242. Chen, L., Doi, M., Durley, R. C., Chistoserdov, A. Y., Lidstrom, M. E., Davidson, V. L., and

Mathews, F. S. (1998) Refined Crystal Structure of Methylamine Dehydrogenase from *Paracoccus denitrificans* at 1.75 Å Resolution. *J. Mol. Biol. 276*, 131-149.

243. Wang, Y., Li, X., Jones Limei, H., Pearson Arwen, R., Wilmot Carrie, M., and Davidson Victor, L. (2005) MauG-Dependent in Vitro Biosynthesis of Tryptophan Tryptophylquinone in Methylamine Dehydrogenase. *J. Am. Chem. Soc. 127*, 8258-8259.

244. van der Palen, C. J., Slotboom, D. J., Jongejan, L., Reijnders, W. N., Harms, N., Duine, J. A., and van Spanning, R. J. (1995) Mutational Analysis of *mau* Genes Involved in Methylamine Metabolism in *Paracoccus denitrificans*. *Eur. J Biochem. 230*, 860-871.

245. Graichen, M. E., Jones, L. H., Sharma, B. V., van Spanning, R. J., Hosler, J. P., and Davidson, V. L. (1999) Heterologous Expression of Correctly Assembled Methylamine Dehydrogenase in *Rhodobacter sphaeroides*. *J. Bacteriol. 181*, 4216-4222.

246. Pearson, A. R., Marimanikkuppam, S., Li, X., Davidson, V. L., and Wilmot, C. M. (2006) Isotope Labeling Studies Reveal the Order of Oxygen Incorporation into the Tryptophan Tryptophylquinone Cofactor of Methylamine Dehydrogenase. *J. Am. Chem. Soc. 128*, 12416-12417.

247. Wang, Y., Graichen, M. E., Liu, A., Pearson, A. R., Wilmot, C. M., and Davidson, V. L. (2003) MauG, A Novel Diheme Protein Required for Tryptophan Tryptophylquinone Biogenesis. *Biochemistry. 42*, 7318-7325.

248. Li, X., Jones, L. H., Pearson, A. R., Wilmot, C. M., and Davidson, V. L. (2006) Mechanistic Possibilities in MauG-Dependent Tryptophan Tryptophylquinone Biosynthesis. *Biochemistry. 45*, 13276-13283.

249. Pearson, A. R., De La Mora-Rey, T., Graichen, M. E., Wang, Y., Jones, L. H., Marimanikkupam, S., Agger, S. A., Grimsrud, P. A., Davidson, V. L., and Wilmot, C. M. (2004) Further Insights into Quinone Cofactor Biogenesis: Probing the Role of MauG in Methylamine Dehydrogenase

Tryptophan Tryptophylquinone Formation. *Biochemistry. 43*, 5494-5502.

250. Erman, J. E., Hager, L. P., and Sligar, S. G. (1994) Cytochrome P-450 and Peroxidase Chemistry. *Adv. Inorg. Biochem. 10*, 71-118.

251. Braaz, R., Armbruster, W., and Jendrossek, D. (2005) Heme-Dependent Rubber Oxygenase RoxA of *Xanthomonas sp*. Cleaves the Carbon Backbone of poly(cis-1,4-Isoprene) by a Dioxygenase Mechanism. *Appl. Environ. Microbiol 71*, 2473-2478.

252. Jensen, L. M. R., Sanishvili, R., Davidson, V. L., and Wilmot, C. M. (2010) In Crystallo Posttranslational Modification Within a MauG/pre-Methylamine Dehydrogenase Complex. *Science. 327*, 1392-1394.

253. Li, X., Feng, M., Wang, Y., Tachikawa, H., and Davidson, V. L. (2006) Evidence for redox cooperativity between c-type hemes of MauG which is likely coupled to oxygen activation during tryptophan tryptophylquinone biosynthesis. *Biochemistry. 45*, 821-828.

254. Fu, R., Liu, F., Davidson, V. L., and Liu, A. (2009) Heme Iron Nitrosyl Complex of MauG Reveals an Efficient Redox Equilibrium between Hemes with Only One Heme Exclusively Binding Exogenous Ligands. *Biochemistry. 48*, 11603-11605.

255. Debrunner, P. G. (1989) Mössbauer Spectroscopy of Iron Porphyrins. *(Book) Phys. Bioinorg. Chem. Ser. 4*, 137-234.

256. Groves, J. T., Quinn, R., McMurry, T. J., Nakamura, M., Lang, G., and Boso, B. (1985) Preparation and Characterization of a Dialkoxyiron(IV) Porphyrin. *J. Am. Chem. Soc. 107*, 354-360.

257. Bill, E., Schunemann, V., Trautwein, A. X., Weiss, R., Fischer, J., Tabard, A., and Guilard, R. (2002) Mössbauer investigations of the hexachlorantimonate salt of the phenyliron 2,3,7,8,l2,13,17,18-octaethyl-5,10,15,20-tetraphenylporphyrinate, [Fe(oetpp)Ph]$SbCl_6$ and X-ray structure of the phenyliron(III) precursor Fe(III)(oetpp)Ph. *Inorg. Chim. Acta. 339*, 420-426.

258. Fu, R., Gupta, R., Wang, S., Geng, J., Dornevil, K., Zhang, Y., Hendrich, M. P., and Liu, A. (2011)

Enzyme reactivation by hydrogen peroxde in heme-based tryptophan dioxygenase. *J. Biol. Chem.*, in press.

259. Horner, O., Oddou, J. L., Mouesca, J. M., and Jouve, H. M. (2006) Mössbauer identification of a protonated ferryl species in catalase from *Proteus mirabilis*: Density functional calculations on related models. *J. Inorg. Biochem. 100*, 477-479.

260. Bollinger, J. M., Jr., and Matthews, M. L. (2010) Remote enzyme microsurgery. *Science. 327*, 1337-1338.

261. Stubbe, J., Nocera, D. G., Yee, C. S., and Chang, M. C. Y. (2003) Radical Initiation in the Class I Ribonucleotide Reductase: Long-Range Proton-Coupled Electron Transfer? *Chem. Rev. 103*, 2167-2201.